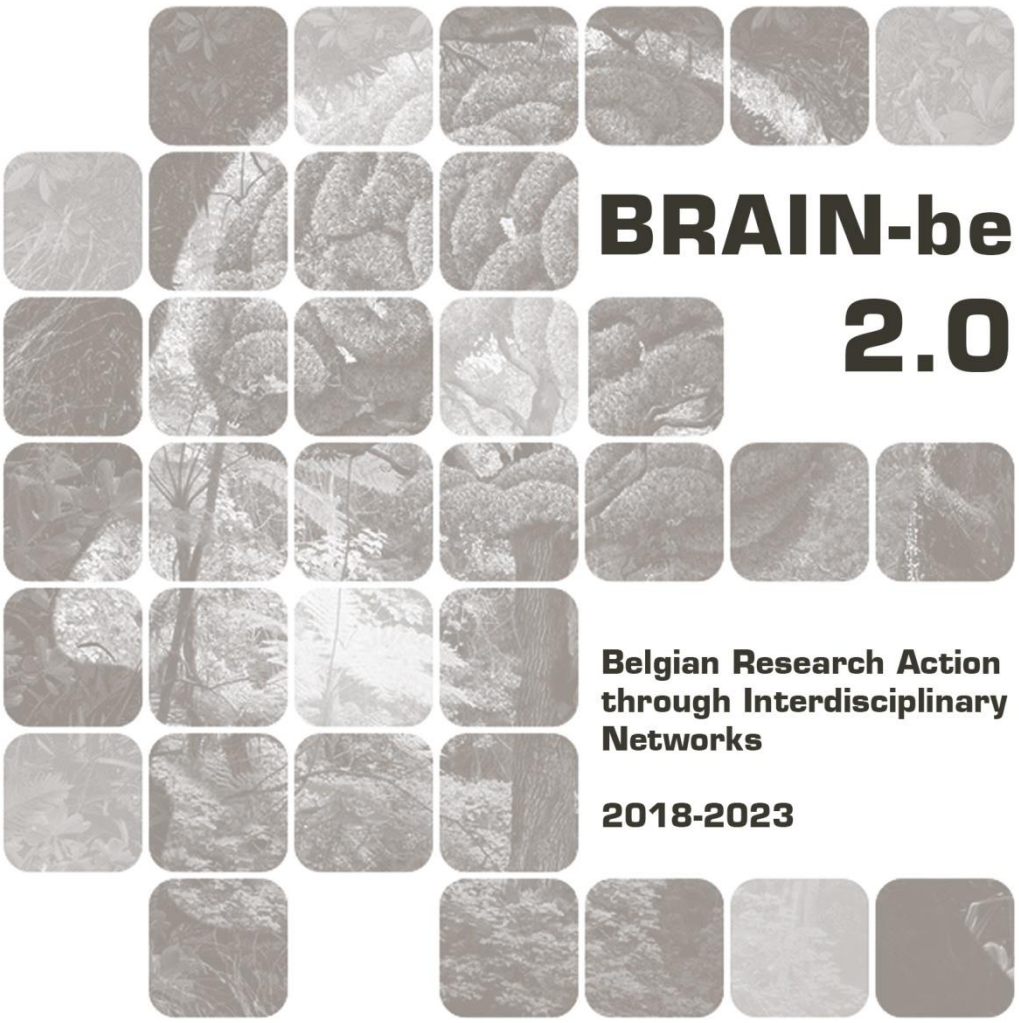

PREDICT

Phase transitions of salt mixtures under changing climatic conditions

Dr. Sebastiaan Godts (KIK-IRPA)
Dr. Hilde De Clercq (KIK-IRPA)
Dr. Julie Desarnaud (KIK-IRPA)
Prof. Dr. Tim De Kock (UAntwerpen)
Prof. Dr. Veerle Cnudde (UGent)

belspo .be

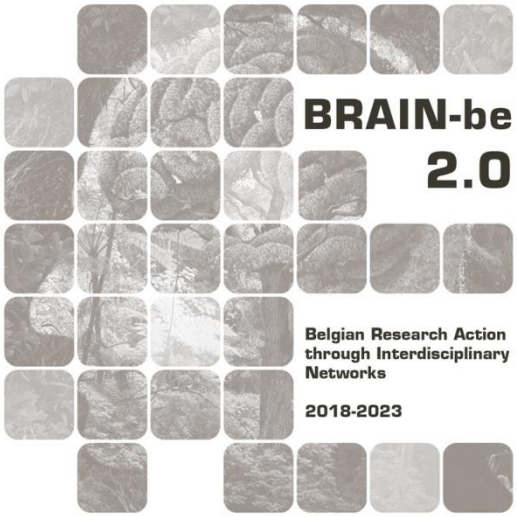

NETWORK PROJECT

PREDICT

Phase transitions of salt mixtures under changing climatic conditions

Contract - B2/191/P1/PREDICT

FINAL REPORT

PROMOTORS: Dr. Hilde De Clercq (KIK-IRPA)
Dr. Julie Desarnaud (KIK-IRPA)
Prof. Dr. Tim De Kock (UAntwerpen)
Prof. Dr. Veerle Cnudde (UGent)

AUTHORS: Dr. Sebastiaan Godts (KIK-IRPA)
Dr. Hilde De Clercq (KIK-IRPA)
Dr. Julie Desarnaud (KIK-IRPA)
Prof. Dr. Tim De Kock (UAntwerpen)
Prof. Dr. Veerle Cnudde (UGent)

ADDITIONAL CONTRIBUTORS: Prof. Dr. Michael Steiger (UHamburg)
Dr. Amelie Stahlbuhk (UHamburg)
Prof. Dr. Scott Allan Orr (UCLondon)
Dr. Katrin Wilhelm (Oxford University)

GHENT UNIVERSITY IRPA KIK belspo .be

Published in 2024 by the Belgian Science Policy Office
WTCIII
Simon Bolivarlaan 30 bus 7
Boulevard Simon Bolivar 30 bte 7
B-1000 Brussels
Belgium
Tel: +32 (0)2 238 34 11
http://www.belspo.be
http://www.belspo.be/brain-be

Contact person: Corinne LEJOUR
Tel: +32 (0)2 238 34 91

Godts, S., et al. ***Phase transitions of salt mixtures under changing climatic conditions***. Final Report. Brussels: Belgian Science Policy Office 2024 – 81 p. (BRAIN-be 2.0 - (Belgian Research Action through Interdisciplinary Networks))

Godts, S., 2024. ***Salts in the Built Environment***. PhD dissertation, Ghent University and the University of Antwerp, Ghent, Belgium.

TABLE OF CONTENTS

EXTENDED ABSTRACT

Context

Built heritage is confronted by extensive challenges in a rapidly changing society and climate. Salts are one of the main causes of stone weathering and are understudied yet critical for conservation management strategies. Ion concentrations in porous materials result from various sources such as groundwater, rainwater, atmospheric, biological, or internal material contamination. Over time, these ions are transported to the surface and deposited at the drying front, where they can crystallize into various solid forms, expanding in volume and exerting pressure on their surroundings. Cycles of crystallization and dissolution, and (de)hydration can lead to material deterioration. Moreover, salt mixtures play a significant role in exogenous processes in geomorphology, planetary research, and industrial processes. Yet, most studies have focused on binary systems.

Objectives

To bridge this knowledge gap, this dissertation explores representative ion mixtures commonly identified in weathered stone materials, including sodium (Na^+), potassium (K^+), magnesium (Mg^{2+}), calcium (Ca^{2+}), chloride (Cl^-), nitrate (NO_3^-), and sulfate (SO_4^{2-}). These ions were analyzed in 11,412 drill samples from 338 historic sites with building materials showing signs of salt decay. This extensive dataset allowed for a more accurate calculation of ion equilibrium, enabling the correct identification of salt content and further investigation into the behavior of common salt mixtures through modeling and experimental verification. One of the main issues in analyzing ion mixtures is interpreting the derived ion balance due to analytical uncertainties and undetected ions, leading to disequilibrium between anions and cations. Thus, corrections are necessary to achieve electrical neutrality for a scientifically accurate evaluation. This dissertation introduced methodological improvements in ion balance calculations, enabling a more precise interpretation of the available salt mixtures. The complete dataset and optimized charge balance calculation method were made available open-source to promote scientific community involvement. Furthermore, based on this dataset, commonly occurring mixture compositions were identified, enhancing our understanding of ions that influence mixture behavior. The corrected ion data also serve as input for thermodynamic modeling, providing insights into salt behavior using the ECOS/Runsalt model, a tool for analyzing the crystallization and dissolution behavior of salt mixtures under different climatic conditions. Specific terminology was recommended, and guidelines on how to use the model and interpret its output were detailed, emphasizing the model's limitations and providing solutions.

Conclusions

The research identified commonly occurring salt mixtures in Belgian architectural heritage, thereby enhancing insight into their behavior and contribution to material deterioration. The results revealed that 92% of the samples contained at least five ions, including sodium, potassium, nitrate, chloride, magnesium, and calcium or sulfate. Furthermore, 14 common salts were identified and four frequently occurring salt mixtures. Their critical relative humidity values for crystallization/dissolution were identified, providing important insights for experimental research into stone weathering and understanding modeling and salt weathering processes under changing climatic conditions. Moreover, innovative combined analytical techniques such as Environmental Scanning Electron Microscopy (ESEM), Dynamic Vapor Sorption (DVS), Raman Spectroscopy, X-ray Diffraction (XRD), and time-lapse micrographs enabled detailed analysis of the crystallization kinetics of salts under changing relative humidity. The kinetics of crystallization of salt mixtures under various conditions were analyzed over

time, showing the effects of relative humidity and mixture composition on crystallization and dissolution behavior, and establishing a correlation between the kinetics and the rate of change of relative humidity. These findings were linked with the results of the thermodynamic model and were confirmed using various analytical techniques.

The combination of results and new techniques introduces significant contributions to determining phase changes over time under different realistic climatic conditions and to the overall understanding of salt crystallization processes. Additionally, a comparison between modeled predictions and experimental outcomes validated the ECOS/Runsalt model's effectiveness and highlighted pitfalls that enhance reliability in predicting salt behavior. The overall results provided new insights into salt-related weathering processes, including identifying critical relative humidity values and crystallization/dissolution times for frequently occurring salts and mixtures, informing conservation efforts. The research provides specific implications for the conservation of built heritage by suggesting targeted management strategies based on specific environmental and material conditions. The findings are crucial for the preservation of built heritage and understanding salt deposition and dissolution mechanisms in general.

Keywords

Salt weathering, Built heritage conservation, Ion mixtures, Thermodynamic modelling, Crystallization kinetics

1. INTRODUCTION

Built heritage faces challenges that are extensive in a rapidly changing society and climate. Salts and consequential weathering are considered understudied and vital to establish proper conservation management strategies. Salt crystallization-dissolution cycles have the potential to weaken and break down porous materials which ultimately leads to loss of the integrity, function and value of cultural heritage. However, salt behavior is a complex subject due to the presence of a wide variety of ions, which are often the result of groundwater infiltration by capillary rising damp, rainwater infiltration, and atmospheric, biological, or internal material contamination. A wide range of literature is available considering the effects of salt crystallization in porous media, broadly defined as salt weathering with several important publications on the impact on natural stone materials such as the milestone references on natural landscape formation by Goudie and Viles (1997) and the review by Evans (1970). In contrast, the literature about stone in the built environment has focused on practical approaches to addressing stone conservation (e.g. Charola, 2000; Doehne, 2002; Doehne and Price, 2010; Siegesmund and Snethlage, 2014).

Fundamental questions, such as the mechanisms of crystallization and the development of crystallization pressure in porous media, remain open questions and active areas of research (e.g., Steiger, 2005a, 2005b; Flatt et al., 2007, 2017; Sawdy and Heritage, 2007; Sawdy et al., 2008; Derluyn, 2012; Desarnaud et al., 2016; Lubelli et al., 2018; Meldrum and O'Shaughnessy, 2020; D'Altri et al., 2021). Nevertheless, there is consensus that the occurrence of repeated cycles of crystallization and dissolution of hygroscopic salts is largely governed by changing conditions in relative humidity and temperature, and that repeated crystallization leads to the degradation of porous stone materials (e.g., Fig. 0.1) through the resulting weakening of intergranular bounds in the substrate. Additionally, moisture stains and biological contamination can be problematic due to the hygroscopic nature of certain mixture compositions, even in the absence of liquid water.

Fig. 0.1 Examples of salt-related deterioration of (a.) 17th-century brick masonry of the Farm Bree-Eik (Lennik, Belgium), (b.) 15th-century limestone (Avenderstone) sculpture in the Church of Saint-Martin (Hainaut, Belgium), and (c.) 18th-century mural on limestone plaster in the Church of Sint-Aldegondis (Mespelare, Belgium).

2. STATE OF THE ART AND OBJECTIVES

Experimental testing and theoretical models are often used to predict the behavior of salt crystallization processes and develop sustainable risk assessment methodologies. Several experimental tests have been designed, debated, and drafted in standard procedures, like the recently published manuscript by the RILEM Technical Committee 271 ASC (Lubelli et al., 2023). In theoretical models, the critical relative humidity thresholds are commonly identified to predict if a single salt will undergo a phase change in certain environmental conditions (e.g., Sabbioni et al. 2012). However, thermodynamic calculations are based on ionic activities, which can introduce uncertainty as kinetics are not considered. Additionally, the deliquescence points of salt mixtures cannot be directly determined from those of the single salt components in the mixture, so they must be calculated, as described by Steiger et al. (2014). To determine the critical crystallization points for salt mixtures, the ECOS/Runsalt model (Price 2000; Bionda, 2005a) is currently the only available model capable of predicting the behavior of salt mixtures found in the built environment under changing climate conditions. The system is based on the thermodynamic approach of Pitzer (based on mole-fractions rather than molalities) (Pitzer, 1981; Pitzer and Simonson, 1986; Clegg et al., 1992; Clegg and Pitzer, 1992) and represents a major achievement, enabling the prediction of the equilibrium behavior of salt mixtures. However, the kinetics of salt behavior are not considered, and the model has several limitations. Additionally, when dealing with salt crystallization, an ambiguous use of terminology and discrepancies can be found in the literature.

The constraints in which the results of such a model should be interpreted are rarely published (Godts et al., 2017). Furthermore, fundamental research on salt mixtures can only be found in recent literature and is rare, (e.g., Steiger et al., 2011; De Clercq et al., 2013; Lindström et al., 2015, 2016; Shen et al., 2020;). The dependency of salt phase transitions on temperature and relative humidity, illustrated by the ECOS/Runsalt outputs, underpin climatic control to mitigate salt damage. Therefore, this environmental risk has frequently been assessed by testing meteorological observations to parameterize relevant phase transitions. Grossi et al. (2011) and Sabbioni et al. (2012) have used thresholds of 75.3% RH and 75.5% respectively, as indicators for sodium chloride (NaCl) crystallization dissolution cycles. They tested average daily relative humidity from meteorological observations and took negative crossings (crystallization) as a proxy for crystallization-dissolution cycles. Establishing a correlation between daily observations and monthly averages for a certain climate allowed them to link the environmental risk to climate variations. Benavente et al. (2011) used a similar single threshold approach of daily averages for NaCl phase transitions for a case study on the Postumius Tomb (Spain) but considered a critical relative humidity difference of 10% for NaCl, setting the RH threshold at 65.3% for two consecutive days. This single-threshold approach can be justified as the relative humidity equilibrium ($^{RH_{eq}}$) of non-hydrating NaCl has a low temperature-dependent variation. Both Grossi et al. (2011) and Benavente et al. (2011) have used a more complex, temperature-dependent indicator for the hydrating sodium sulfates. Godts et al. (2017) counted phase transitions of complex salt mixtures based on thresholds of the ECOS/Runsalt outputs for a fixed temperature, using six- and twelve-hourly RH variations in the case of the St. James Church (Liège, Belgium). Menéndez (2017, 2018) has considered relative humidity changes and temperature to estimate the occurrence of salt transitions. However, the state-of-the-art is limited when dealing with realistic situations in which complex salt mixtures are present and crystallization/dissolution kinetics are understudied.

In response, an initial paper was published on NaCl-related weathering of stone, focusing on the importance of crystallization and dissolution kinetics of salt mixtures in environmental risk assessment (Godts et al., 2021). This paper includes results of an investigation into salt weathering assessment methodology, considering the temporal and kinetic behavior of salts present in porous media in both urban or rural environments. The methodology investigates an ideal situation with pure unconfined and confined NaCl, directly influenced by changing RH, and NaCl in a mixture. The dissolution and crystallization rates of NaCl under realistic changing climatic conditions are investigated. This in turn was the basis for this dissertation, intended to enhance our understanding of salt mixture behavior, by identifying phase transitions of salts in a mixture and moving toward a better understanding of kinetics and thermodynamics (model issues). Thereby paving the way toward predicting stone decay in changing climatic conditions, past and future. The initial research conducted for this dissertation highlight the limitations of current approaches, forming the key research objectives, which are systematically addressed, and are essential for achieving better risk assessment and addressing the necessary work to enable these improvements.

The research presents an in-depth investigation to further our understanding of salt mixture behavior. With an initial focus on the calculations necessary to evaluate the charge balance of ions detected in porous building materials and optimize data input for modeling purposes. For heritage materials, showing signs of salt damage (see Fig. 0.1), it is common practice to take small powder-drilled samples and analyze the ion content of the aqueous extract. Due to the diversity of ions available in building materials and the complexity of the analysis, data treatment is essential for the overall interpretation. Thus, the research focusses on the analysis of salt mixtures, presenting improved charge balance calculations of mixtures including sodium (Na^+), potassium (K^+), magnesium (Mg^{2+}), calcium (Ca^{2+}), chloride (Cl^-), nitrate (NO_3^-), and sulfate (SO_4^{2-}), as published in Godts et al. (2022a). The procedure applied to the dataset illustrates the quantification of salt mixture compositions and highlights the extent of adjustments applied in relation to the sample mass to aid interpretation. The data analysis allows the identification of theoretical carbonates that could influence the mixture behavior. Additionally, the data can be used as direct input for thermodynamic modeling. The dataset and calculations have been made available at Godts et al. (2022b).

The continued research explores model issues, terminology for salt mixture behavior, and the overall understanding of model results. The majority of the results are published in Godts et al. (2022c). To understand the crystallization behavior of a mixed salt solution as a function of changing climatic conditions, excluding factors such as the internal pore structure, the thermodynamic model ECOS/Runsalt is the only freeware available that includes the most relevant ions in the built environment. Considering the extensive variety of terms used to describe processes involving salt mixtures, specific terminology is suggested to enhance comparability across scientific studies. Additionally, the methodology on how to use the model and interpret the output is described. While emphasis is placed on key limitations of the model for which solutions are provided. However, salt mixture kinetics and the internal pore structure remain crucial parameters that are not considered. These aspects need further attention to develop a better understanding and correctly model salt damage in relation to climatic changes.

Accordingly, relevant salt mixtures are identified. This part of the research incorporates the publication Godts et al. (2023a) and explores questions concerning frequently occurring salt mixture compositions and their calculated behavior. Despite the prevalence of salt mixtures in natural

environments, most experimental work in literature has focused on single salts. Thus, the identification of salt mixture compositions and their behavior is necessary to understand weathering. The ECOS/Runsalt model is used to analyze several thousand realistic salt mixtures found in weathered stone materials and explores common mixture types and their behavior. From a wide range of salt species theoretically possible, common salts are identified that occur most frequently and their critical RH points are discussed. This research section focuses on understanding salt weathering processes based on relative humidity (RH) changes, which is a key driver for dissolution and crystallization processes. The results informed the design of the experimental work explored in the following research.

Following we explore the calculated behavior of common mixtures in relation to experimental behavior under variable humidity and fixed temperature. The results are published in Godts et al. (2024). The described processes allow us to verify the model outputs and add the dimension of time, which is crucial for understanding the kinetics involved. Specifically, looking into the dissolution and crystallization times in relation to the rate of RH changes. The kinetics of unconfined salt mixtures are studied under RH conditions, varying between 15% and 95% (at 20 °C). The focus here is placed on the four most frequently identified mixture types, sulfate-rich (Type 1) and calcium-rich (Type 2), each type containing five or six ions, Cl^-, NO_3^-, Na^+, K^+, including or excluding less common Mg^{2+}, and including either an excess of SO_4^{2-} or Ca^{2+}, with respect to gypsum. Using time-lapse micrographs and Dynamic Vapor Sorption (DVS) measurements, crystallization and dissolution behavior are explored. A range of RH change rates are studied to simulate realistic weather events. Microstructural analyses are carried out through Environmental Scanning Electron Microscopy (ESEM) to identify crystal habits corresponding with RH transitions and elemental mapping via Energy Dispersive X-ray Spectroscopy (EDX). Phases predicted from thermodynamic modeling (ECOS/Runsalt) are investigated using micro-Raman spectroscopy, X-ray Diffraction (XRD).

Finally, the dissertation that is the result of this project includes an overview of the results in the context of preservation strategies in built heritage. These results link to salt deposition and mechanisms in diverse geological and environmental sciences, laboratory experiments, future modeling efforts and the understanding of stone decay in general. Specifically, the general conclusions outline the key findings, implications for practice, limitations, and future work. It summarizes the impact on salt mixture analysis, thermodynamic modeling, terminology, and the behavior of mixtures involving kinetics. The results are placed into perspective to benefit the development of sustainable conservation and risk management strategies for salt crystallization in a wide range of contexts.

3. METHODOLOGY

Analysis of salt mixtures: charge balance calculations

The following text is primarily based on the work originally published as: Godts, S., Steiger, M., Orr, S.A., De Kock, T., Desarnaud, J., De Clercq, H., Cnudde, V., 2022. Charge balance calculations for mixed salt systems applied to a large dataset from the built environment. Sci Data 9, 324. 10.1038/s41597-022-01445-9.

The charge balance procedure is applied to ion concentrations of soluble salts found in the built environment, including the following (most common) ions: cations Na^+, K^+, Mg^{2+}, Ca^{2+}, and anions Cl^-, NO_3^-, SO_4^{2-}. The current dataset includes 11412 samples analyzed with ion chromatography, thus 79884 ion values, from 338 different monuments, archaeological sites, or sculptures, further described as sites. 330 of these sites are in Belgium, while the remaining sites in the Czech Republic (4 sites), 2 in the Netherlands, 1 in Germany, and 1 in Italy. The different sites in Belgium are spread out over 186 cities. The dataset includes general information, such as, the sampling date, location, object name, material, height, and depth. More specifically, a range of different materials are included, such as, traditional lime-based mortar, cement, plaster (including wall-paintings), brick, natural stone (mainly limestone), and efflorescence.

Samples were drilled (6 mm, drill diameter) without the use of water at different depths and heights, respectively in a wide range of intervals from the surface to 0.1, 1, 2, 3, 5 or 10 cm to a depth of maximum 20 cm in the masonry, and from the ground level to heights up to 20 meters (such as church vaults). To illustrate the spread of samples, 788 samples were taken in 25 different sites in Antwerp (Belgium), here in one site '*Museum Vleeshuis*' 108 samples were taken in 6 different areas, at 3 different heights per area, and at each height the drill samples were taken in the limestone and lime mortar at three different depths from the surface (0-1, 1-3 and 3-5; all in cm).

The ion analysis was carried out on the filtered extract of the dry sample mass by the addition of ultra-pure water and mixed for several hours (no constant time was upheld or noted, however extensive tests in our lab showed that all salts of interest were dissolved after approximately two hours. Logically, the final content of less soluble salts is dependent on the time and the water to sample ratio. The mean sample mass of all 11412 samples was 1.026 g (median: 0.865 g) while the water content added to the samples was on average 0.1 L per g dry sample mass.

The raw data derived from the ion analysis is given as a concentration of each ion as milligram per liter (mg/L). To facilitate the interpretation of the ion content in the material it is common practice to present the raw ion data as a weight percentage relative to the dry sample mass. Here, this is presented as weight fraction:

$$w_i = \frac{c_i V_w}{m_s} \tag{1}$$

where w_i is weight fraction of each individual ion, c_i is the concentration of the ion (mg/L), V_w the volume of water (L) used for the extraction of ions from the dry sample mass represented with m_s (mg).

This approximation assumes a liter of solution is equal to a kilogram of pure water (1.000 g/cm³). Although a correction could be applied if the solution density of each individual sample solution was known, the calculated deviation is considered negligible, as the solutions are highly diluted, thus resulting in an acceptable deviation of several tenths to hundredths of mg/L.

Salt mixtures are always electrically neutral, thus, any deviation from electrical neutrality must be the result of either a measurement error or ions not analyzed. Some deviation from the analysis is common. Therefore, to correctly evaluate the salt content in each individual sample and facilitate the calculations of the ionic balance, the concentration of each ion is converted to equivalents per kilogram (Eq/kg).

The calculation eliminates the charge difference between ions and allows direct comparison between cation and anion balance:

$$e_i = \frac{w_i |z_i|}{M} \tag{2}$$

here e_i is Equivalents per kilogram (Eq/kg) per ion, z_i the absolute charge of the ion and M the molar mass of the ion in question (kg/mol).

With the values in equivalents per kilogram an initial analysis is carried out to determine the charge imbalance (Δe), thus the charge excess between the total sum of amount of all cations (e_{cat}) and all anions (e_{ani}), by:

$$\Delta e = |e_{\text{cat}} - e_{\text{ani}}| \tag{3}$$

The charge balance adjustments are applied in the next equations and are based on the charge balance with a charge excess limit of 2%. This limit is dependent on the analytical method/equipment, calibration, and is ideally adjusted accordingly, further specified by Steiger and Heritage (2012). Naturally, some variation is possible, which should not reflect in the final evaluation of the ion content when considering weight fraction. The data follows one of two pathways: when the charge excess limit is equal or smaller than 2% or the anion content is greater than the cation content pathway I is followed, if it exceeds 2% Pathway I is skipped and then, the data follows Pathway II, as illustrated in the flowchart (Fig. 0.1).

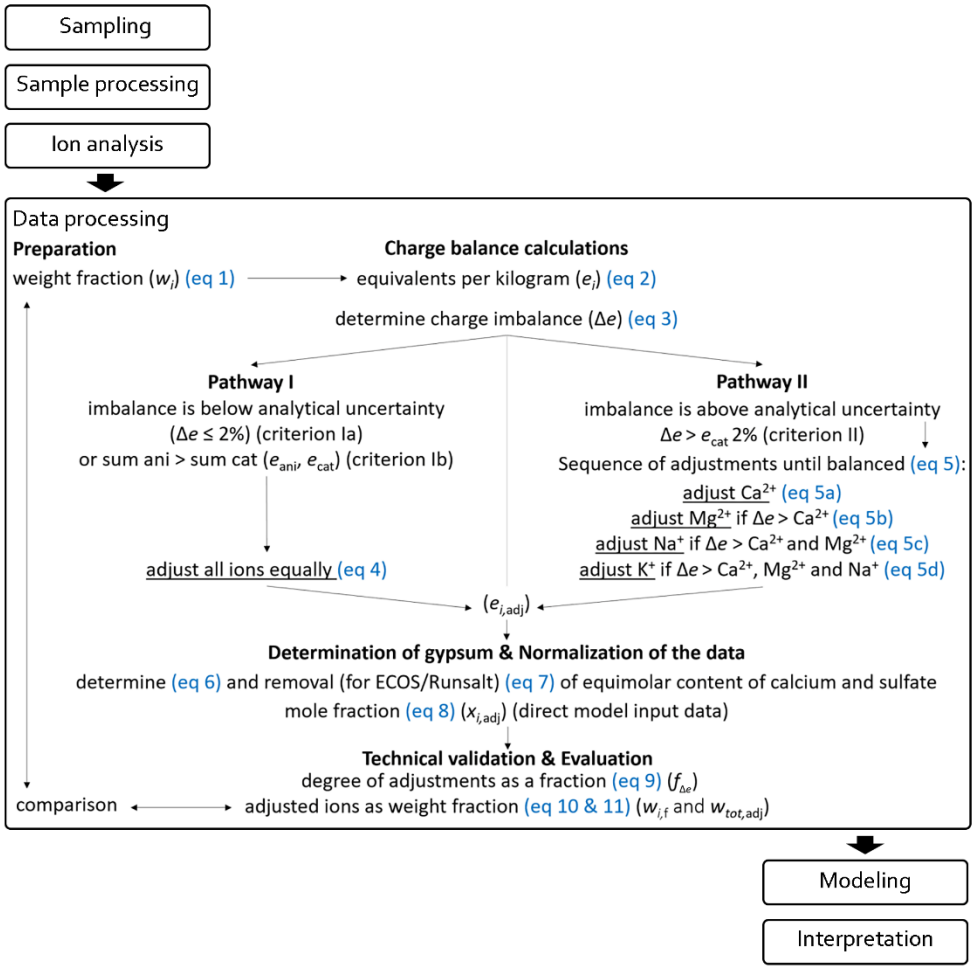

Fig. 0.1 Flowchart illustrating the entire data processing sequence starting with the preparation of the data, charge balance calculations, and addressed later in the manuscript the gypsum determination, normalization of the data for modeling purposes, technical validation, and evaluation section, ending with a comparison of the data before and after adjustments.

Pathway I is followed when either one of two criteria are met:

- criterion Ia: an analytical uncertainty is probable when the excess (Δ_e) is less or equal to 2% compared to the greatest value between the total sum of amount of all anions (e_{ani}) and all cations (e_{cat}):

  $$\Delta e \leq (0.5(e_{\text{ani}} + e_{\text{cat}} + |e_{\text{ani}} - e_{\text{cat}}|))2\%$$

  or,
- criterion Ib: when the sum of all anions is greater than the sum of all cations:

  $$e_{\text{ani}} > e_{\text{cat}}$$

However, when criterion Ib is met and the charge imbalance exceeds the estimated analytical uncertainty, the results should be carefully interpreted, as described by Steiger and Heritage (2012). The evaluation is dependent on the specific analytical method, and one should determine if the contribution of the anions in excess is important compared to the total charge imbalance, while considering the analytical uncertainty, this evaluation is carried out in 1.4 the **Error! Reference source not found.** section.

When either of the two criteria comply, an equal adjustment to all ions is applied to reach charge balance, by:

$$e_{i,\text{adj}} = \frac{e_i(e_{\text{cat}} + e_{\text{ani}})}{2\begin{Bmatrix} i \text{ is a cation } e_{\text{cat}} \\ i \text{ is an anion } e_{\text{ani}} \end{Bmatrix}} \quad (4)$$

where $e_{i,\text{adj}}$ is the adjusted and balanced concentration of the single ion, e_i is the initial charge equivalent content of either the single cation or anion to be corrected, e_{cat} and e_{ani} are the sum of respectively all cations and all anions. In the denominator the sum of either cations or anions is considered in the equation for the adjustment of respectively the individual cation or anion in question (e_i), all as Eq/kg.

If both criteria Ia and Ib are not met, pathway II is followed.

Pathway II is considered when the following criterion is met:

- criterion II: the excess of cations is greater than 2% compared to the sum of all cations: $\Delta e > e_{\text{cat}} 2\%$

When the charge imbalance is associated with an undetected anion, it is assumed that the excess is related to the least soluble theoretical solids in sequence of their solubility. The balancing procedure abstains from considering the rare contribution to the total charge balance by fluoride, phosphate, oxalate, ammonia, acetate, or formate as partly described by Arnold and Zehnder (1987). Here forth a reasonable assumption can be made to adjust the calcium and magnesium content. Calcium carbonate or calcium hydroxide is present in nearly every lime-based building material, and it is partly dissolved by the extraction procedure. In certain cases, this is also applicable for magnesium carbonate. However, in the intact material these solids cannot go in solution as there is much less water available in the pores to dissolve them compared to what is available in the extraction procedure. This means that there is a maximum excess that can be adjusted reasonably, which is specific to the analytical procedure.

The above reasoning can thus follow the rule of the solubility of possible solids within the extracted solution. Specifically, the lowest soluble salt in the mixture will crystallize first, which are: calcite ($CaCO_3$): 0.0005 mol/kg, portlandite ($Ca(OH)_2$): 0.02 mol/kg, followed by nesquehonite ($MgCO_3 \cdot 3H_2O$): 0.01 mol/kg (Silcock, 1979). Thus, the adjustment of calcium is carried out until equilibrium is reached, limited to zero calcium content, followed by an adjustment of magnesium. More specifically, when charge balance in excess surpasses the calcium content (e_{Ca}) the adjustment continues to magnesium (e_{Mg}). Any additional excess is related to carbonate salts that have a much higher solubility and are relevant within the mixture behavior. Consequently, the following cation associated with carbonates in the sequence of solubility is sodium, and then potassium. These salts are two to three orders of magnitude more soluble compared to calcium and magnesium carbonates; thus, the solubility values of these single salts are not shown as the solubility changes are more relevant within the mixture compositions. The equations below are carried out in sequence until charge balance is reached:

$$e_i^* = \begin{cases} e_i - \Delta e \geq 0 = e_i - \Delta e \\ e_i - \Delta e < 0 = 0 \end{cases}$$
$$\Delta e_i = \begin{cases} e_i - \Delta e \geq 0 = 0 \\ e_i - \Delta e < 0 = \left| e_i - \Delta e \right| \end{cases} \quad (5)$$

$$e_{i,\text{adj}} = \begin{cases} e_{\text{Ca,adj}} = e_{\text{Ca}}^* & (5a) \\ e_{\text{Mg,adj}} = e_{\text{Mg}}^* - \Delta e_{\text{Ca}} & (5b) \\ e_{\text{Na,adj}} = e_{\text{Na}}^* - \Delta e_{\text{Mg}} & (5c) \\ e_{\text{K,adj}} = e_{\text{K}}^* - \Delta e_{\text{Na}} & (5d) \end{cases}$$

Here e_i^* is the adjusted ion content (limited to 0) considering the charge balance in excess (Δe), applicable to the initial ion content (e_i) in (eq 5). When the excess exceeds the ion content in question the adjustment continues with the difference (Δe_i), following the sequence calcium, magnesium, sodium and potassium until anions and cations are balanced, thus $e_{i,\text{adj}}$ is the final adjusted ion content, all as Eq/kg.

Determination of gypsum and balanced outputs

With the results ($e_{i,\text{adj}}$) the theoretical content of gypsum is determined for appropriate interpretation of the results, and this, because gypsum is often present in high quantities and overshadows the importance of more soluble salts. This procedure also allows the removed equimolar contents of calcium and sulfate from the data, when required for modeling. For example, the ECOS/Runsalt model does not compute the full range of calculations when including equimolar contents of calcium and sulfate, in the mixture. In fact, ECOS can only handle solutions with six ions, including either Ca^{2+} or SO_4^{2-} in the system with Na^+, K^+, Mg^{2+}, Cl^-, NO_3^-.

The above reasoning is grounded on the basis that gypsum overshadows other important solids in the mixture and its low solubility. Seen that gypsum ($CaSO_4 \cdot 2H_2O$) has a low solubility (0.015 mol/kg) (Silcock, 1979) a reasonable assumption can be made that gypsum will crystallize rapidly from any system during evaporation, the latter as described by Clegg and Brimblecombe (Price, 2000). Although gypsum is presumed less relevant to influence the mixture behavior under environmental changes (Sawdy & Heritage, 2007), some questions remain unanswered as described by Charola et al. (2007). Thus, it remains crucial to determine and evaluate the gypsum content as the salt remains highly important as a primary cause of deterioration, especially in the presence of liquid water.

The determination and exclusion of gypsum is thus necessary for i) general interpretation of the results and ii) for ECOS to compute, noting that this step has no bearing on the balance between anions and cations. The following equation is considered to determine and evaluate the theoretical gypsum content in the sample:

$$e_{\text{lim}_{\text{CaSO}_4}} = 0.5(e_{\text{Ca,adj}} + e_{\text{SO}_4\text{,adj}} - \left| e_{\text{Ca,adj}} - e_{\text{SO}_4\text{,adj}} \right|) \quad (6)$$

where $e_{\text{lim}_{\text{CaSO}_4}}$ is the limited content of Ca and SO_4 in Eq/kg to determine the theoretical gypsum content; $e_{\text{Ca,adj}}$ and $e_{\text{SO}_4\text{,adj}}$ are the (adjusted) calcium and sulfate content from Eq. 4 and Eq. 5.

The removal of the theoretical gypsum content is carried out on the individual calcium and sulfate ions, by:

$$e_{\mathrm{Ca,adj,f}} = e_{\mathrm{Ca,adj}} - e_{\mathrm{lim}_{\mathrm{CaSO_4}}}$$
$$e_{\mathrm{SO_4,adj,f}} = e_{\mathrm{SO_4,adj}} - e_{\mathrm{lim}_{\mathrm{CaSO_4}}} \quad (7)$$

here, $e_{\mathrm{Ca,adj,f}}$ and $e_{\mathrm{SO_4,adj,f}}$ are the final adjusted calcium and sulfate contents.

After the removal of gypsum either calcium or sulfate are always zero.

To allow the mutual comparison between different mixture compositions derived from samples with a different weight, the data is normalized, under the condition that the excess (Δe) (as a control) is less than or equal to $1x10^{-12}$ Eq/kg. This value was selected to eliminate rounding errors without implications to data interpretation. The anion and cation values after removal of the theoretical gypsum content as mole fraction ($x_{i,\mathrm{adj}}$) is determined by:

$$x_{i,\mathrm{adj}} = \frac{\frac{e_{i,\mathrm{adj}}}{|z_i|}}{\sum_{k=1}^{n} \frac{e_{k,\mathrm{adj}}}{|z_k|}} \quad (8)$$

The ion concentrations as mole fraction can be used as direct input for, amongst others, the ECOS/Runsalt model without the need for ambiguous corrections. Furthermore, batch model analysis from different samples can be used for statistical determinations of common ions and salt mixtures found in the built environment, following an approach that was suggested in 2014 (Godts et al., 2014). Several considerations before using the processed data remain important and are further described.

Modeling salt behavior

The following text is primarily based on the work originally published as: Godts, S., Steiger, M., Orr, S.A., Stahlbuhk, A., Desarnaud, J., De Clercq, H., Cnudde, V., De Kock, T., 2022. Modeling Salt Behavior with ECOS/RUNSALT: Terminology, Methodology, Limitations, and Solutions. Heritage, 5, 3648-3663. 10.3390/heritage5040190.

Terminology and methodology for using Runsalt

Understanding salt mixture behavior in porous media under changing climatic conditions is not a straightforward task and requires in-depth knowledge of the mixture composition and material characteristics, as well as internal and external factors. However, a first step is knowing the correct salt mixture present, which requires data input preparation for the model, as described further in Steiger and Heritage (2012) and is verified by applying the method to a large dataset including several additional steps to calculate the charge balance of all ions as detailed earlier.

Before moving forward with the methodology for using RUNSALT, Table 0-1 is given to overcome the ambiguous use of terminology found in the literature and to clarify the crystallization pathways of mixed salt systems shown in RUNSALT plots (see example Fig. 0.2). Specific RH points of interest are linked to the suggested symbols presented in the table, and the letters A to F are further detailed in the legend of Fig. 0.2. Note how RH points of interest overlap depending on how a plot is read from a humid to a dry environment or vice versa. The term mutual (m) is chosen as the behavior of each solid

is influenced by the mixture composition, and m is removed when dealing with single salts. The symbols are recommended for future use to make scientific information comparable.

Table 0-1 Overview of terminology and suggested symbols to describe RUNSALT plots showing the crystallization pathway of mixed salt systems under changing RH. Refer also to Fig. 0.2, the legend of Fig. 0.2, and Table 3-2.

	Meaning	Base Symbol	Species-Specific Symbol [1]
	Explanation following RUNSALT plots (example Fig. 0.2)		
1.	Mutual crystallization relative humidity	RH^{m}_{cry}	$RH^{m}_{cry_1}$
RH point at the onset of any line shown in a plot corresponding to the start of crystallization; the number shown in the specific symbol refers to the species/solid in order of appearance from a humid to a dry environment. The use of the number (e.g., 1) in relation to the solids can be useful to understand the sequence of crystallization. The solution at this point is saturated with respect to a specific solid. When available, the first letters of the mineral name or chemical formula can be used to replace the number, e.g., $RH^{m}_{cry_1}$ is aphthitalite = aph and thus $RH^{m}_{cry_{aph}}$ (Fig. 0.2 A). Aphthitalite is the first that crystallizes in the mixture and the same base symbol is used for the mutual crystallization relative humidity of all solids that crystallize (indicated with the letter B in Fig. 0.2). This is only relevant when solution is still available before crystallization takes place (reactions in solution in Table 3-2.			
2.	Mutual dissolution relative humidity	RH^{m}_{dis}	$RH^{m}_{dis_1}$
RH point at the end of a horizontal line in a plot, looking from a dry to a humid environment, equals the start of dissolution; e.g., in Fig. 0.2 this is illustrated by the RH points indicated with the letter C, and thus when solution becomes available.			
3.	Mutual deliquescence relative humidity	RH^{m}_{del}	$RH^{m}_{del_1}$
RH point at the end of a horizontal line in a plot when no more solution is available, looking from a dry to a humid environment, e.g., indicated as letter D in Fig. 0.2. Here, the last solid that crystallizes is darapskite, and afterwards no more solution is available. Thus, $RH^{m}_{del_{dar}}$, as further illustrated by reaction number 2 shown in Table 3-2.			
4.	Mutual transition relative humidity	RH^{m}_{tra}	$RH^{m}_{tra_{[3-5]}}$
RH point at which salt transitions occur. The numbers refer to the solids involved in the transition, starting with solids before the dash (e.g., 3 in [3–5]) at more humid conditions transitioning to solids after the dash (e.g., 5 in [3–5]) at dryer conditions. Either a phase change (hydration, dehydration), decomposition, or the formation (addition) of solids occur under both wetting and drying conditions. For example, the transition of mirabilite to thenardite is $RH^{m}_{tra_{[mir-the]}}$, or is more complicated, as shown by reaction 3 in Table 3-2 (Fig. 0.2 E).			
Additional terms that are useful when calculating water activities or concentrations.			

Values that are not included in the RUNSALT output data yet could be derived from the ECOS calculations.

5. Mutual equilibrium relative humidity RH^{m}_{eq}

Any RH point at which a solution is in equilibrium with its environment = water activity at any concentration if solution is available, e.g., in Fig. 0.2 any *RH p*oint above D, and thus $RH^{m}_{del_{dar}}$.

6. Mutual saturation relative humidity RH^{m}_{sat}

Any RH point at which a solution is saturated (points on the curves, e.g., in Fig. 0.2, all RH points between A and C on the curve of aphthitalite crystallization), equal to the RH^{m}_{eq} points during crystallization (when solid and solution are available).

[1] For practical considerations, double subscripts can be replaced by a comma between subscripts, e.g., $RH^{m}_{cry,aph}$.

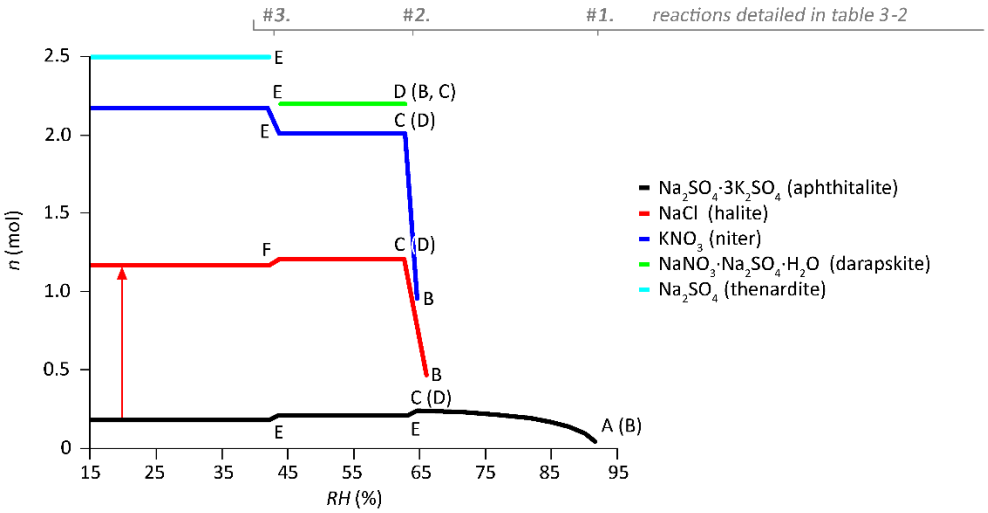

Fig. 0.2 Example of an ECOS/RUNSALT output with 2 mol Na^+ and K^+, and 1 mol Cl^-, NO_3^-, and SO_4^{2-}, calculated at 20 °C with RH (%) from 15% to 95% (resolution 1.6% RH points), with the latter on the *x*-axis and the amount of crystalline salt, *n* (mol), stacked on the *y*-axis. The red arrow illustrates the absolute amount of the solid NaCl (halite) at the specific RH, here from 0.16 to 1.16 mol, thus with an absolute amount of 1 mol. The letters A to F indicate specific RH points of interest and are explained in the legend below. The numbers 1 to 3 indicate the RH points at which reactions take place when looking from a humid to a dry environment, as further detailed in Table 3-2.

Legend by Fig. 0.2, with the letters A to F indicating specific RH points of interest:

A. The first mutual crystallization relative humidity of the mixture ($RH^{m}_{cry_1}$) represents the RH at which crystallization initiates for the first solid that appears under drying conditions (aphthitalite here, and thus $RH^{m}_{cry_{aph}}$). The solution is saturated with respect to aphthitalite, and above this RH all solids are dissolved.

B. The mutual crystallization relative humidity of all the following solids that crystallize from the solution in the mixture, and thus is the RH at which crystallization first begins for $RH^{m}_{cry_{hal}}$, $RH^{m}_{cry_{nit}}$ and $RH^{m}_{cry_{dar}}$.

C. The mutual dissolution relative humidity of all solids in the mixture when solution becomes available is equal to the RH points when a crystal starts to dissolve for $RH^{m}_{dis_{aph}}$, $RH^{m}_{dis_{hal}}$, $RH^{m}_{dis_{nit}}$ and $RH^{m}_{dis_{dar}}$. B and C are often at the same RH; here, the resolution of the plot distorts the position for halite and niter, a phenomenon explained further on.

D. The mutual deliquescence relative humidity of the mixture is the RH determined by the solids in the mixture at which the first dissolution starts to occur and solution becomes available; here, $RH^{m}_{del_{dar}}$ also equals the dissolution relative humidity of $RH^{m}_{dis_{aph}}$, $RH^{m}_{dis_{hal}}$ and $RH^{m}_{dis_{nit}}$.

E. The mutual transition relative humidity $RH^{m}_{tra_{[dar/aph]-[nit/the]}}$. Here, under drying conditions, thenardite is formed and the amount of niter increases from the decomposition of darapskite and aphthitalite in a solid-state reaction.

F. Plot stacking artifact caused by transition reactions, herein identified by chloride that is not available in other solids.

The reactions presented in the RUNSALT plot shown in Fig. 0.2 are further detailed in Table 3-2.

Table 0-2 Summary of the reactions under drying conditions shown in the RUNSALT plot (Fig. 0.2, noted as # 1, 2 and 3 above the figure).

Start composition of the solution (mol): $2Na^+ + 2K^+ + 1Cl^- + 1NO_3^- + 1SO_4^{2-}$	
#	Reactions in solution
1.	$2Na^+ + 6K^+ + 4SO_4^{2-} \rightarrow Na_2SO_4{\cdot}3K_2SO_4$ (cr)
2.	$Na_2SO_4{\cdot}3K_2SO_4$ (cr) + $11Na^+ + Cl^- + 10NO_3^- + 4H_2O \rightarrow NaCl$ (cr) + $6KNO_3$ (cr) + $4NaNO_3{\cdot}Na_2SO_4{\cdot}H_2O$ (cr)
	Solid state (decomposition) reactions
3.	$6NaNO_3{\cdot}Na_2SO_4{\cdot}H_2O$ (cr) + $Na_2K\,SO_4)_4$ (cr) $\rightarrow 6KNO_3$ (cr) + $10Na_2SO_4$ (cr)

As described in section **Error! Reference source not found.**, the ions used for the model input are Cl^-, NO_3^-, Na^+, K^+, and Mg^{2+}, with either SO_4^{2-} or Ca^{2+}. This excludes, amongst others, carbonates and the equimolar contents of calcium and sulfate, with the latter considered as the gypsum content. Hence, the model primarily calculates a maximum of six ions. The system composition is entered into the RUNSALT interface as mol or weight, with the selection of either a RH range between 15% and 98%, or a T range between −30 and +50 °C, after which either the T or RH value is fixed. The RUNSALT interface generates a temporary .DAT file that includes the inputs required by the model. These inputs are read in by the batch executable .EXE file which then initiates the model. In another temporary file, ECOS outputs the equilibrium composition at 50 equally spaced intervals for either the specific temperature or humidity range and is then read by RUNSALT to produce a graphical representation of the crystallization behavior. The output can be exported in graphical and textual (.CSV) formats for further analysis through RUNSALT.

The crystallization behavior of the mixture is graphically represented by RUNSALT with the specified RH or T range on the *x*-axis, while the *y*-axis returns the amount of substance (mol) (Fig. 0.2). After the plot is generated, one can choose to show the *y*-axis as volume (*V*) in cm^3 (molar volume of salt, that is, equilibrium crystal volume) (Fig. 0.3), which gives a more realistic visualization of the salt content in the pores. For example, aphthitalite is present in approximately one tenth of the total mol content (Fig. 0.2), and at least a third of the total solid volume (Fig. 0.3). The latter is thus more indicative of risk in the pore structure and will determine the overall interpretation and conservation advice. The use of volume in the outputs was recently illustrated in relation to climatic conditions by Costa et al. (2022). Expressing the results as volume is additionally useful to estimate pore filling, as the molar

volume (V_m) can be used as an input value in the calculation, as described in Gulotta et al. (2021). All values on the *y*-axis are cumulative (stacked), meaning that the amount of the first solid should be deducted from the second to know the absolute value of each individual solid. The individual amount of salt is illustrated for halite (NaCl) at the given RH with the red arrow in Fig. 0.2.

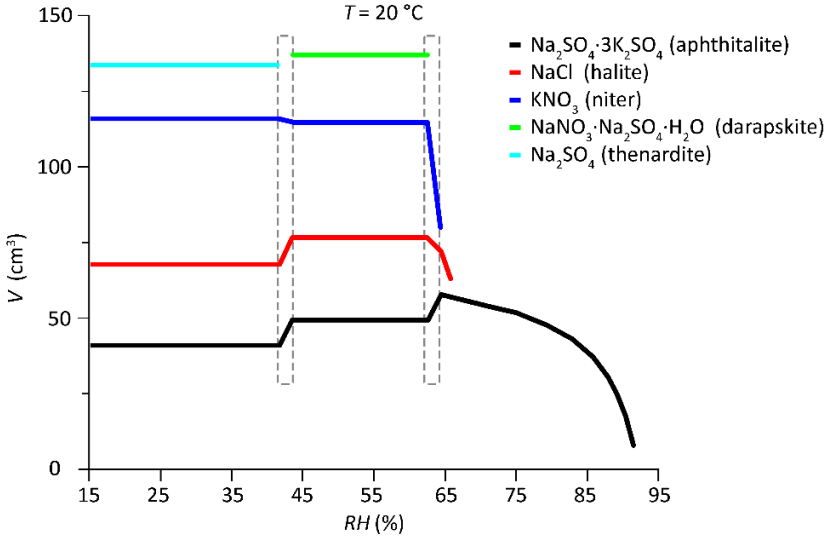

Fig. 0.3 Example of an ECOS/RUNSALT output of 2 mol Na^+ and K^+, and 1 mol Cl^-, NO_3^- and SO_4^{2-}, calculated at 20 °C with RH (%) from 15% to 95% (resolution 1.6% RH), with the latter on the *x*-axis and the amount of crystalline salt in volume, *V* (cm^3), stacked on the *y*-axis. The dashed rectangles illustrate plot artifacts caused by the RH resolution; the non-vertical lines are to be read as vertical ones and the gap between darapskite and thenardite is closed.

As the data points are systematically calculated for 50 points within the chosen range of environmental parameters (RH or T), the smaller the range the higher the resolution. Hence, data related to smaller successive intervals can be stitched together to obtain a more detailed output. However, changes in stacking order in the detailed plots can occur at higher resolution. This process can be an important step to correct certain artifacts caused by the resolution of the chosen environmental parameters. For example, in Fig. 0.4, if the RH range between 60 and 70% is entered into RUNSALT, the resolution of the plot increases to 0.2% RH, as opposed to 1.6% RH when generating a plot from 15 to 95% RH (Fig. 0.2). Thus, the thermodynamically calculated mutual relative humidity points of interest, for example, $RH^m_{cry_{nit}}$ and $RH^m_{cry_{hal}}$, are more accurate. The plot also shows that $RH^m_{cry_{dar}}$ or $RH^m_{del_{dar}}$ is equal to $RH^m_{dis_{nit}}$, $RH^m_{dis_{hal}}$, and $RH^m_{tra_{[aph]-[hal/nit/dar]}}$. The resolution makes little to no difference to the final conservation advice given to the field in terms of the risk assessment of RH ranges of crystallization/dissolution.

However, selecting a narrower range in the environmental parameters can clarify certain artifacts and uncertainties in the plot. In particular, the slightly non-vertical lines of aphthitalite, halite, and niter are caused by the resolution 0.2% RH, and these lines are in fact to be read as vertical (location shown by the dashed rectangles in Fig. 0.3 and Fig. 0.4). The same is true for the gap (transition $RH^m_{tra_{[dar/aph]-[nit/the]}}$) and all non-vertical lines at lower RH at approximately 43% (shown in Fig. 0.3).

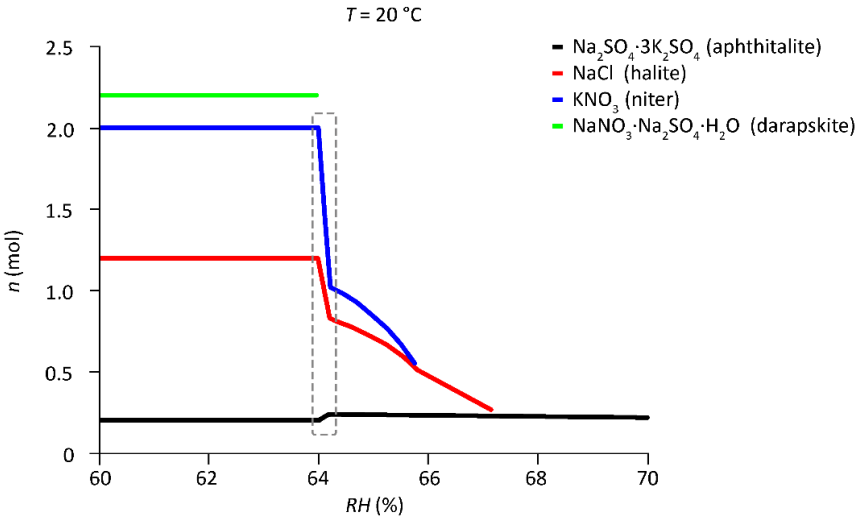

Fig. 0.4 Detail of the ECOS/RUNSALT output shown in Figure 2.1, calculated at 20 °C with RH (%) from 60% to 70% (resolution 0.2% RH points), with the latter on the *x*-axis and the amount moles of crystalline salt, *n* (mol), stacked on the *y*-axis. The dashed rectangle illustrates plot artifacts caused by the RH resolution; the non-vertical lines are to be read as vertical.

When reading the complete RUNSALT plot, we can start looking at the *x*-axis from a more humid environment on the far right (95% RH) to a dry environment on the far left (15% RH). Under more humid conditions, and before the first line appears, all salts are in solution. The solution has a certain concentration corresponding to the given RH; the further away from the first solid, the more the solution is diluted, which is theoretically infinite until pure water is reached at 100% RH. Just before the RH at which the first solid crystallizes (for example, in Fig. 0.2, aphthitalite ($Na_2SO_4 \cdot 3K_2SO_4$)), the solution is at its highest degree of saturation. The solution is saturated and in equilibrium with the environment and is referred to as mutual saturation relative humidity (RH^m_{sat}). In a mixture, this can be defined at any RH point where curved lines are visible in the RUNSALT outputs.

The lines indicate the crystallization of a solid. Looking further at Fig. 0.2, aphthitalite starts to crystallize at approximately 92% (20 °C). This point is the mutual crystallization relative humidity of the solution (RH^m_{cry}). Following the crystallization of aphthitalite to dryer conditions, the remaining ions are still in solution and become more concentrated until halite starts to crystallize, followed by niter and darapskite. Each solid has a crystallization relative humidity (RH^m_{cry}) of 67, 66, and 64% (±0.1), respectively. Similar to aphthitalite, for both halite and niter, the solid amount increases over a RH range, while all darapskite crystallizes at a specific RH point, as shown in Fig. 0.4. This RH of 64% is also the point at which no more solution is available. This is the mutual deliquescence relative humidity (RH^m_{del}) of the mixture.

Looking further down the remaining crystallization pathway at dryer conditions below $RH^m_{cry_{dar}}$ ($=RH^m_{del}$ of the mixture), while keeping in mind that no solution is available, the following solid-state (decomposition) reactions can be observed. First, a small amount of aphthitalite decomposes at the same RH as $RH^m_{cry_{dar}}$, and from 64% to 43% RH all solids remain crystallized. For this mixture, the RH of 64% is the most important to avoid crystallization cycles and damage to porous materials. In practice, it would be common to advise a stable RH between 50% and 60% RH at 20 °C; that is, if all water sources are eliminated, if other artifacts in the area remain well preserved under these conditions, if

the mixture compositions are representative for the entire salt risk assessment, and if the location allows such a narrow range of RH to be maintained. However, some flexibility should be considered, specifically toward the lower RH range as the solid-state reactions might have limited effect on the substrates. Additionally, an RH increase over a limited time should be acceptable due to the kinetics considering dissolution/crystallization rates (Godts et al., 2021). However, more research is needed to further understand these processes for common mixture compositions.

As shown in Table 0-2 the formation of thenardite is the result of the decomposition of aphthitalite and darapskite, which also explains the increase in niter at the same RH of approximately 43%. The decrease in halite at the same RH is an artifact of plot stacking (amount of substance or volume) on the *y*-axis. This can be derived from the fact that no other salt is formed with Cl^-. In drier conditions (below 43%), all salts remain crystallized.

Looking back at higher RH in the figures, it is important to understand that, for example, aphthitalite in the system will only start to dissolve if all other salts have gone into solution and the solution has reached the specific dilution above 64% RH. Specifically, the dissolution of aphthitalite is dependent on the concentration of the surrounding solution. The solution will accumulate moisture, which can cause discoloration, moisture stains, the peeling of paint layers, and attract biological growth. At $RH^{m}_{cry_{aph}}$ of 92%, the solution is saturated with respect to aphthitalite. Above this RH point, the solution becomes further diluted (until infinity at 100%). The amount of water vapor absorbed by the solution at a given RH can be calculated with ECOS. However, this data is currently not given in RUNSALT. Details on the backend calculations of the model are extensively described in Price et al. (2000).

The above example shows the value of the model to derive specific advice for environmental salt risk assessment. The model has proven extremely valuable for the field and certain aspects have been verified with four ion mixtures by Rörig-Dalgaard (2021). However, several limitations and issues should be taken into consideration before application. In the following, the most common limitations and solutions are provided, while we abstain from considering deviations in the crystallization pathways if a solid becomes isolated from the remaining solution.

Identification of relevant salt mixtures

The following text is primarily based on the work originally published as: Godts, S., Orr, S.A., Steiger, M., Stahlbuhk, A., De Kock, T., Desarnaud, J., De Clercq. H., Cnudde, V., 2023. Salt mixtures in stone weathering. Sci Rep 13, 13306. 10.1038/s41598-023-40590-y.

The complete dataset used in this study includes 11412 drill samples analyzed with ion chromatography, specifically 79884 ion concentrations of chloride, nitrate, sulfate, sodium, potassium, magnesium, and calcium. The ion analysis and data treatment were detailed earlier, with the complete dataset and calculations available at (Godts et al., 2022b). The samples were taken from weathered stone materials in 338 monuments, archaeological sites, mural paintings, and sculptures, primarily in Belgium (Fig. 0.5). The related building materials were mostly produced between the 10th and 20th centuries and consist of traditional lime-based mortar, cement, plaster (including wall paintings), brick, and natural stone (mainly limestone). The ions detected are to an important degree representative of the diverse mixtures found in stone materials globally.

The identification of common mixtures, solids, and behavior under changing RH conditions is based on the ion dataset, corrected to achieve an equilibrium charge balance within each individual sample. The balanced ion concentrations are presented as mole fraction and equimolar contents of calcium

and sulfate, considered as the gypsum content, were removed (further detailed in **Error! Reference source not found.**), which identified three mixture types:

- Type 1: a sulfate-rich mixture includes an excess of sulfate ions, with respect to the removal of equimolar contents of calcium and sulfate (70% of samples). The most important ions of this mixture type (median) derived from the dataset in order of magnitude were SO_4^{2-}, Na^+, K^+, NO_3^-, Cl^-, and Mg^{2+}.
- Type 2: calcium-rich mixture includes an excess of calcium ions, with respect to the removal of equimolar contents of calcium and sulfate (30% of samples). The most important ions of this mixture type (median) derived from the dataset in order of magnitude were NO_3^-, Ca^{2+}, Cl^-, Na^+, K^+, and Mg^{2+}.
- Type 3: a mixture containing an important content of carbonates related to an excess of sodium or potassium (relevant within 3% of samples in Type 1).

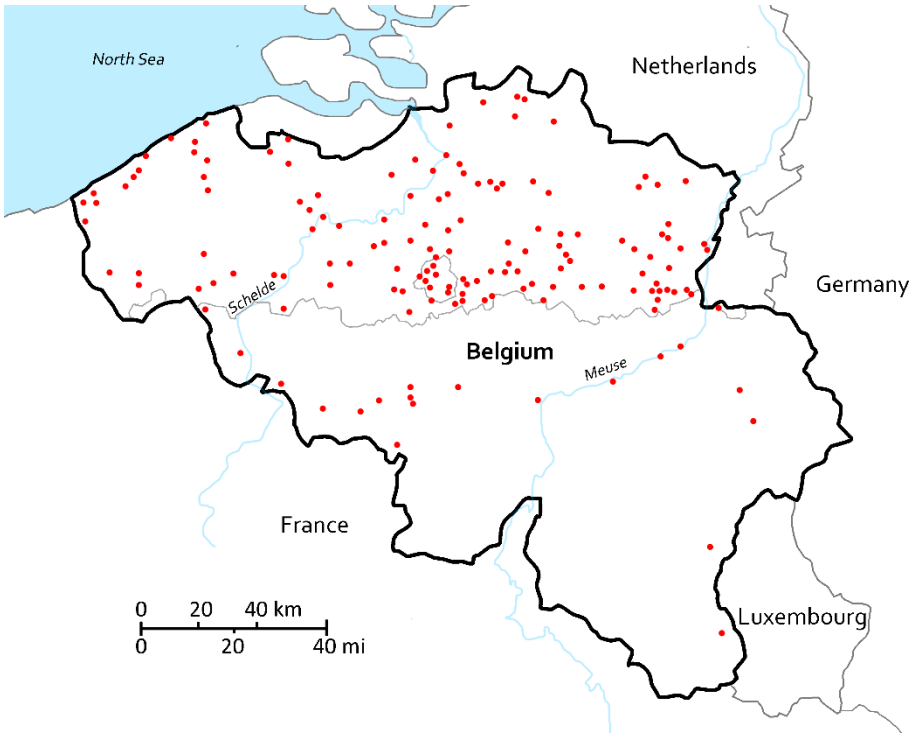

Fig. 0.5 Overview of the locations of 338 sites where in total 11412 drill samples were taken for the determination of the quantitative ion concentrations of Cl^-, NO_3^-, SO_4^{2-}, Na^+, K^+, Mg^{2+}, and Ca^{2+}. Several sites were located in a single city, for example: 30 in Brussels and 25 in Antwerp. The dataset (Godts et al., 2022b) also includes one site in Germany, one in Italy, two in The Netherlands and four in the Czech Republic. Drawn with Adobe Photoshop 2022, map data available at (Godts, 2023).

The results presented further, focus on mixtures Types 1 and 2. The data were used as direct input for the ECOS/Runsalt model (Price, 2000; Bionda, 2005a). The model has equivalent principles to the molality based model, generally known as the Pitzer–Simonson–Clegg model, includes ion concentrations expressed as mole fractions (Clegg & Brimblecombe, 2000). The outputs of the model are investigated to determine the crystallization behavior of salt mixtures under changing RH between 15% and 95% with a 0.2% resolution at 20 °C. Further input details, limitations, issues, and solutions for the model were taken into consideration. Special attention was given to certain issues with the representation of hydrate behavior in the outputs, such as calcium nitrates, magnesium sulfates and potassium sulfates. The removal of equimolar contents of calcium and sulfate ($CaSO_4$, here regarded as the gypsum content ($CaSO_4 \cdot 2H_2O$)) was carried out before inputting the ion data into the user

interface (Runsalt) to avoid the software prompting to remove gypsum from the system before it can run the model. Thus, calcium sulfate double salts were not considered in this study, e.g., glauberite ($Na_2Ca(SO_4)_2$), wattevillite ($Na_2Ca(SO_4)_2{\cdot}4H_2O$), eugsterite ($Na_4Ca(SO_4)_3{\cdot}2H_2O$), hydroglauberite ($Na_{10}Ca_3(SO_4)_8{\cdot}6H_2O$), syngenite ($K_2Ca(SO_4)_2{\cdot}H_2O$), görgeyite ($K_2Ca_5(SO_4)_6{\cdot}H_2O$), and polyhalite ($K_2Mg_2Ca_2(SO_4)_4{\cdot}2H_2O$). Carbonate salts and more complex salts such as humberstonite ($Na_7K_3Mg_2(SO_4)_6(NO_3)_2{\cdot}6H_2O$), kainite ($KMg(SO_4)Cl{\cdot}3H_2O$), $Ca(NO_3)_2{\cdot}KNO_3{\cdot}3H_2O$ (R. Flatt & Bocherens, 1962) and $Ca_2Cl_2{\cdot}Ca(NO_3)_2{\cdot}4H_2O$ (Ehret, 1932) were also not considered in the model.

To identify common salt mixtures and their behavior, datasets were compiled with ion data as mole fraction to derive mean ion values. These values were then used to generate ECOS/Runsalt outputs. Mole fraction was selected to normalize the quantity of ions between samples and mean values were chosen to maintain charge balance between anions and cations. The following datasets were evaluated:

- All 11412 samples (338 sites) (3340 bricks, 3693 mortars, 799 plasters, 1318 stones, and 2262 unidentified).
- 7946 samples identified as Type 1 (sulfate-rich mixture), subsets: 2317 bricks, 2405 mortars, 483 plasters, 1089 stones and 1652 unidentified.
- 3466 samples identified as Type 2 (calcium-rich mixture), subsets: 1022 bricks, 1286 mortars, 316 plasters, 229 stones, and 619 unidentified.

Additional subsets were considered which focus on a sampling depth from the material surface to a depth of maximum 2 cm, and a total salt content equal or greater than 0.8 wt.% (excl. $CaSO_4$) compared to the dry material mass. The depth was selected due to practical considerations of sampling depths on site and because the first centimeters of a substrate contain the highest salt load directly influenced by external environmental conditions. The salt content value selected was derived from on-site investigations where limited damage was seen at lower salt contents. This subset results in a total of 1867 samples from 218 sites:

- 921 samples from 186 sites were allocated to Type 1 (sulfate-rich mixture)
- 946 samples from 132 sites were identified as Type 2 (calcium-rich mixture)

The data of all samples were further investigated to evaluate the distribution of mixture types per site considering different sampling heights classified in groups between 0 to 30 cm (including samples taken at the base of a building near the ground), 30 to 50 cm, 50 to 100 cm, 100 to 200 cm, 200 to 400 cm, and above 400 cm, the latter often reaching ceiling vaults. Hereby, evaluating the occurrence of sulfate- and calcium-rich mixtures to understand salt distribution in terms of fractionation as described by Arnold and Zehnder (1987).

ECOS/Runsalt outputs of all samples were generated to identify common solids as a percentage within the given mixture Types 1 and 2. For each sample, eight iterations of ECOS were run to achieve a resolution of 0.2% RH, thus for each 10% between 15 and 95% RH (removing duplicates), all calculated at 20 °C. The median, minimum and maximum mutual crystallization and dissolution relative humidity points (RH^m_{cry} and RH^m_{dis}, respectively) were determined for each solid from all Runsalt outputs (see **Error! Reference source not found.** for detailed explanations of these terms and nomenclature). The RH ranges were compared to the relative humidity equilibrium of the individual solids (single salt behavior) to outline the range of crystallization and dissolution RH points of salts in a mixture.

The composition and behavior of mixtures were analyzed, specifically focusing on crystallization under changing relative humidity (RH) at 20 °C and the mutual deliquescence of common solids.

Understanding the RH ranges for crystallization and dissolution in different mixtures can help us understand the damage phenomena in weathered stones due to repeated phase changes. This study also investigates the distribution of ions and changes in mixture composition in traditional building materials, particularly regarding their influence on crystallization behavior under varying RH conditions.

Modeled versus experimental salt mixture behavior

The following text is primarily based on the work originally published as: Godts, S., Steiger, M., Stahlbuhk, A., Orr, S.A., Desarnaud, J., De Clercq, H., Cnudde, V., De Kock, T., 2024. Modeled versus experimental salt mixture behavior under variable humidity. ACS Omega. 10.1021/acsomega.4c01486.

The ECOS/Runsalt (Price, 2000; Bionda, 2005a) model is used to calculate the crystallization behavior of four different mixture compositions (Table 0-3). Two different compositions are selected per mixture type based on their frequency of occurrence. The outputs of the model are investigated to determine the crystallization behavior of salt mixtures under changing RH between 15 and 95% at 20 °C. The results are compiled from several outputs of the model, stitching together 5% RH ranges to achieve 0.1% RH resolution. Input details, terminology, limitations, issues, and solutions for the model are taken into consideration.

Table 0-3 Initial mixture composition (mol·kg^{-1}). Each mixture is given a sample name corresponding to either Type 1 mixture (sulfate-rich) = T1, or Type 2 mixture (calcium-rich) = T2, while subscripts $_{V}$ and $_{VI}$ refer to five or six ions.

	Cl^-	NO_3^-	SO_4^{2-}	Na^+	K^+	Mg^{2+}	Ca^{2+}
mix T1$_V$	1.0	1.0	1.0	2.0	2.0	0.0	0.0
mix T1$_{VI}$	1.0	2.0	1.0	2.0	1.0	1.0	0.0
mix T2$_V$	1.9	4.7	0.0	1.9	1.9	0.0	1.4
mix T2$_{VI}$	2.2	3.8	0.0	1.1	1.1	1.1	0.8

The model outputs show solids that can crystallize from the solution. For example, at a given RH the amount of crystalline solids is indicated. Because a limited number of independent variations of coexisting phases in a system are possible, generally known as the phase rule, a maximum of four and five solids can coexist at a given temperature (T) and relative humidity (RH) within the five and six ion mixtures. The salts under investigation in this section were:

- aphthitalite ($Na_2SO_4 \cdot 3K_2SO_4$)
- thenardite ($NaSO_4$)
- mirabilite ($NaSO_4 \cdot 10H_2O$)
- darapskite ($NaNO_3 \cdot Na_2SO_4 \cdot H_2O$)
- nitratine ($NaNO_3$)
- halite (NaCl)
- niter (KNO_3)
- bloedite ($Na_2SO_4 \cdot MgSO_4 \cdot 4H_2O$)
- magnesium sulfate hydrates ($MgSO_4 \cdot xH_2O$)
- nitromagnesite ($Mg(NO_3)_2 \cdot 6H_2O$)
- carnallite ($KCl \cdot MgCl_2 \cdot 6H_2O$)
- sylvite (KCl)
- bischofite ($MgCl_2 \cdot 6H_2O$)
- hydrated calcium nitrate $Ca(NO_3)_2 \cdot xH_2O$.

This analysis excludes the double salts $Ca(NO_3)_2{\cdot}KNO_3{\cdot}3H_2O$ (R. Flatt & Bocherens, 1962) and $Ca_2Cl_2{\cdot}Ca(NO_3)_2{\cdot}4H_2O$ (Ehret, 1932) as these solids are currently not considered in the model.

Experimental mixture composition

The experiments were carried out with the solutions presented in Table 0-3, further defined as mixtures $T1_V$, $T1_{VI}$, $T2_V$ and $T2_{VI}$. Solutions were prepared with analytical grade salts (Merck KGaA, EMSURE) below the saturation degree to allow complete dissolution, the mixtures are considered to be saturated with respect to aphthitalite ($T1_V$), epsomite ($T1_{VI}$), and niter ($T2_V$ and $T2_{VI}$) at 20 °C.

Time-lapse micrographs under rapid changing RH

Dissolution and crystallization times were captured using time-lapse micrographs from a 3D-digital microscope (HIROX) with the following settings: 100× to 200× magnification, lens MXG-2500REZ, KH-8700, a diameter of 2079.49 µm field of view, and 1.30 µm spatial resolution. It is important to note that while the resolution of the micrographs impacts the granularity of the obtained data, the research prioritizes understanding the overall crystallization timeline over the exact moment of nucleation, due to the study's focus on the decay of porous materials. The need for pore filling in such decay processes makes the specific timing of nucleation less important. Instead, the study concentrates on the delay and duration of complete crystallization, offering insights into the decay processes of porous materials, where the completion time of crystallization is more relevant to assessing the environmental impact. The processes were monitored in a windowed climate chamber with a 0.2 L/min constant gas flow of nitrogen with controlled RH (GenRH/Mcell, with a rotronic HC2-IC 102 high temperature industrial humidity probe, accuracy: ±0.8% RH). Micrograph intervals of 2, 5, 30, or 60 seconds were chosen based on observed phase transitions in initial runs. All tests were conducted at a lab temperature of 20 °C (±1) and 15 to 95 % RH. Solid phases were examined using a portable Raman spectrometer (Renishaw, Virsa) at specific RH levels where crystals became visible. After 3 months of conditioning at 15% RH and 20 °C, micro-Raman spectroscopy (Renishaw InVia) was performed for further verification.

For both methods, Raman spectra were obtained using a 785 nm, 100-400 mW near-infrared diode laser and a long-distance objective at magnifications of 5×, 20×, or 50×. A 10 s exposure time and 100-2000 cm^{-1} measurement range were sufficient for identifiable spectra against an in-house reference library (see 'Data records'). Lastly, X-ray diffraction (XRD) analysis (Bruker D8 in theta/2theta configuration) was performed on the dried samples after the same 3-month conditioning period. In each experiment, six 0.5 µL droplets of solution (per mixture: $T1_V$, $T1_{VI}$, $T2_V$ and $T2_{VI}$) were placed on an 18 mm × 18 mm glass slide within the windowed climate chamber. The droplets were initially conditioned at 95% RH and then dried at 15% RH, with each step lasting one hour. Following this preconditioning the droplets were subjected to RH cycles returning to either 95 or 15% RH after each intermediate step *x* (1 h) (Fig. 0.6).

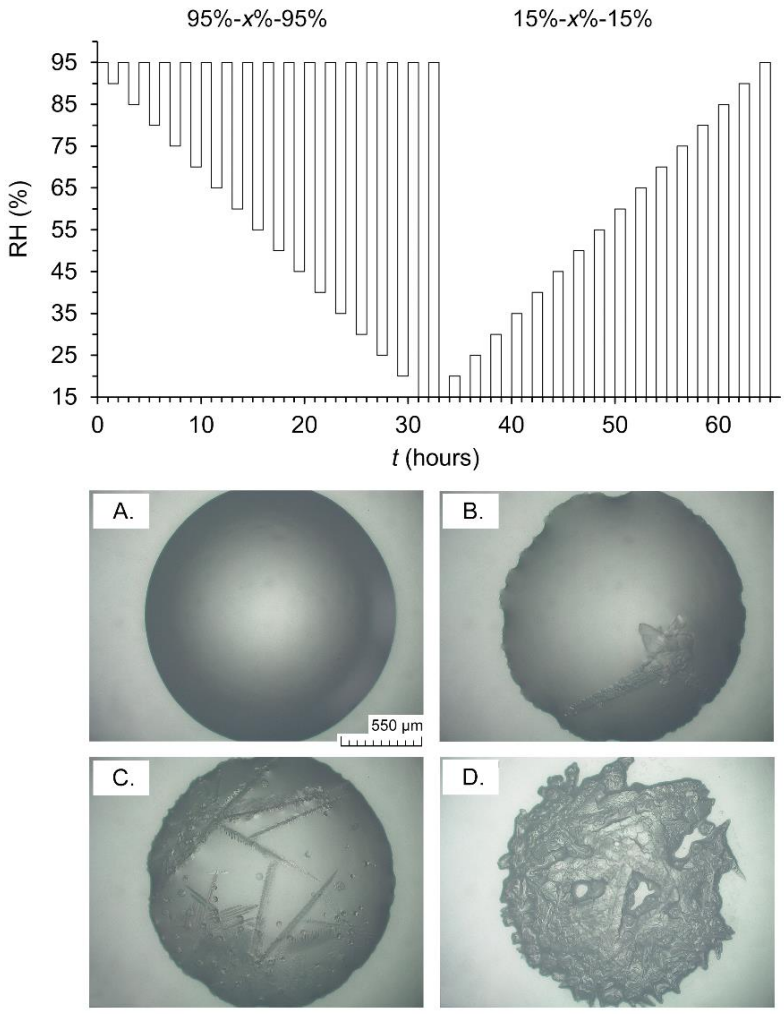

Fig. 0.6 Top: Relative humidity cycles to explore crystallization and dissolution of salt mixtures ($T1_V$, $T1_{VI}$, $T2_V$, $T2_{VI}$) using time-lapse micrographs in a climate chamber. Bottom: Images A-D illustrate micrographs (0.5 µL initial vol.) of a $T2_{VI}$ droplet at 95% RH and its crystallization, respectively, at 30%, 20%, and 15% RH, at 20 °C. The micrographs quantify visible crystallization and dissolution times at different RH levels.

The mean rate of RH change was derived from the calculated slopes of the obtained data points. For rapid RH changes, the mean slope is approximately 0.6% RH s^{-1}. A full procedure of one mixture includes up to 24,000 micrographs to identify the exact moment when visible crystallization occurs, how long the process takes, and vice versa the time for completed dissolution at a given RH. Specifically, the experimental procedure is as follows:

- For the cycles starting at 95%, the pattern is 95%-*x*%-95%, where *x* decreases from 90 to 15% RH in 5% steps. *x* = 90, 85, 80, 75, 70, and so forth until 15%.
- For the cycles starting at 15%, the pattern is 15%-*x*%-15%, where *x* increases from 20% to 95% RH in 5% steps. *x* = 20, 25, 30, 35, 40, and so forth until 95%.

The experimental series reaches a total of 66 steps: thus, a duration of 66 h per mixture type. RH and T were logged every 2 seconds in the climate chamber near the droplets. The experimental method involves identifying kinetic properties and deviations concerning the crystallization or dissolution RH and times (see below), which are correlated to the mutual crystallization or dissolution relative humidity for each solid as calculated (ECOS/Runsalt).

Vapor sorption under slowly changing RH

Sorption and desorption isotherms of the four mixtures were determined via dynamic vapor sorption measurements (SPSx-1 µ high load, ProUmid, SPS: sorption testing system, 1 µg resolution). All isotherms were recorded at 20 °C between 15 and 95% RH for sorption and desorption. For each run, 20 µL droplets of the mixed solution were placed in an aluminum sample pan of the SPS autosampler. To ensure reliability, data from four runs per mixture type were averaged to obtain mean values and standard deviations were calculated to assess the variability among replicates. The sample mass was recorded at 15 min intervals. Equilibrium conditions are met by performing a linear regression on net weights observed over the time period. The equilibrium gradient, determined by the slope of the regression line is considered achieved if it falls within the specified limit, defined as change in mass of less than 0.01% per 40 min. The initial conditions were set to 40 °C and 15% RH to ensure a stable mass, reaching a mean equilibrium time for all mixtures of 2.8 h (standard deviation (SD) = 0.01 h), followed by the experiments carried out at 20 °C and RH steps of 2% each maintained for a maximum of 6 hours or until equilibrium conditions were met. The mean experimental time of the latter was 159 h (SD = 5 h) for the sorption phase (15 to 95% RH) and 171 h (SD = 3 h) for desorption (95 to 15% RH), reaching a total experimental time of 330 h (SD = 8 h). Thus, the mean rate of change is approximately 0.5% h^{-1}. Besides a general investigation of the hysteresis between sorption and desorption curves, the first derivative of the individual curves is calculated to identify RH points of interest where crystallization and dissolution occur.

Raman spectra and imaging were conducted separately during the experiments, with each method being performed in two separate runs out of the four total. Images were obtained at each RH step with a 50 mm lens and CMOS sensor (11.3 mm × 11.3 mm, 2046 × 2046 pixel resolution, 5.5 × 5.5 µm pixel size). A Wasatch Photonics WP 785 (nm laser) was used to obtain Raman spectra at approximately each 5% RH step, with the following parameters: laser power 450 mW (100% intensity), wavelength resolution 7 cm^{-1}, 200 ms integration time, 2 scan average, 1 pixel boxcar smoothing, 270-2000 cm^{-1} spectral range, working distance 50 mm.

An additional experimental run was conducted, which included imaging, under slower conditions compared with previous runs. The primary difference in this run was that it was performed with two samples for each mixture type. RH steps of 2% were maintained for a maximum of 50 h or until equilibrium conditions were met. On average, the sorption phase (from 5 to 93% RH) took 885 h, while the desorption phase (from 91 to 5% RH) took 789 h. The total experimental duration amounted to 1674 hours. Consequently, the average rate of change in relative humidity was approximately 0.1% h^{-1}.

Time steps considered to identify processes

The effective crystallization and dissolution times observed by microscopy were recorded under rapid and slowly changing RH. As illustrated in Fig. 0.7 we consider:

- t_1 = the start time of the experiment until the first mutual crystallization or dissolution RH is reached, as modeled by ECOS/Runsalt. Thus, approximately 0.6% s^{-1} for rapid (GenRH) and 0.5% and 0.1 h^{-1} for slow RH changes (SPS).
- t_2 = from the end of t_1 until the first visible crystal or dissolution, which is considered as the induction time.
- t_3 = the time from the end of t_2 until complete visible crystallization or dissolution, hence the effective crystallization/dissolution time.
- t_4 = from the end of t_1 to the end of t_3, the induction time plus completed crystallization/dissolution, thus equal to $t_2 + t_3$.

- t_{exp} = the total experimental time from the start of t_1 until complete visible crystallization or dissolution (end of t_3). This can be less or exceed the experimental cycle time (1 h for rapid and maximum 6 h and 50 h for slow changing RH)

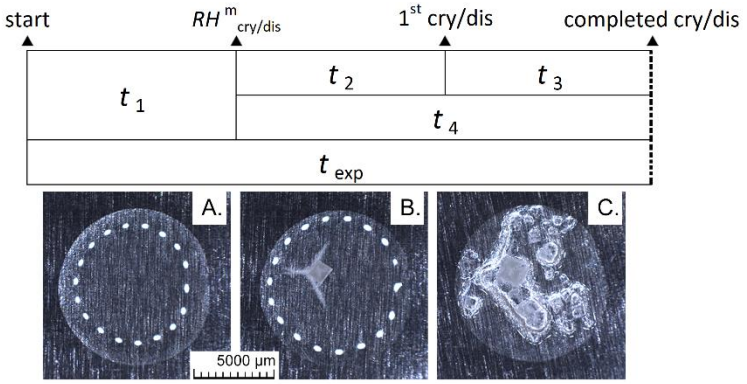

Fig. 0.7 The table on the top illustrates the time intervals of the experiments. t_1 : from start of the RH step to first mutual (m) crystallization (cry) or dissolution (dis) RH target (as defined by the modeled behavior, ECOS/Runsalt), t_2 : from the end of t_1 until first visible crystal or dissolution (1st cry/dis), t_3 : from the end of t_2 until complete visible crystallization or dissolution (completed cry/dis); t_4 : $t_2 + t_3$, t_{exp} : start of t_1 until the end of t_3, thus the total experimental time for each RH step. Figures A, B, and C display images acquired throughout the SPS experiments (initial volume 20 µL), illustrating a salt solution droplet ($T2_V$) at 63% RH, initial crystallized salts at 49% RH and completed crystallization at 15% RH and 20 °C, respectively. The white dots in figures A and B are the result of light reflection.

Investigating crystal habit

Environmental Scanning Electron Microscopy combined with Energy Dispersive X-ray Spectroscopy (ESEM-EDX) was performed for all four mixtures (EVO system from Carl Zeiss Microscopy GmbH). The method aims to compare the crystal habit and elemental variations in salt mixtures after undergoing both rapid and slow (evaporation) crystallization. To ensure stable imaging and video capture at higher RH levels the Peltier stage temperature was set to 5 °C, allowing higher vacuum. Key experimental parameters included an accelerating voltage (Extra High Tension, EHT) at 20.00 kV, a LaB6 (Lanthanum Hexaboride) cathode filament, and the use of an NTS BSD detector (Nano Technology Systems BackScattered).

4. SCIENTIFIC RESULTS AND RECOMMENDATIONS

Analysis of salt mixtures: charge balance calculations

The following text is primarily based on the work originally published as: Godts, S., Steiger, M., Orr, S.A., De Kock, T., Desarnaud, J., De Clercq, H., Cnudde, V., 2022. Charge balance calculations for mixed salt systems applied to a large dataset from the built environment. Sci Data 9, 324. 10.1038/s41597-022-01445-9.

The charge balance of all 11412 samples is illustrated in Fig. 0.1. As a result of the charge balance calculations applied to the large dataset several important considerations can be derived for the further consideration of ion mixtures. The processed data is evaluated and shows that after the applied adjustments three samples contain zero ions, leaving the dataset with 11409 samples.

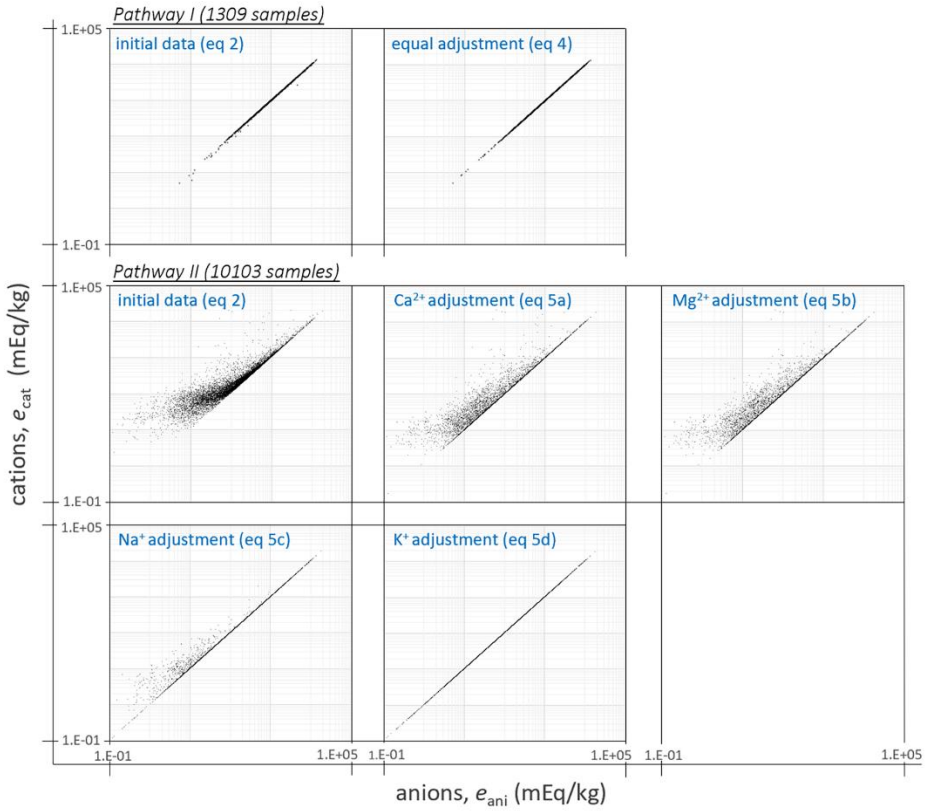

Fig. 0.1 Charge balance sequence in logscale with all anions on the *x*-axis and all cations on the *y*-axis (mEq/kg). Top left: initial data (Eq. 2) of samples following pathway I (1309 samples), top right: equal adjustment of all ions (Eq. 4). Middle left: initial data (Eq. 2) of samples following pathway II (10103 samples): middle center: after calcium adjustment (Eq. 5a), middle right: after magnesium adjustment (Eq. 5b), bottom left: after sodium adjustment (Eq. 5c), and bottom right: after potassium adjustment (Eq. 5d).

After charge balance is achieved the gypsum content is determined and removed. The removal of equimolar contents of calcium and sulfate follows the assumption that gypsum is mostly present in crystalline form, which is required for the input data of ECOS/Runsalt. Therefore, it is reasonable to assess the balance between both ions (after Eq. 4 and Eq. 5), as illustrated in Fig. 0.2. All sulfate and calcium ions not balanced, respectively right and left in the figure, are not related to gypsum and belong to different mixture types. Each salt mixture includes either remaining calcium or sulfate ions. This results in two types of mixture compositions typically found in the built environment, as described

in Brimblecombe (2003) and Steiger et al. (2014), and validates the charge balance procedure applied to the dataset. Details on the mixture types, the distribution and their behavior are explored further.

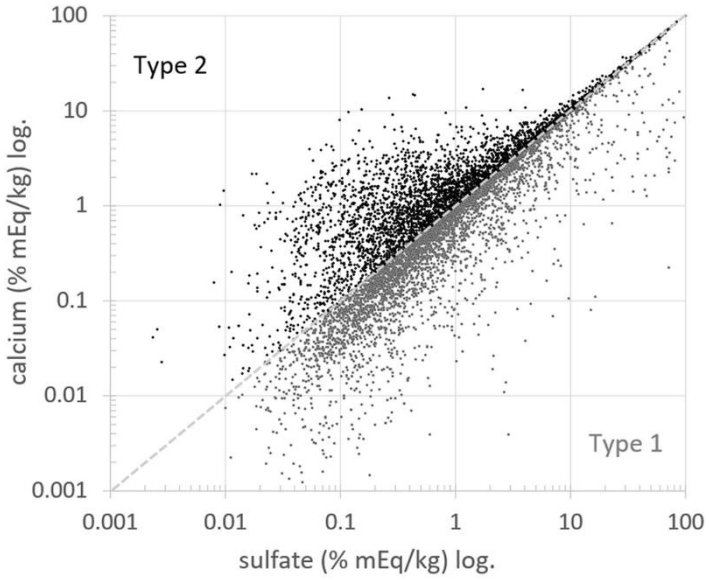

Fig. 0.2 Representation of the ion balance between calcium and sulfate after Eq. 4 and Eq. 5 (% mEq/kg in logscale, as a percentage of the maximum ion content within the dataset per mixture type). Samples including sulfate ions on the *x*-axis (Type 1: 7946 samples) and samples including calcium ions on the *y*-axis (Type 2: 3463 samples), all calcium and sulfate ions that fall together on the dashed diagonal line are equimolar contents of calcium and sulfate, thus the theoretical gypsum content, as determined and removed in Eq. 6 and Eq. 7.

Type 1) Mixtures including an excess of SO_4^{2-} ions, with respect to gypsum removal (70% of samples)
Type 2) Mixtures including an excess of Ca^{2+} ions, with respect to gypsum removal (30% of samples)

With the adjusted results in Eq/kg and after the removal of the theoretical gypsum content (Eq. 7) an overview is given of the individual ion content in all samples per mixture type (Fig. 0.3). In mixtures that are part of Type 1 the systems are primarily dominated by sodium and sulfate, followed by potassium and in lesser contents nitrate and chloride ions. The ion ratio in this mixture Type 1 is typically less hygroscopic. While in mixtures part of Type 2 tend to be more hygroscopic, and are dominated by nitrate, sodium, and chloride, followed by calcium and smaller amounts of potassium ions. Magnesium is in both mixture types the least common ion. The ions that dominate the mixture will significantly influence the mutual crystallization and deliquescence relative humidity, thus the analysis validates the rank of the most important ions that occur in the built environment (Steiger et al., 2014).

Another important aspect derived from the results is the overall ion content in the two mixture types. With the total salt content (excluding gypsum) translated to weight percent compared to the dry sample mass, the content is 0.9 and 1.1 wt.% for mixture Type 1 and 2, respectively. Seen that the majority of samples are taken in areas where salt damage or chromatic alteration (Vergès-Belmin, 2008) (specifically, moisture stains) are visible a generalized assumption can be made: a total salt content of 1 wt.% (±0.1), excluding gypsum, can be considered a limit value in common building materials, to be further defined. Nevertheless, to avoid misinterpretation after the applied adjustments, and to complete the validation, as per (Brimblecombe, 2003; Steiger et al., 2014), the applied adjustments need to be evaluated further to identify a third mixture composition of interest:

Type 3) Mixtures containing carbonates (relative within 3% of samples in Type 1)

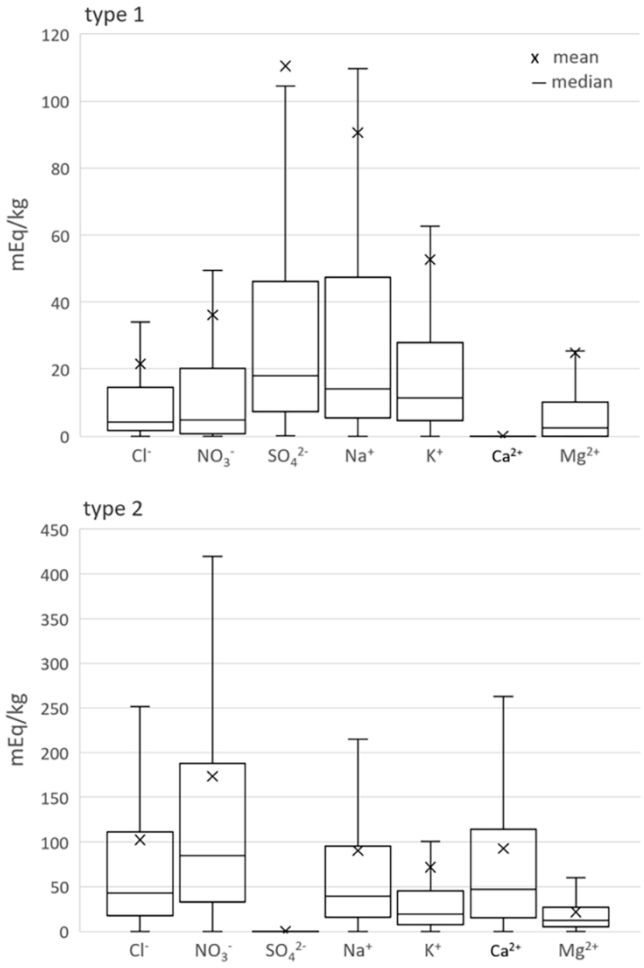

Fig. 0.3 Representation of the most important ions per mixture type derived from the dataset. Left: Type 1 mixtures (7946 samples), right: Type 2 mixtures (3463 samples). Ion content of all samples (mEq/kg) derived from the results after eq 7 (excluding equimolar contents of Ca^{2+} and SO_4^{2-}). Boxplots: bottom 25% top 75%, not showing outliers (x 1.5 quartile range).

Naturally carbonate-rich mixtures within Type 2 (including calcium) are excluded after the applied adjustments under Eq. 5a, because of the assumption that calcium carbonates will rapidly crystallize from the system due to low solubility. Furthermore, the amount of dissolved calcium carbonates in the solution is depended on the time, and ratio between the amount of pure water added to the dry sample mass to dissolve salts, thus the result will be subject to the individual methodological approach. To avoid error on this front and for completeness of the evaluation, the adjustment of calcium (Eq. 5a) was additionally checked for each sample by evaluating the solubility limit of calcium hydroxide within the specific analytical procedure. Here the solubility of calcium hydroxide instead of calcium carbonate is considered as it is likely that uncarbonated lime is available in the depth of historical lime mortars or recent cement. Accordingly, the theoretical assumption where calcium hydroxide surpassed the solubility limit, was only seen in 0.04% of the samples. In view of the sample size this can be considered a measurement error or the presence of other undetected anions, no further evaluation was carried out at this time.

In the case zero is reached after the adjustment of potassium (Eq. 5d) the sample can be disregarded as no ions are left, excluding perhaps gypsum. This situation occurred for three samples in the entire dataset. Furthermore, the excess contents of calcium, magnesium, sodium, and potassium (Δe_{Ca}, Δe_{Mg}, Δe_{Na}, and Δe_{K} respectively) can be used to calculate a theoretical carbonate content. To allow a proper interpretation of the mixture composition (presented above as mixture types 1, 2 or 3) and to avoid misinterpretation of the total system composition, the degree of each adjustment is calculated to a fraction of the initial cation sum by:

$$f_{\Delta e} = \frac{e_i - e_{i,\mathrm{adj}}}{e_{\mathrm{cat}}} \tag{9}$$

where $f_{\Delta e}$ is the amount of substance in excess as a fraction (for calcium, magnesium, sodium, and potassium) compared to the initial sum of cations (before adjustments), e_i is the initial single cation content, $e_{i,\mathrm{adj}}$ is the adjusted single cation content derived from Eq. 5 and e_{cat} the initial sum of cations (Eq. 2).

From the result of Eq. 9 and the number of samples for which the ions are equally adjusted (Eq. 4), an overview of the applied corrections can be given (Table 0-1). With 11.5% of all samples corrected equally (pathway I), while for pathway II calcium was corrected in the majority of samples (88.4%), followed by sodium (17.9%) and less common a correction for magnesium 11.8% and potassium 4.8%. All four cations required correction in 2.1% of the samples.

Table 0-1 Overview of applied adjustments, number and percentage of samples adjusted (total number of samples 11409) following Pathway I (equal adjustment of all ions, Eq. 4) and Pathway II (adjustment of calcium, magnesium, sodium, and/or potassium, Eq. 5)

	Pathway I	**Pathway II**			
Sample size 11409	**Eq. 4** all ions	**Eq. 5a** Ca^{2+}	**Eq. 5b** Mg^{2+}	**Eq. 5c** Na^{+}	**Eq. 5d** K^{+}
Adjustments applied per sample	1309 (11.5%)	10085 (88.4%)	1351 (11.8%)	2044 (17.9%)	552 (4.8%)
	/	1336 (11.7%)		/	
	/	917 (8.0%)			/
	/	234 (2.1%)			

Table 0-1 presents how often corrections are applicable and specifies the presence of undetected anions in the system. However, the importance of these adjustments in view of the total salt content compared to the sample mass is yet to be determined. The quantity of ions corrected in the mass of the individual sample is equally important to evaluate the probable effect on the mixture composition/behavior. To rank this probable effect, the adjusted ion values are calculated from Eq/kg back to weight fraction and the latter is then compared to the initial ion content.

$$w_{i,\mathrm{f}} = \frac{e_{i,\mathrm{adj}} \cdot M}{|z_i|} \tag{10}$$

where $w_{i,\mathrm{f}}$ is the final corrected amount of substance as weight fraction per individual ion in the dry sample mass, $e_{i,\mathrm{adj}}$ is the (adjusted) concentration of the ion (Eq/kg), M the molar mass (kg/mol) z_i its absolute charge. The results give a more representative indication of the ions corrected in view of the salt content compared to the sample mass. Fig. 0.4 shows the adjusted content of each ion and the total amount after the charge balance calculations.

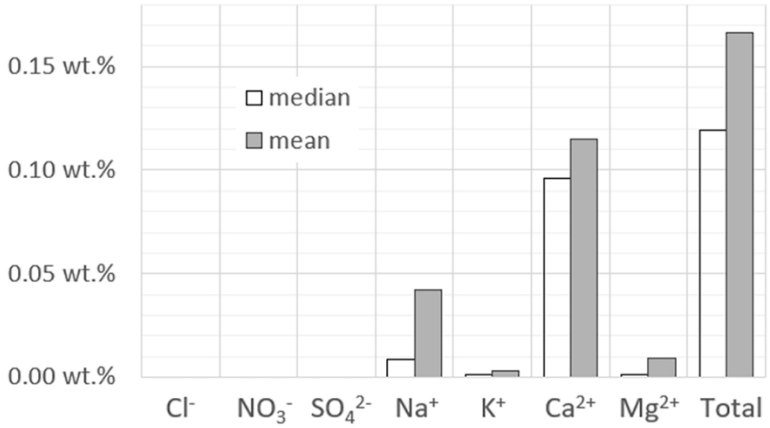

Fig. 0.4 Representation of the adjusted content per ion and the total in wt.% compared to the dry sample mass. Median and mean values of the difference between the initial ion content and the corrected ion content of all 11412 samples are shown.

The adjustments carried out following pathway I are insignificant, which is clearly illustrated by the indistinguishable anion content adjusted at this scale, that is, for the given dataset. After pathway II the adjustments are more important, with calcium being the most adjusted ion at almost 0.1 wt.% (median), followed by sodium at 0.01 (median) and less significant amounts of magnesium and potassium are adjusted. The valuation specifies the limited changes to the systems, yet they are crucial for individual evaluation of sample composition, statistics, and modeling purposes. The individual sample evaluations are described further.

As mentioned earlier the gypsum content plays an important role in the deterioration of building materials yet is considered to have limited influence on the mixture behavior and is thus removed for modeling purposes. However, it remains crucial when giving advice to the field, therefore the theoretical gypsum content is presented separately as weight fraction ($w_{\mathrm{CaSO_4}}$) derived from Eq. 10. In the dataset (11409 samples) the median gypsum content is 0.3 wt.%, while the mean gypsum content is 1.8 wt.%, and excluding 0 the content is 2.6 wt.% (with a standard deviation of 6.3), the latter considering 8100 samples. In view of the determined gypsum content, it is clearly an important salt in building materials which in turn can overshadow more soluble salts.

After the determination of gypsum, the total ion content adjusted ($w_{tot,\mathrm{adj}}$) as a fraction compared to the dry sample mass, excluding gypsum, gives us an overview of the total amount of adjustments applied. The extent of these corrections should be carefully interpreted when compared to visual deterioration patterns *in-situ*. The following equation returns the content of adjustments applied to determine their overall significance compared to the initial ion content:

$$w_{tot,\mathrm{adj}} = \sum_{k=1}^{n} (w_i - e_{i,\mathrm{f}}) - w_{\mathrm{CaSO_4}} \tag{11}$$

The results correspondingly give an indication of how important the theoretical carbonate content in each sample might be. This is further detailed by calculating the content of corrected Ca^{2+} ions and separately the sum of Na^+ and K^+ ions. This allows a better understanding of the less relevant calcium ions likely associated with carbonates and the more relevant magnesium, sodium or potassium ions associated with carbonates in the system. However, it is currently not possible to give a limit value for this assessment. Especially due to the absence of experimental data involving different salt mixture compositions including carbonates to assess the crystallization behavior and damage potential to porous materials. Therefore, an assumption is made based on field experience, i.e., in cases where an excess of cations (excluding calcium) is detected from 0.6 wt.% upwards, carbonate salts such as trona, are regularly detected by XRD-analysis in the efflorescence. In view of this limit value, and possible solids related to carbonates relevant in the pore solution, the calculated number of samples that include ≥0.6 wt.% adjusted sodium, and potassium (sum) is only 1.2% of all samples or 1.8% of all samples in Type 1. When considering a lower threshold ≥ 0.3 wt.%, the number of samples containing possible carbonate salts of importance increases to 2.5 and 3.6%, respectively. This shows the limited importance of soluble carbonate salts in the presented data.

However, these salt mixtures (samples) should be treated with caution when applying the charge balance corrections and attempting to model the crystallization behavior. The same applies to samples for which the total anion content exceeds the total cation content as described earlier in the section ‘charge balance calculations under pathway 1. In the entire dataset we found that the anion content was in surplus for 41 samples, here Eq. 4 was carried out when criterion Ib was met, for 6 of these sample an excessive correction is observed when evaluating the contribution of the anions in excess to the total charge imbalance. Thus, within the entire dataset not so relevant at 0.05% of all samples, yet crucial for individual evaluation of a salt mixture in a single sample. The full integrated database and charge balance calculation sheet, including raw ion concentrations and balanced outputs are available at (Godts et al., 2022b).

The described charge balance calculations applied to the ion data from 11412 samples follow two main pathways based on the charge imbalance. When an analytical uncertainty is probable, pathway 1 results in an equally adjustment of all ions, which was applicable to approximately one tenth of all samples. When the analytical uncertainty is passed the calculation follow pathway 2 assuming that the measured imbalance is related to undetected anions. Accordingly, cations in surplus are identified in sequence of the solubility of the related solids associated with carbonates. Here, when applicable the initial adjustments correct calcium and magnesium in excess, which are dissolved by the extraction procedure. The following adjustments are carried out for any access related to sodium and potassium. Each of the above ions until charge balance is reached. When using the data and calculations it remains important to understand that the adjustments of sodium and potassium remain relevant within the system behavior. Therefore, when using the dataset, the validation and evaluation remain relevant in all cases. In the dataset presented, calcium is naturally the most corrected cation, while sodium is the next most common ion adjusted, followed by the less common adjustments needed for potassium and magnesium.

For modeling purposes, the output data as mole fraction is represented after removal of the theoretical gypsum, if gypsum is required the calculation needs to be adjusted. However, the current method allows the identification of each sample within common mixture types found in the built environment. Type 1 mixtures included remaining sulfate and zero calcium ions. This type contains

higher amounts of sodium and sulfate, which renders the mixtures less hygroscopic, other important ions, are potassium and nitrate, followed by lesser contents of chloride and magnesium. Type 2 mixtures with remaining calcium and zero sulfate ions are more hygroscopic mixtures containing considerable amounts of nitrate followed by sodium, chloride, calcium, and lesser contents potassium and magnesium. A third type can be classified as a sub-type within approximately 3% of Type 1 mixtures. This sub-type includes carbonates and is only identified by evaluating the content of corrected cations. The identification of this type is important to avoid misinterpretation of the mixture composition and is most relevant when an access of sodium is found, that is, within the given dataset.

Here, the evaluation method is important as it allows the final comparison between the initial ion content with the corrected values, thus the user can assess the adjustments made in the mixture composition in relation to the mass of the material under investigation. The results of this evaluation show quantitatively the corrections applied to the individual ions, identifying when primarily sodium and potassium are adjusted and caution is necessary. The data as mole fraction can be used as direct input for modeling the crystallization behavior under changing climatic conditions without the need for ambiguous corrections.

Modeling salt behavior

The following text is primarily based on the work originally published as: Godts, S., Steiger, M., Orr, S.A., Stahlbuhk, A., Desarnaud, J., De Clercq, H., Cnudde, V., De Kock, T., 2022. Modeling Salt Behavior with ECOS/RUNSALT: Terminology, Methodology, Limitations, and Solutions. Heritage, 5, 3648-3663. 10.3390/heritage5040190.

Comparable to any model, ECOS/RUNSALT has limitations and pitfalls. An important obstacle in the calculations is caused when there are extremely high concentrations or supersaturation in hygroscopic mixtures, including calcium nitrate and calcium chloride, resulting in water activities higher than expected from thermodynamics. This obstacle was overcome by the incorporation of certain assumptions and non-verified solids, such as $MgCa(NO_3)_4 \cdot 10H_2O$, which rarely appears in the outputs. However, it is yet unclear whether extreme hygroscopic solids crystallize in these conditions.

Concerning the input data, an issue occurs with the autobalance option in RUNSALT, a simplified calculation method to reach charge balance. When using theoretical charge input data with integer numbers (e.g., $1Cl^-$ and $1Na^+$), the autobalance works correctly. However, with experimental output of ion analyses, values with several decimal places are common and the autobalance only corrects the chloride content, rendering the output incorrect. It is thus recommended to abstain from using the 'autobalance' feature and consider the use of charge balance calculations, including the downloadable calculation sheet and R script (.R and .xlsx) at (Godts et al., 2022b). Furthermore, an error message can occur due to rounding issues produced by the thermodynamic calculations, which is caused by the number of decimals of each ion value entered. This can be resolved by changing the place values of all ions equally to ones, tens, hundreds, or thousands, depending on the initial concentration; although the total amount on the *y*-axis (mol or volume) varies, the output remains identical.

In certain cases, an error message appears when either entering the full RH range from 15 to 98% as input in the environmental parameters, or under certain temperatures, depending on the mixture composition. Both errors are easily overcome by limiting the RH to 95% or increasing or decreasing the temperature by one to five degrees. In either case, the results obtained from the model for the limitations of output values are considered more than sufficient. Another issue in the environmental parameters is the possibility to use values below 0 °C, although the formation of ice is not incorporated in the outputs. It is thus advised not to use a temperature input values below 0 °C in Runsalt.

Moving forward to complications specifically related to single salts in the ECOS calculations and Runsalt outputs, inconsistencies are seen with more recent studies related to $Ca(NO_3)_2$, K_2SO_4, and $MgSO_4$ hydrates (Steiger et al., 2011). The critical RH values calculated by the ECOS of $Ca(NO_3)_2$, K_2SO_4, and $MgSO_4$ are presented in the Runsalt output in Fig. 0.5 and Fig. 0.6, respectively. The crystallization behaviors of Ca^{2+} and NO_3^- show two critical RH values (Fig. 0.5, top), the first at 51.82% for tetrahydrate (nitrocalcite) and the second at 37.98% for anhydrous calcium nitrate (at 20 °C, RH resolution = 0.02%; resolution not represented in the figure). However, it is known that dehydration of the tetrahydrate only occurs over extended periods of time and at extreme low RH with transition values between the anhydrous di-, tri-, and tetrahydrate at 8.3%, 12.4%, and 20.5%, respectively (Steiger, 2011). Thus, considering that the dehydration of nitrocalcite is kinetically hindered, one can expect that the crystallization RH of the tetrahydrate is the only one to be considered, keeping in mind that more research is needed to understand the in-pore effects under realistic climatic conditions.

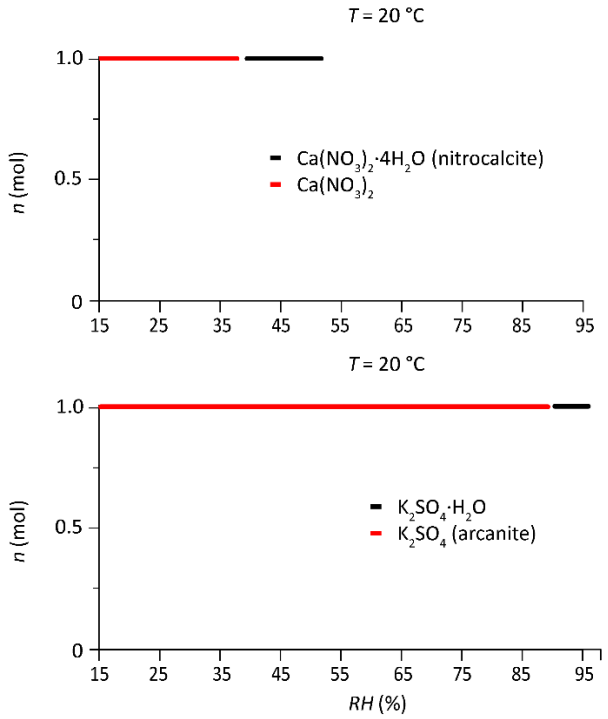

Fig. 0.5 ECOS/Runsalt outputs, 1 mol Ca^{2+} and 2 mol NO_3^- (top), and 2 mol K^+ and 1 mol SO_4^{2-} (bottom). Calculated at 20 °C for RH ranging from 15% to 95% or to 98% (bottom) (resolution 1.6% RH), with the latter on the *x*-axis and the amount of crystalline salt, *n* (mol), on the *y*-axis.

The Runsalt outputs of K^+ and SO_4^{2-} (calculated at 20 °C) show two critical RH values (Fig. 0.5, bottom) with a relative humidity crystallization of potassium sulfate monohydrate starting at 97.7%, followed by dehydration to form arcanite at 89.7%. However, as detailed further by Archer and Kirklin (2002), it has been found in several studies that the monohydrate phase does not occur below 9 °C, and if stable at all this is less probable at higher temperatures. Furthermore, the RH_{cry} should decrease with decreasing temperature; currently, the outputs show the opposite at lower temperatures, with a decreasing amount of the monohydrate (not illustrated). Thus, caution should be taken when looking at the critical RH values of potassium sulfate. Here, at 20 °C, K_2SO_4 is likely to start at 97.7% and the monohydrate can be ignored.

For magnesium sulfate (Fig. 0.6), four critical RH values are shown at 20 °C, starting with the crystallization relative humidity, $RH_{cry_{eps}}$ at 91.54% for $MgSO_4 \cdot 7H_2O$ (epsomite), followed by the

transition to $MgSO_4 \cdot 6H_2O$ (hexahydrite), $RH_{tra_{[eps\text{-}hex]}}$ at 81.94%, and to $MgSO_4 \cdot 4H_2O$ (starkeyite) and $MgSO_4 \cdot 1H_2O$ (kieserite), with $RH_{tra_{[hex\text{-}sta]}}$ and $RH_{tra_{[sta\text{-}kie]}}$ at 62.3% and 27.16%, respectively. However, from experimental results and improved thermodynamic calculations, see (Steiger et al., 2008, 2011), important deviations specifically concerning starkeyite are derived. The data shows that the values used in ECOS for this phase are inaccurate and no change in the mixtures from one to the other hydrate should be taken into consideration within the range of 5–40 °C. The original data from the ECOS/Runsalt outputs are shown in Fig. 0.6, while the corrected data are given in Fig. 0.7.

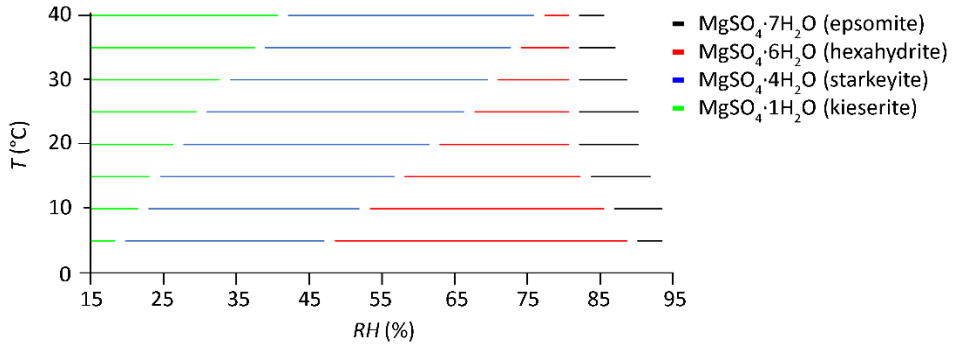

Fig. 0.6 Calculated $MgSO_4$ phases at different temperatures derived from ECOS/Runsalt plots (with equimolar contents of Mg^{2+} and SO_4^{2-}); relative humidity from 15 to 95% on the *x*-axis (resolution 1.6% RH) and temperature, temperature (°C) is on the *y*-axis

In Fig. 0.7, the RH_{del} of $MgSO_4 \cdot 7H_2O$ (epsomite) is 91.2% RH at 20 °C, with a transition to $MgSO_4 \cdot 1H_2O$ (kieserite) at 46.6% RH; the hexahydrate only occurs at higher temperatures. This figure illustrates how ECOS/Runsalt outputs with a wide RH range calculated in a variety of temperatures can correspond to the phase diagram, following the transition between kieserite, hexahydrite, and epsomite, and the RH_{del} at different temperatures. In addition to the described issues that should be considered in the model outputs, it remains important to understand that certain phases can be metastable and kinetically hindered, as further described for magnesium sulfates in Steiger et al. (2011).

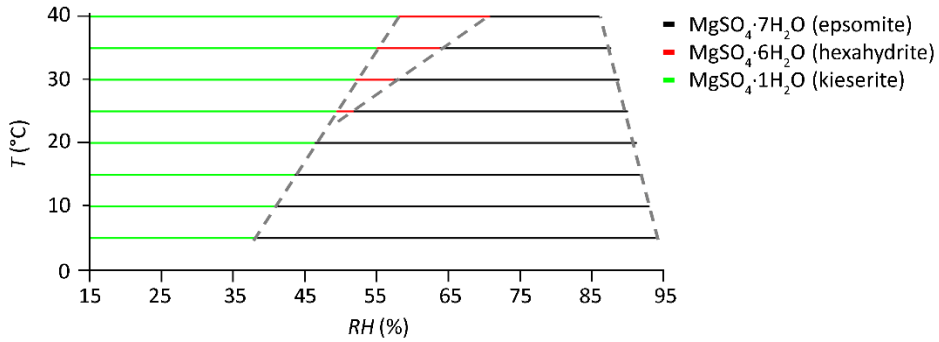

Fig. 0.7 Calculated and experimental $MgSO_4$ phases at different temperatures derived from Steiger et al. (2011) (the dashed lines correspond to data of the phase diagram); the relative humidity from 15 to 95% (resolution 1.6% RH) is on the *x*-axis, and temperature (°C) is on the *y*-axis

Several solids are missing in ECOS/Runsalt, although they can play a role in the crystallization pathways and deterioration processes, such as Ca-K-NO_3 double salts (R. Flatt & Bocherens, 1962). The

efflorescence found on monuments (Charola and Lewin, 1979; Arnold and Küng, 1985; Arnold and Zehnder, 1987; Von Konow, 2002; Bionda, 2006; Morillas et al., 2015; Siedel, 2018; Benavente et al., 2020) reveals salts that are currently not available or not consistently incorporated in the model outputs, for example, humberstonite ($Na_7K_3Mg_2(SO_4)_6(NO_3)_2{\cdot}6H_2O$).

Moreover, the removal of equimolar contents of calcium and sulfate (gypsum) can alter the Runsalt outputs, including double salts such as glauberite ($Na_2Ca(SO_4)_2$), gorgeyite ($K_2Ca_5(SO_4)_6{\cdot}H_2O$), and syngenite ($K_2Ca(SO_4)_2{\cdot}H_2O$). However, the formation of the latter three might be kinetically hindered or occur as solid-state reactions over longer periods of time.

As detailed in Godts et al. (2017), the model is not capable of systematically integrating the presence of an equimolar amount of calcium and sulfate ions. In rare cases, when the model allows calculations with calcium and sulfate, the crystallization pathway can change. In these cases, it is often observed that the common salt darapskite ($NaNO_3{\cdot}Na_2SO_4{\cdot}H_2O$) is replaced by glauberite ($Na_2SO_4{\cdot}CaSO_4$), as illustrated in Fig. 0.8. As mentioned earlier, several issues are visible in the plot on the right, such as the kinetically hindered solid-state phase change between gypsum and anhydrite. Additionally, due to the stacking of the solids and the RH resolution, the vertical lines for glauberite and nitratine should remain horizontal; thus, the latter is simply an artifact of the gap between the transition $RH^{m}_{tra_{[gyp\text{-}anh]}}$. Further research is needed to understand the formation of double salts containing calcium and sulfate.

Furthermore, relevant carbonate salts such as thermonatrite ($Na_2CO_3{\cdot}H_2O$), natron ($Na_2CO_3{\cdot}10H_2O$), trona ($Na_3CO_3HCO_3{\cdot}2H_2O$), and kalicinite ($KHCO_3$) are absent from the model outputs. However, these soluble carbonates are rare and only seen in approximately 2% of samples taken in Belgium heritage (Godts et al., 2022a). Other rare ions not included but contributing to the total charge balance and crystallization pathway are fluoride, phosphate, oxalate, acetate, ammonium, and formate (Steiger & Heritage, 2012).

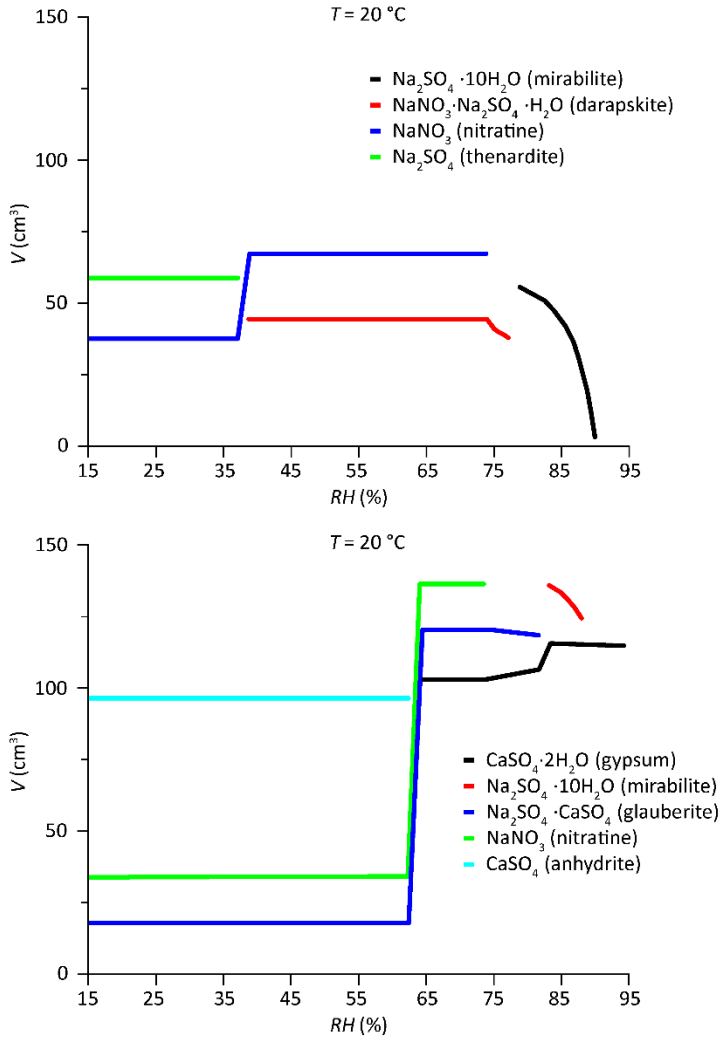

Fig. 0.8 ECOS/Runsalt outputs to illustrate the influence of Ca^{2+} and SO_4^{2-} (considered as the gypsum content) on the crystallization behavior of a salt mixture. Top: excluding equimolar contents of Ca^{2+} and SO_4^{2-}, input parameters in mol are Na^+: 1.8, Ca^{2+}: 0, NO_3^-: 1, and SO_4^{2-}: 0.4. Bottom: including equimolar contents of Ca^{2+} and SO_4^{2-}, thus Na^+: 1.8, Ca^{2+}: 3.6, NO_3^-: 1, and SO_4^{2-}: 4. Both outputs show the RH (%) on the *x*-axis and the amount of crystalline salt in volume, *V* (cm^3), on the *y*-axis.

ECOS/Runsalt is currently the only model that includes the most relevant salt phases found in built heritage. This section provides an overview to further the understanding of its use and to introduce specific terminology for salt mixture behavior. This to clarify the model, making scientific information comparable. Furthermore, as several limitations and pitfalls exist when using the model, possible incorrect interpretations of the derived outputs can occur. However, when the presented issues and solutions are taken into consideration, the Runsalt outputs can be considered accurate. The most important issues described concern calcium nitrate, potassium sulfate, and magnesium sulfate phases (hydrates), and the possible influence of calcium sulfate on the formation of different solids under specific conditions.

It also remains important to examine the variety of factors that can cause deviations from the modeled crystallization behavior. Some of these factors include the in-pore situation, the material characteristics, impurities in the system, and salt kinetics. The latter is specifically relevant to environmental conditions, the separation of solids from the solution, gradients in solution concentrations, kinetically hindered salt crystallization, and rates of crystallization/dissolution, including long-term solid-state (decomposition) reactions. In any case, if a specific range of RH is considered safe when interpreting Runsalt outputs, meaning salt crystallization/transition cycles are less likely to occur in the specific environment, the model outputs can be trusted, keeping in mind that different crystallization pathways are possible when certain salts are separated from the solution. Overall, there is a need for further research into salt mixture kinetics. An essential focus should be on understanding dissolution and crystallization times under realistic rates of relative humidity changes. Additionally, the modeled phases and RH point of interest need verification. Consequently, it becomes important to update the current model and enhance the accessibility of the source codes for future studies. However, before we can continue, it is crucial to identify relevant salt mixtures encountered in the context of stone weathering.

Identification of relevant salt mixtures

The following text is primarily based on the work originally published as: Godts, S., Orr, S.A., Steiger, M., Stahlbuhk, A., De Kock, T., Desarnaud, J., De Clercq. H., Cnudde, V., 2023. Salt mixtures in stone weathering. Sci Rep 13, 13306. 10.1038/s41598-023-40590-y.

338 sites have been investigated for a wide variety of salt-induced deterioration of porous building materials. Besides the salt mixture composition, the salt concentration was also indicative for decay, where sufficient pore filling occurred, and daily environmental conditions influence the substrate, further detailed by Flatt et al. (2014) and Godts et al. (2017). Thus, the first centimeters of the drying front of the substrate were of primary concern when evaluating the already induced deterioration, while the salt distribution at further depths allowed the understanding of salt transport properties over time and possible concerns for treatment methods. The frequency of samples taken from the first two centimeters of the substrates that include a total salt content ≥0.8 wt.% (including Cl^-, NO_3^-, Na^+, K^+, Mg^{2+}, and SO_4^{2-} or Ca^{2+}) are shown in Fig. 0.9. Additionally, the equimolar content of calcium and sulfate ($CaSO_4$), considered as the theoretical gypsum content ($CaSO_4 \cdot 2H_2O$), as a function of the two mixture types of interest is included in the figure.

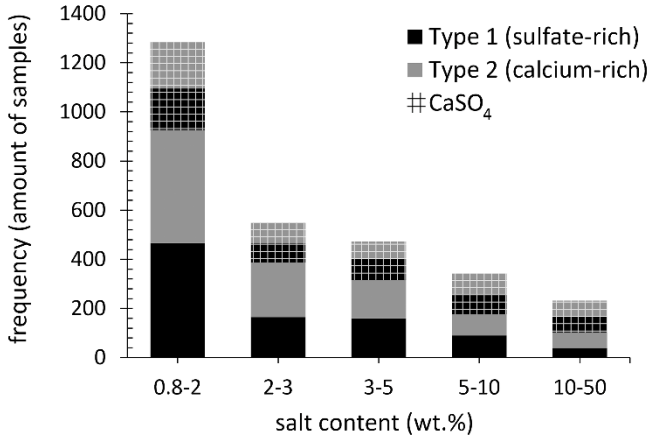

Fig. 0.9 The total salt content (*x*-axis, bin range wt.%-wt.%) per mixture type (excl. $CaSO_4$), with Type 1: sulfate-rich (black) and Type 2: calcium-rich (gray), and the $CaSO_4$ content per mixture type (grid) as a frequency of the samples (*y*-axis). The dataset is limited to samples with a depth from the material

surface to 2 cm and a total balanced ion content ≥ 0.8 wt.% (excl. $CaSO_4$). 1867 samples from 218 sites in total, with 921 samples from 186 sites allocated to Type 1 mixtures, and 946 from 132 sites to Type 2. Excluded from the chart are 13 samples with a total salt content above 50 wt.%.

In the first two centimeters of the substrate where salt weathering of stone materials was mostly visible, approximately 50% of the 1867 samples had a total salt content between 0.8 and 2 wt.% (excl. $CaSO_4$). Both mixture types were almost equally represented over the samples, with 466 and 460 allocated to mixture Type 1 (sulfate-rich) and Type 2 (calcium-rich), respectively. The frequency of samples with salt contents above 2 wt.% declined significantly, indicating that a salt content between 0.8 wt.% and 2 wt.% was more common. Gypsum was always present and remained relatively similar in terms of frequency from 0.8 wt.% upwards. However, what is most important to note is the almost equal distribution of the two mixture types within this subset, with 921 samples from 186 sites allocated to Type 1 mixtures, and 947 from 132 sites to Type 2 mixtures. While in the complete dataset (11412 samples), thus including all sampling depths (as detailed in section **Error! Reference source not found.**) a higher frequency of up to two thirds was observed for Type 1 mixtures, indicating that sulfate-rich mixtures tend to be further distributed in depth.

The analysis of the complete dataset (11412 samples) revealed the frequency of different ions, with at least five charge-balanced ions included in >92% of all samples, indicating the significance of mixtures opposed to single salts. The only ion that occurred less frequently was Mg^{2+}, which was detected in 66% of the samples (above 0.1 wt.%). When focusing on the two mixture types, Mg^{2+} occurred in 86% of all Type 1 and in 56% of all Type 2 samples. Additionally, NO_3^- occurred less in all Type 1 samples at 88%. The most important ion mixtures are presented in Table 0-2.

Table 0-2 Representation of ions in common mixture compositions considering two mixture types. Left Type 1 (sulfate-rich) mixture and right Type 2 (calcium-rich) mixture, followed by the complete mixture of seven ions including calcium and sulfate (considered as gypsum). >92% of 11412 samples from the built environment contain at least five ions, thus four mixture compositions ($T1_V$, $T1_{VI}$, $T2_V$, $T2_{VI}$) were investigated further with ECOS/Runsalt with mean ion values derived from the dataset.

Type 1							Type 2						
					Na^+	SO_4^{2-}	Ca^{2+}	NO_3^-					
				K^+	Na^+	SO_4^{2-}	Ca^{2+}	NO_3^-	Cl^-				
			NO_3^-	K^+	Na^+	SO_4^{2-}	Ca^{2+}	NO_3^-	Cl^-	Na^+			
$T1_V$		Cl^-	NO_3^-	K^+	Na^+	SO_4^{2-}	Ca^{2+}	NO_3^-	Cl^-	Na^+	K^+		$T2_V$
$T1_{VI}$	Mg^{2+}	Cl^-	NO_3^-	K^+	Na^+	SO_4^{2-}	Ca^{2+}	NO_3^-	Cl^-	Na^+	K^+	Mg^{2+}	$T2_{VI}$
			K^+	Na^+	SO_4^{2-}	Ca^{2+}	NO_3^-	Cl^-	Mg^{2+}				

A separation of salt mixture types, as described by Arnold and Zehnder (1987), with more Type 1 (sulfate-rich mixture, including less soluble solids, thus less hygroscopic) nearer to the ground, and more Type 2 (calcium-rich mixture, including more soluble solids, thus more hygroscopic) at greater heights is likely. However, no statistical significance was obtained from the full dataset as a 0.95 *p*-value was determined from a chi-square test between the number of samples per mixture type identified at different heights: 0 to 30, 30 to 50, 50 to 100, 100 to 200, 200 to 400, and greater than 400 cm. This indicates that both mixture types are possible at any given height. However, both are most often found between a height of 100 and 200 cm. This height primarily experiences salt accumulation and decay, particularly when ground water is, or was, readily available to migrate upwards due to the capillary forces within the porous media.

Moving forward to the identification of common mixture types, mean values of the ion content for the different subsets and groups were used as input data for the ECOS/Runsalt model to evaluate the crystallization behavior of the mixture compositions. The outputs show common mixtures for each

dataset as specified in the method section. Similar mixture composition and behavior under changing RH conditions were identified, with minor differences in the number of solids and RH ranges of interest per mixture type. Furthermore, no significant differences were seen in the solids shown in the plots between the different heights, depths, and materials (brick, mortar, plaster, and stone). The mean ion values of the two mixture types derived from all samples (all materials and heights) taken from the material surface to a depth of maximum 2 cm and a total salt content ≥0.8 wt.% (excluding $CaSO_4$) are shown in Fig. 0.10 and Fig. 0.11. The results present common mixture types and solids, and their behavior under changing relative humidity.

Common solids identified in Type 1 mixtures are: aphthitalite ($Na_2SO_4 \cdot 3K_2SO_4$), bloedite ($Na_2SO_4 \cdot MgSO_4 \cdot 4H_2O$), magnesium sulfates ($MgSO_4 \cdot xH_2O$), halite (NaCl), niter (KNO_3), darapskite ($NaNO_3 \cdot Na_2SO_4 \cdot H_2O$), and thenardite ($Na_2SO_4$). Type 2, on the other hand, includes halite, niter, nitratine ($NaNO_3$), calcium nitrates ($Ca(NO_3)_2 \cdot xH_2O$), nitromagnesite ($Mg(NO_3)_2 \cdot 6H_2O$), and carnallite ($KCl \cdot MgCl_2 \cdot 6H_2O$). Three salts occur in both mixture types: halite, niter, and nitratine, the latter however is part of the double salt darapskite in Type 1. Solids that are shown in the plots that include magnesium can simply be removed without significant changes to the behavior when considering five ion mixtures (Cl^-, NO_3^-, Na^+, K^+, and SO_4^{2-} or Ca^{2+}). The outputs are evaluated following the method described in section **Error! Reference source not found.**, with an example output provided and a summary of the reactions under drying conditions for a common Type 1 mixture with five ions. From the common mixture compositions and behaviors presented in Fig. 0.10 and Fig. 0.11 the statements made by Arnold and Zehnder (1987) and Steiger et al. (2014) and are verified in the presented analysis based on the relative composition of the two mixture types, with:

- **Type 1:** a sulfate-rich mixture is less hygroscopic:
  SO_4^{2-}, Na^+, K^+, NO_3^-, Cl^-, Mg^{2+}
- **Type 2:** a calcium−rich mixture is more hygroscopic:
  NO_3^-, Ca^{2+}, Cl^-, Na^+, K^+, Mg^{2+}

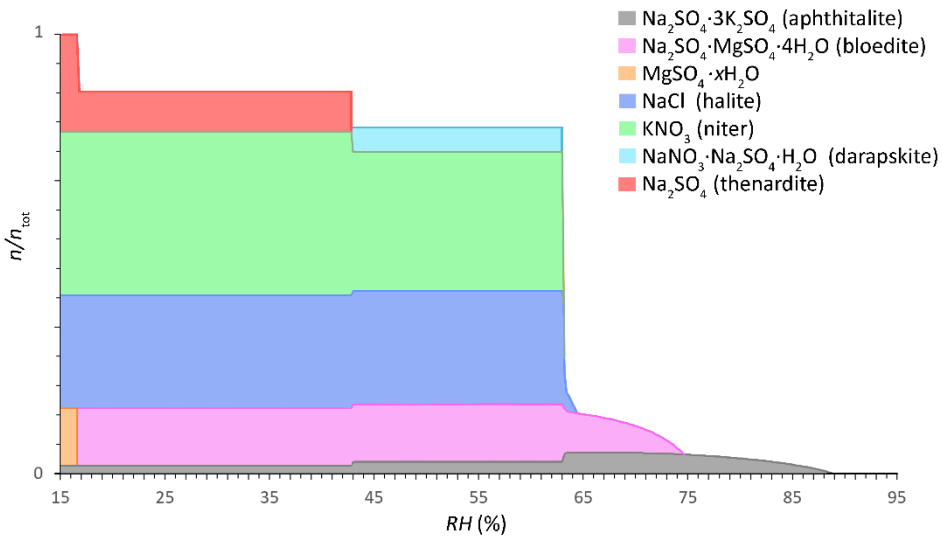

Fig. 0.10 Common salt mixture behavior of Type 1 mixtures (sulfate-rich, less hygroscopic) calculated between 15 and 95% RH (0.2% resolution) (*x*-axis) at 20 °C. The relative amount of substance is given as a fraction of crystalline salt (n / n_{tot}) (*y*−axis), mean of 921 samples from 186 sites (considering a maximum sampling depth from the surface to 2 cm and a total salt content ≥0.8 wt.% (excl. $CaSO_4$)).

Mole fractions: Cl^- : 0.1070, NO_3^- : 0.1543, SO_4^{2-} : 0.1771, Na^+ : 0.3063, K^+ : 0.2012, and Mg^{2+} : 0.0540. Modified ECOS/Runsalt output (Price, 2000; Bionda, 2005a).

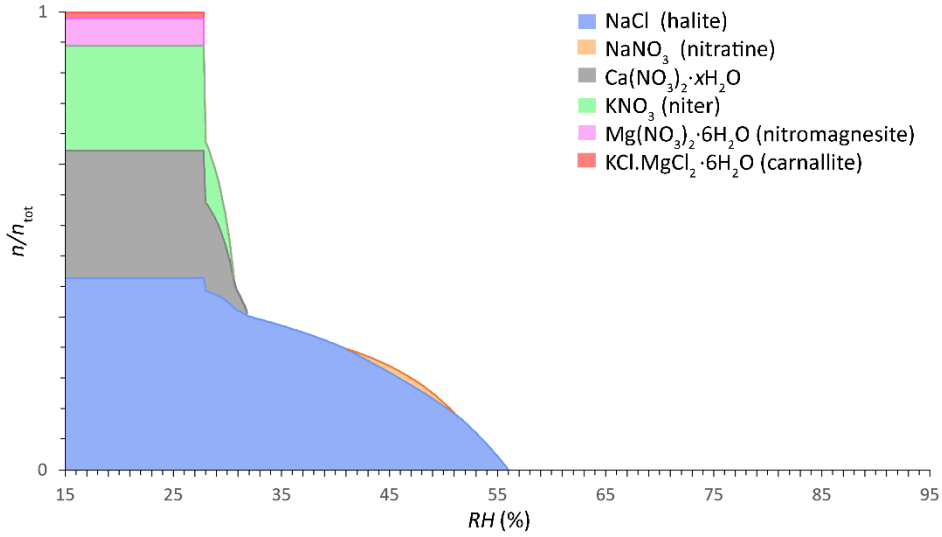

Fig. 0.11 Common salt mixture behavior of Type 2 mixtures (calcium-rich, more hygroscopic) calculated between 15 and 95% RH (0.2% resolution) (*x*-axis) at 20 °C. The relative amount of substance is given as a faction of crystalline salt (n / n_{tot}) (*y*-axis), mean of 946 samples from 132 sites (considering a maximum sampling depth from the surface to 2 cm and a total salt content ≥0.8 wt.% (excl. $CaSO_4$)). Mole fractions: Cl^- : 0.1937, NO_3^- : 0.3801, Na^+ : 0.1770, K^+ : 0.1016, Mg^{2+} : 0.0308 and Ca^{2+} : 0.1168. Modified ECOS/Runsalt output (Price, 2000; Bionda, 2005a).

Specific trends are derived from the outputs for both mixture types. Here, the common solids and mutual crystallization RH (with a resolution of 0.2%) at 20 °C for the Type 1 mixture under drying conditions are (cf. Fig. 0.10): 88.8% for aphthitalite, 74.6% for bloedite, 64.4% for halite, 63.2% for niter, and 63% for darapskite. Partial decomposition of aphthitalite occurs under drying conditions below 65% and 43%, during the first step this coincides with an increase of bloedite and crystallization of halite, niter and darapskite, followed by a slight increase of niter and thenardite, respectively. The latter is a solid-state reaction and overlaps with the decomposition of darapskite. The last solid-state reaction occurs at 17% when bloedite decomposes completely to form $MgSO_4{\cdot}xH_2O$ and thenardite. Further research is needed to verify the solid-state reactions and identify the magnesium sulfate hydrates, as detailed in **Error! Reference source not found.**.

For the Type 2 mixture, the common solids and mutual crystallization RH of interest are (cf. Fig. 0.11): 56% for halite, 51% for nitratine, 31.8% for $Ca(NO_3)_2{\cdot}xH_2O$, 30.6% for niter, and 27.8% for both nitromagnesite and carnallite. The solid phase $Ca(NO_3)_2$ was incorrectly calculated by ECOS as the anhydrous phase is not able to form under these climatic conditions. The only feasible form of crystallization is the tetrahydrate (nitrocalcite), however its crystallization is often observed to be kinetically hindered. Likewise, an unverified phenomenon is shown with nitratine as it decomposes below 41%, returning to solution as the amount of crystalline NaCl and the solution concentration increases.

Common solids and their behavior are derived from the ECOS outputs of all 11412 samples and presented in Fig. 0.12. The RH-range (distribution) of the solid behavior in the mixture compositions are shown and grouped per mixture type. The median, minimum and maximum mutual crystallization,

and dissolution/transition relative humidity points ($RH^{m}_{cry}, RH^{m}_{dis}, RH^{m}_{tra}$) are determined for each solid from all samples and compared to the single salt $RH_{cry}, RH_{dis}, RH_{tra}$. See section **Error! Reference source not found.** for a detailed explanation of these terms and nomenclature.

Additionally, the distribution of the behavior of all solids per mixture type including less frequent ones (occurring in less than 20% of samples per mixture type) are summarized to evaluate the overall possible behavior of the type. The *RH* points for the (single) salt are the same in both sides of Fig. 0.12, to clarify the RH_{cry} and RH_{dis} of the salt is identical to the RH equilibrium (RH_{eq}). While for solids in a mixture both points can be different, for example as shown in Fig. 0.11, the $RH^{m}_{cry_{hal}}$ for halite is 56% and the $RH^{m}_{dis_{hal}}$ is 27.8%.

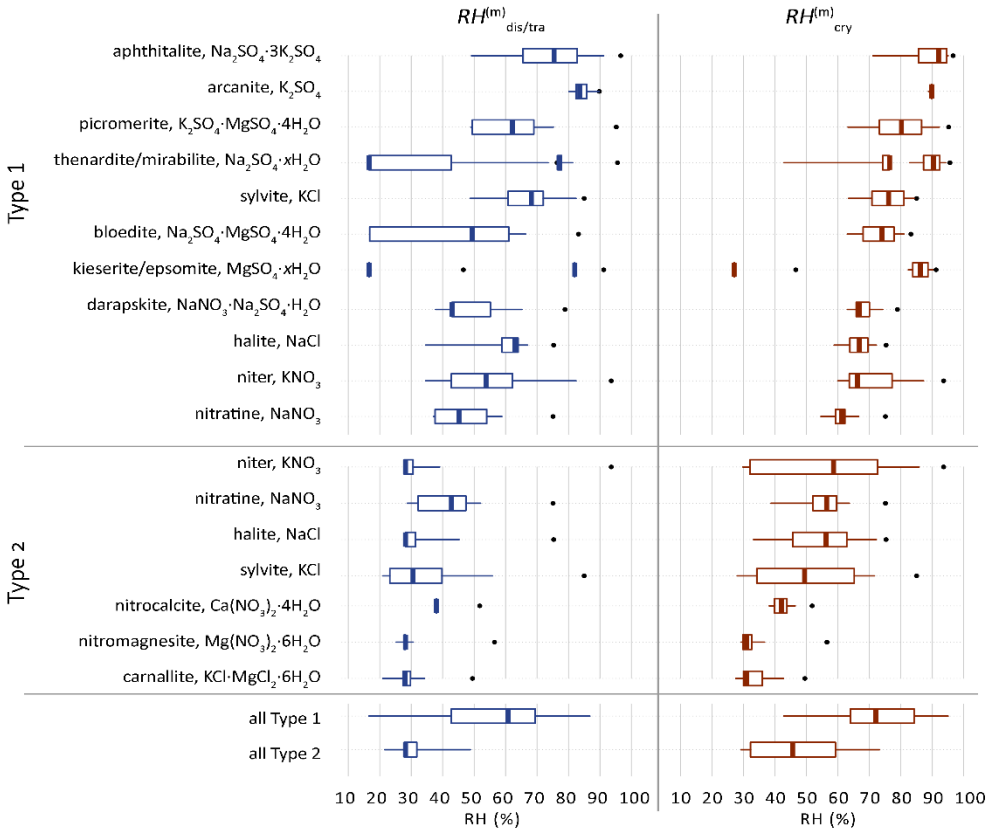

Fig. 0.12 Distribution of the mutual crystallization and dissolution or transition relative humidity points ($RH^{m}_{cry}, RH^{m}_{dis}, RH^{m}_{tra}$) of common solids identified for Type 1 (sulfate-rich) or Type 2 (calcium-rich) mixtures, limited to solids that occur in at least 20% of samples per mixture type, excluding three solids per mixture type in addition to gypsum. Solids are identified from the ECOS outputs of all 11412 samples. Boxplots: 25% left, 75% right, with whiskers drawn to the 5th and 95th percentiles, excluding outliers. The dots indicate the single salt $RH_{cry}, RH_{dis}, RH_{tra}$. Solids with a variety of possible hydrate phases are shown as xH_2O and their calculated RH points of interest are shown with increasing hydrate from left to right, excluding unverified metastable phases. The crystallization behavior has been calculated between 15% and 95% at 20 °C with a resolution of 0.2%. Corrections are applied following identified issues for $MgSO_4$, $Ca(NO_3)_2$, and K_2SO_4 (see **Error! Reference source not found.**). The two last boxplots (all Type 1 and 2) show a summary of all solids identified including ones below 20% of samples per mixture type.

From Fig. 0.12, common solids are identified that occur in at least 20% of the samples per mixture type: eleven in Type 1 and seven in Type 2. The RH points of interest are vastly different compared to the relative humidity equilibrium for the corresponding individual salts, with the critical crystallization RH of salts in a mixture always below the RH_{eq} of the (single) salt. A main RH threshold at 60% is identified for the median mutual crystallization RH at 20 °C for all common solids. The solids identified in Type 1, excluding kieserite, show a median RH^{m}_{cry} above 60% RH, and for solids in Type 2 they remain below this value.

The median trends of all solids between the RH^{m}_{dis} and RH^{m}_{cry} are 61% and 72% for Type 1, and 28% and 46% for Type 2, respectively. These median values for both mixture types are the critical RH ranges in which common mixtures will dissolve and crystallize, thus causing decay. However, the median, maximum and minimum RH ranges between the RH^{m}_{dis} and RH^{m}_{cry} are also defined for each solid in all the mixture compositions and indicate the range in which the solid can crystallize and dissolve. It is important to consider this for each individual solid in the given mixture separately, while keeping in mind that the phase transitions shown for sodium and magnesium sulfate can either exist as the specific phase given or a phase transition can occur in the mixture. The latter was not evaluated in terms of frequency, thus keeping in mind that phase transitions ((de)hydration) of a single solid can or cannot occur in a given mixture, and that the single salts related to a double salt often coexist or form within the given crystallization pathway.

The results of the statistical analysis show 14 common salts that occur in at least 20% of samples per mixture type. The frequency of occurring solids is further defined in Table 0-3. Five of these solids are double salts, aphthitalite, bloedite, darapskite, and picromerite, found in Type 1 and carnallite is frequently identified in Type 2 mixtures. Less frequent solids that are not included in the table are for Type 1: nitromagnesite ($Mg(NO_3)_2{\cdot}6H_2O$) (10.2%), carnallite ($KCl{\cdot}MgCl_2{\cdot}6H_2O$) (2.6%), and bischofite ($MgCl_2{\cdot}6H_2O$) (0.6%), and for Type 2: antarcticite ($CaCl_2{\cdot}6H_2O$) (15.8%), bischofite ($MgCl_2{\cdot}6H_2O$) (3.5%), and $MgCa(NO_3)_4{\cdot}10H_2O$ (2.9%). Remarking that the results presented do not include the amount of solid as they appear in the mixtures.

Table 0-3 Common solids and their frequency of occurrence (%) as identified in the samples per mixture type, excluding solids below a frequency of 20% and anhydrite/gypsum. (B) indicates solids that occur in both mixture types. (E) shows salts that overlap with the ones identified in the ECOS outputs of the mean ion values per mixture type. *x*H_2O implies different possible states of hydration, while (m) indicates unverified metastable phases not considered.

	Common solids	Frequency %
Type 1 sulfate-rich mixture	(B) (E) niter, KNO_3	86%
	(B) (E) halite, NaCl	86%
	(E) aphthitalite, $Na_2SO_4{\cdot}3K_2SO_4$	72%
	(E) thenardite/(m)/mirabilite, $Na_2SO_4{\cdot}xH_2O$	69%
	(E) kieserite/(m)/epsomite, $MgSO_4{\cdot}xH_2O$	56%
	(E) bloedite, $Na_2SO_4{\cdot}MgSO_4{\cdot}4H_2O$	48%
	(E) darapskite, $NaNO_3{\cdot}Na_2SO_4{\cdot}H_2O$	46%
	(B) nitratine, $NaNO_3$	30%
	arcanite, K_2SO_4	24%
	(B) sylvite, KCl	21%
	picromerite, $K_2SO_4{\cdot}MgSO_4{\cdot}6H_2O$	20%
Type 2 calcium-rich mixture	(B) (E) halite, NaCl	100%
	(E) (m)/nitrocalcite, $Ca(NO_3)_2{\cdot}xH_2O$	100%
	(B) (E) niter, KNO_3	79%
	(E) nitromagnesite, $Mg(NO_3)_2{\cdot}6H_2O$	65%
	(B) (E) nitratine, $NaNO_3$	60%
	(E) carnallite, $KCl{\cdot}MgCl_2{\cdot}6H_2O$	47%
	(B) sylvite, KCl	23%

Four solids, halite (NaCl), niter (KNO_3), nitratine ($NaNO_3$), and sylvite (KCl) occur in both mixture types. Above a frequency of 45% the solids overlap identically with the results of the Runsalt outputs of the mean ion values considering a maximum sampling depth from the surface to 2 cm, as shown in Fig. 0.10 and Fig. 0.11. Thus, concluding with the identification of the most common solids found in the built environment with seven solids identified in Type 1 and six in Type 2 mixtures.

It remains important to note that due to kinetics and possible separation of solids from the solution during crystallization in realistic situations, that is, the in-pore situation, deviations from the modeled crystallization pathway can take place. Additionally, the individual salts of each double salt can occur, resulting in an increase of the frequency regarding the solids arcanite (K_2SO_4), sodium sulfates ($Na_2SO_4{\cdot}xH_2O$), magnesium sulfates ($MgSO_4{\cdot}xH_2O$), and nitratine ($NaNO_3$) in Type 1, and in Type 2 mixtures sylvite (KCl) and bischofite ($MgCl_2{\cdot}6H_2O$). Furthermore, the result corresponds well with efflorescence detected on sites, the frequency was compared to reported efflorescence in 112 journal articles and conference papers (M. Steiger, personal communication, Unpublished). Excluding calcium sulfate and related double salts, the salts as efflorescence relevant to this study are presented as a percentage of times they were mentioned in these papers: halite (49%), thenardite (45%), niter (35%), nitronatrite (32%), epsomite (30%), aphthitalite (23%), mirabilite (22%), hexahydrite (21%), syngenite (20%), darapskite (13%), nitrocalcite (11%), arcanite (7%), starkeyite (7%), picromerite (7%), bloedite (5%), and 19 others below 5%, of which kieserite, antarcticite, and pentahydrate ($MgSO_4{\cdot}5H_2O$). Naturally, more hygroscopic salts are less likely to effloresce on the surface of in-situ building materials.

In future research, it would be beneficial to examine the different mixture types and their connections to decay phenomena observed on-site. Type 1 mixtures include more hydrating and double salts and would cause, for example, visible efflorescence and sub/crypto-florescence with severe powdering, material disintegration and/or delamination under regular RH fluctuations around 61% and 72%. While Type 2 mixtures are more likely to result in moisture stains, biological contamination and/or surface powdering caused by RH fluctuations around 28% and 46%. These statements can be verified

through on-site investigations and experimental determination of salt mixture kinetics over time, including solid state (decomposition) reactions.

The kinetic aspects require specific attention toward a better understanding of crystallization cycles under realistic climatic conditions within the pore structure of the material. The focus includes several key factors: pore filling, crystallization pressure, changes in the solution viscosity, separation of solids from the solution, pore clogging effects, capillarity, crystallization pathways and climatic buffering of the material. Moreover, the study did not delve into the quantification of the solids identified, which would enhance our comprehension of the extent of these solids in typical mixture composition. Finally, certain hydrating salts and double salt phases need further attention, such as magnesium sulfates, calcium nitrates, potassium calcium nitrates, humberstonite, and calcium sulfate double salts. When evaluating the risk of material decay from salt mixtures and understanding the damage mechanisms over time under changing climate conditions, it is crucial to take all these factors into account. This information can then be used to evaluate the potential for salt decay, guide the design of future experiments, and develop preventive measures, such as, adjusting the climate or limiting the amount or time people can enter an area where salts are of concern.

Common salt mixtures in the built environment, governed by the behavior of two mixture types, were investigated. Upon removal of equimolar amounts of calcium and sulfate, Type 1 mixtures (sulfate-rich) and Type 2 mixtures (calcium-rich) were identified. This process is based on gypsum crystallizing rapidly from a solution because of its low solubility. Due to the formation of more hydrating and sulfate-containing (double) salts in Type 1 these tend to be less hygroscopic, while the presence of more nitrate salts in Type 2 cause these to be more hygroscopic by nature. The data showed that in 92% of samples at least five ions are available, with magnesium seen less frequently. Thus, four common mixtures are identified including sodium, potassium, nitrate, chloride, and calcium or sulfate, either including or excluding magnesium.

The mean ion data entered in the thermodynamic model (ECOS/Runsalt) showed common solids and their behavior for each mixture type. In Type 1 these are niter, halite, aphthitalite, sodium and magnesium sulfate (phases), bloedite, and darapskite, while for Type 2 these are halite, calcium nitrate, niter, nitromagnesite, nitratine, and carnallite. The same common solids were identified, occurring with a frequency in at least 46% per mixture type, from the statistical analysis of all 11412 modeled samples. Salts that occur in at least 20% of the samples per mixture type showed 14 common solids, which is a valuable reduction of the more than 85 possible phases to consider. The modeled crystallization behavior of all mixtures revealed an overview of the vast range of possible mutual crystallization and dissolution RH ranges of the 14 common solids compared to the (single) salt behavior. These results are important to understand the overall behavior of salts in terms of RH ranges in which they can crystallize and dissolve in real world situations, where a mixture of ions is always present.

If building materials display signs of salt damage or moisture stains, even in the absence of liquid water, it has been commonly observed that the total salt content (excluding gypsum) in the first two centimeters is within the range of 0.8-2 weight percent relative to the dry material weight. Both mixture types occur with a similar frequency in the first two centimeters of the substrate in different materials and at different heights. The main distinction is that Type 1 mixtures are more commonly found at greater depths, while Type 2 mixtures tend to accumulate closer to the surface. Both mixture types are present together in 64% of the 338 sites, indicating the importance of sampling different areas of one site. It is important to consider the presence of liquid water, as gypsum is often found in high quantities in nearly all samples and is likely the primary source of damage in such cases. While, when liquid water is not or no longer present a total salt content (excluding gypsum) of approximately

1 wt.% is sufficient to cause damage or moisture related problems in a wide range of porous materials, dependent on the past and future climatic conditions. This value is determined on the material properties and any external factors that may impact the cycles of salt crystallization over time.

Modeled versus experimental salt mixture behavior

The following text is primarily based on the work originally published as: Godts, S., Steiger, M., Stahlbuhk, A., Orr, S.A., Desarnaud, J., De Clercq, H., Cnudde, V., De Kock, T., 2024. Modeled versus experimental salt mixture behavior under variable humidity. ACS Omega. 10.1021/acsomega.4c01486.

The modeled crystallization behavior of the four common mixtures ($T1_V$, $T1_{VI}$, $T2_V$ and $T2_{VI}$), as derived from the ECOS/Runsalt model are shown in Fig. 0.13 and Fig. 0.14. In mixture Type 1 ($T1_V$ and $T1_{VI}$), the solid phases that typically crystallize include aphthitalite, halite, niter, darapskite, thenardite, magnesium sulfate hydrates, bloedite, and nitratine. In these sulfate-enriched mixtures, most solid phases tend to crystallize around 65% and 60% RH for the five- and six-ion mixtures, respectively. An important note here is that the transition to thenardite in mix $T1_V$ is a solid-state reaction (see **Error! Reference source not found.**), which is not likely to be observed in the experimental results as described further.

Turning to mixture Type 2 ($T2_V$ and $T2_{VI}$), frequently occurring solids are niter, halite, nitrocalcite, carnallite, and nitromagnesite. In these calcium-rich mixtures, a wider range of mutual crystallization RH is often observed between 65% and 30% RH. Notably, significant crystallization activities are commonly found under extremely dry conditions, below 35% RH, while anhydrous calcium nitrate is not stable (Piqué et al., 1992; Steiger, 2005a), which is an identified issue in the model. Additionally, the dissolution of niter under drying conditions and its recrystallization as seen in mix $T2_{VI}$ has also been observed in mix $T2_V$ as further detailed in section **Error! Reference source not found.**.

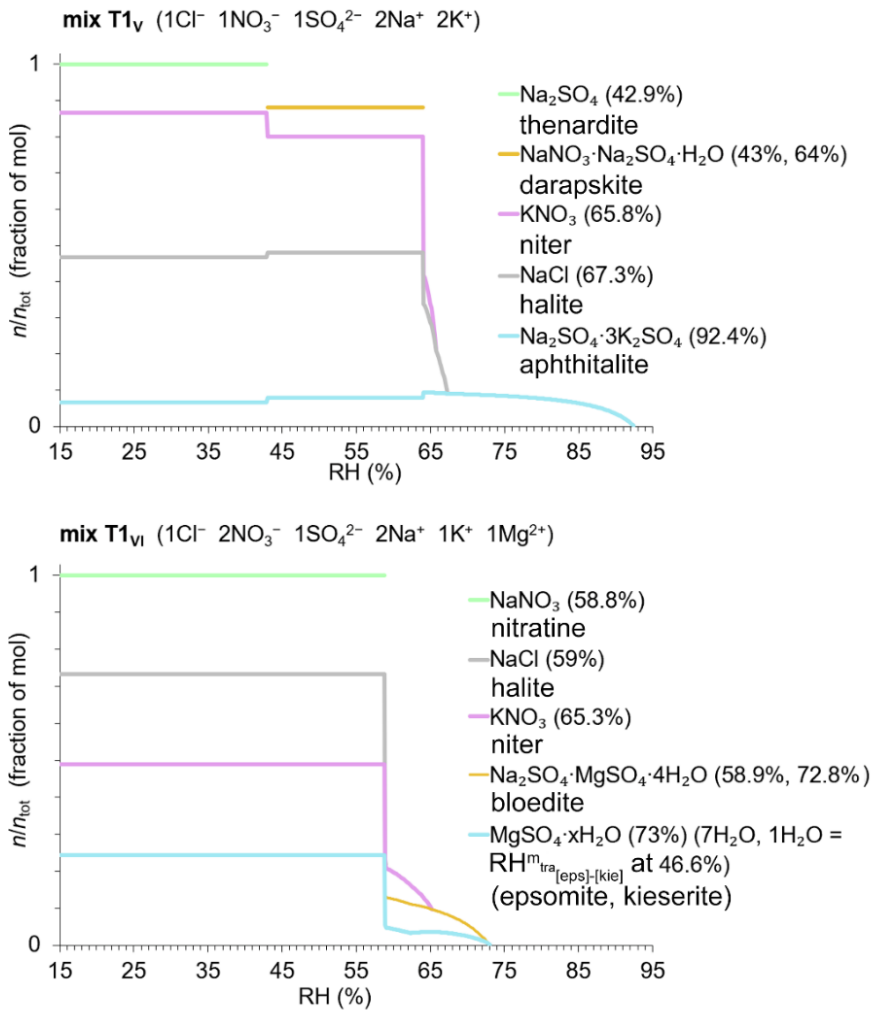

Fig. 0.13 Crystallization behavior showing solid phases of the Type 1 salt mixtures and their mutual crystallization relative humidity (%), as modeled by ECOS/Runsalt (Price, 2000; Bionda, 2005a). Model limitations for magnesium sulfate hydrates are considered, as detailed in (Godts, Steiger, Orr, Stahlbuhk, et al., 2022). The y-axes depict crystalline solid as a fraction of mol in a stacked format, calculated at 20 °C, across 15%-95% RH (x-axes: with 0.1% resolution). See Table 0-4 (method A) for an overview of RH points of interest.

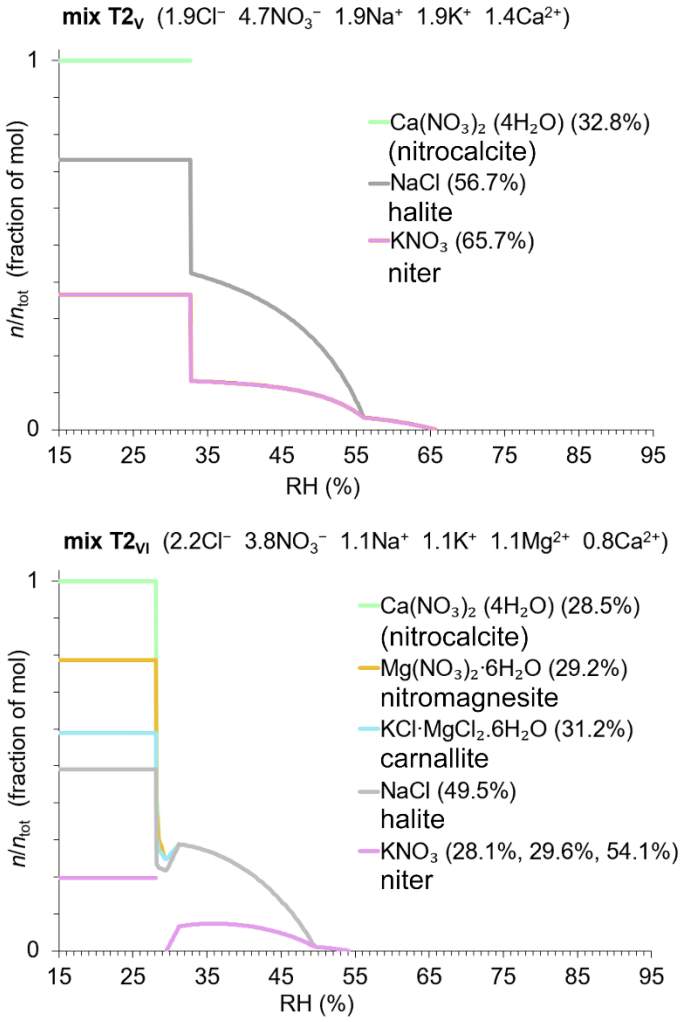

Fig. 0.14 Crystallization behavior showing solid phases of the Type 2 salt mixtures and their mutual crystallization relative humidity (%), as modeled by ECOS/Runsalt (Price, 2000; Bionda, 2005a). Model limitations for calcium nitrate hydrates are considered, as detailed in (Godts, Steiger, Orr, Stahlbuhk, et al., 2022). The y-axes depict crystalline solid as a fraction of mol in a stacked format, calculated at 20 °C, across 15%-95% RH (x-axes: with 0.1% resolution). See Table 0-4 (method A) for an overview of RH points of interest.

Time-lapse micrographs under rapid changing RH

The time-lapse micrographs (Fig. 0.15, plots A and B) illustrate dissolution and crystallization times of salt mixtures under rapidly changing relative humidity conditions (0.6% s^{-1}). For dissolution, the mixtures showed a rapid onset (t_2) and a faster completion with increasing RH (mean time, t_3: 10 min, SD = 3). However, when the RH target approached the modeled mutual crystallization RH, a significant increase in dissolution time was observed with a mean t_4 at 49 min and up to 225 min when considering aphthitalite in mix $T1_V$. Interestingly, little influence is noticed on the dissolution times considering the crystal habit in all mixtures, specifically when comparing the dissolution of bulk crystals that are formed when the RH was set closer to the crystallization relative humidity or smaller crystals formed at lower RH (detailed further below). The crystallization times of the salt mixtures also showed significant variations under rapidly changing RH conditions (Fig. 0.15, plots C and D).

For crystallization, in mix $T2_V$ a gradual increase in time to onset (t_2) and from first crystallization to completed crystallization (t_4) was observed as the starting RH was increased, ranging from 2 to 7 min and 12 to 41 min respectively (Fig. 0.15, plot D). In contrast a gradual decrease in time to onset was observed with 15 to 7 min and completion (t_4) at 56 to 27 min when the target RH is increased (Fig. 0.15, plot C). Mix $T1_V$ showed faster crystallization times, especially at lower RH targets, with onset times (t_2) as low as 0 min due to the continuous presence of aphthitalite (not shown). The more hygroscopic calcium-rich mixtures ($T2_{VI}$ and $T2_V$) generally required longer times for crystallization completion, particularly when the RH was reduced from 95% to lower levels, reaching up to 59 minutes in mix $T2_{VI}$, excluding crystallization of calcium nitrate (Fig. 0.15, plot C). The sulfate-rich, less hygroscopic, mixtures ($T1_V$ and $T1_{VI}$), on the other hand, showed fast crystallization for $T1_V$ and slower crystallization for $T1_{VI}$, especially at RH levels of 15% (Fig. 0.15, plot D).

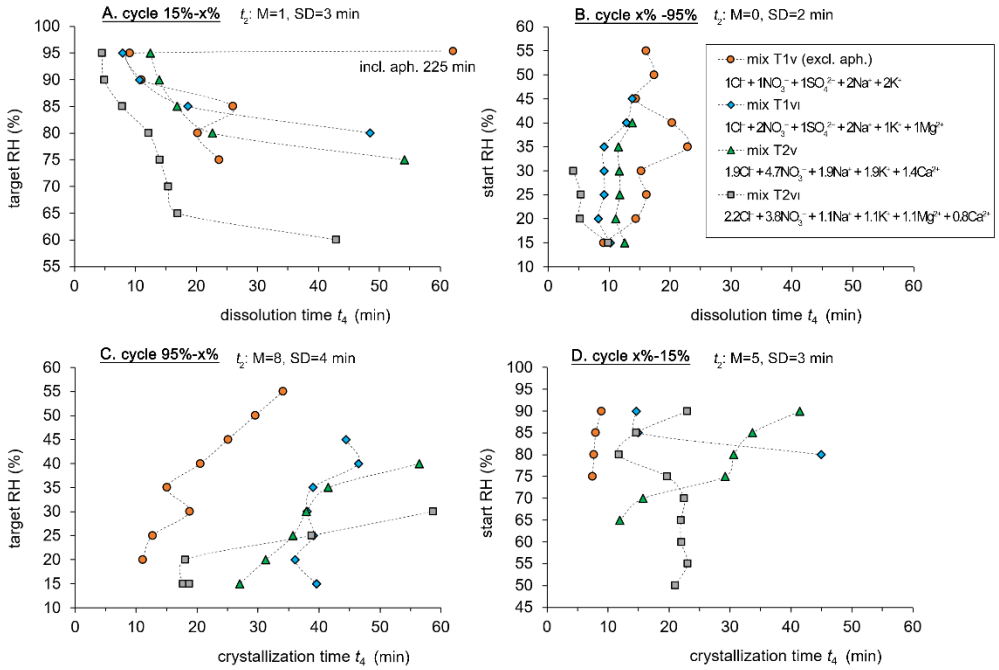

Fig. 0.15 Time-lapse micrograph-based analysis of dissolution and crystallization for four mixture compositions ($T1_V$, $T1_{VI}$, $T2_V$ and $T2_{VI}$) under variable RH. The x-axes show time in minutes t_4, equivalent to t_2 (induction time) + t_3 (completion time). Median (M) and standard deviation (SD) for t_2 is specified. Plots A and B show dissolution times for cycles from 15% to x% and x% to 95% RH, respectively. Plots C and D depict crystallization times for cycles from 95% to x% and x% to 15% RH, respectively. Only complete processes are included. Aphthitalite in mix $T1_V$ is excluded due to dissolution times exceeding the 60-min RH step. Complete crystallization in mixes $T2_V$ and $T2_{VI}$ is also excluded due to kinetically hindered calcium nitrate crystallization.

Completed dissolution processes were mostly in agreement with the modeled outputs for less hygroscopic sulfate-rich mixtures, this occurred above 75% and 95% RH for $T1_V$, respectively excluding and including aphthitalite, and above 80% RH for $T1_{VI}$ (Fig. 0.15, plot A). For the more hygroscopic, calcium-rich mixtures, the observations deviate more from the model with completed dissolution above 75% RH for $T2_V$ and above 60% RH for $T2_{VI}$ (Fig. 0.15, plot A). These results indicate that completed dissolution processes under rapid RH changes occurred at least 5% above the modeled dissolution RH. A notable deviation was observed for mix $T2_V$, where this occurred approximately 10% RH above the indicated mutual crystallization relative humidity of niter (65.7%) (Fig. 0.15, plot A). In

contrast, completed crystallization processes diverged further from the model outputs, likely due to supersaturation, which is a key factor influencing the kinetics. When a solution is supersaturated, it holds more dissolved material than what is predicted by thermodynamics at a given temperature and RH. Furthermore, the experimental parameters, particularly the rate of RH change, are linked to the observed RH at which crystallization occurs. In the less hygroscopic sulfate-rich mixtures completed crystallization was observed at 55% RH for $T1_V$, excluding aphthitalite, and at 45% RH for $T1_{VI}$ (Fig. 0.15, plot C). For more hygroscopic, calcium-rich mixtures, completed crystallization was seen from 40% and 30% RH for $T2_V$ and $T2_{VI}$, respectively (Fig. 0.15, plot C). Thus, deviating 10% to 25% RH from the modeled values at which all solids should crystallize, that is, under the experimental rate of RH decrease (0.6% s^{-1}) and each RH step maintained for 1 hour.

Vapor sorption under slowly changing RH

As shown in the previous section, the rate of RH change has an impact on the crystallization and dissolution behavior of mixed ion solutions. Thus, the verification of the modeled behavior is further evaluated from sorption and desorption experiments under (equilibrium) conditions with steps of 2% each 6 h and 50 h (maximum time). The mean results of four sorption and desorption measurements (2% each 6 h) of mix $T1_V$ and $T2_V$ are shown in Fig. 0.16 in comparison to the modeled crystallization behavior.

The results of $T1_{VI}$ and $T2_{VI}$ are similarly consistent with the modeled values as illustrated for $T1_V$ and $T2_V$ (refer to Data records). The initial hysteresis observed during the transition from sorption to desorption, starting from 95% relative humidity (RH) and decreasing, is attributed to kinetics, specifically evaporation is slower than sorption and the measurement time is too fast for evaporation to achieve equilibrium conditions at the respective RH. The subsequent hysteresis demonstrates a similar phenomenon but is associated with the kinetics, most likely due to the supersaturation of the solution in relation to the rate at which the RH changes to achieve effective crystallization. Specifically, the hysteresis at lower RH is attributed to crystallization kinetics, probably supersaturation, before crystallization and the deviation of the branches is therefore useful to identify the critical crystallization humidity. Interestingly, when a slower experimental run is conducted (2% each 50 h), both forms of hysteresis become significantly less pronounced, thereby adding complexity to the interpretation. A logical phenomenon in which at high RH more time is needed for evaporation to approach the equilibrium concentration. In our results the hysteresis between sorption and desorption is clearly visible and in good agreement with the modeled values for mixtures $T1_V$ (Fig. 0.16, top) and $T1_{VI}$ where the majority of salts crystallize. However, the crystallization of aphthitalite in $T1_V$ cannot be determined from the mass changes alone, likely because the crystallization RH is too high. The results are also in close agreement with the modeled values for the more hygroscopic mixtures $T2_V$ and $T2_{VI}$, even though the hysteresis is less defined for these mixtures.

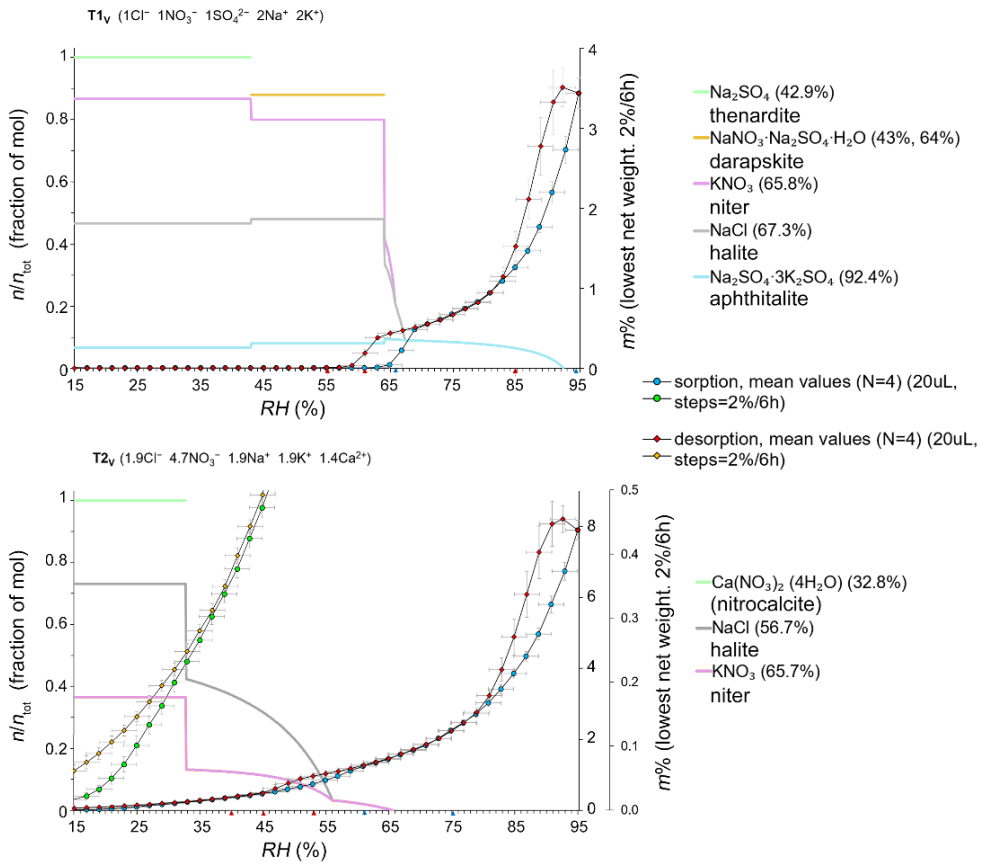

Fig. 0.16 Crystallization behavior of five ion mixtures under slow RH changes (0.5% RH h^{-1}) (maximum RH steps 2% per 6h). $T1_V$ (top) and $T2_V$ (bottom). Calculations were performed using ECOS/Runsalt at a temperature of 20 °C, with a 0.1% resolution. The primary *y*-axes shows the modeled crystalline solid as a fraction of moles, presented in a stacked format, with the legend describing the various modeled solid phases. A secondary right *y*-axes displays dynamic vapor sorption data (circles = sorption, diamonds = desorption), recorded at 20 °C in 2% RH intervals every 6 h (maximum time per step). The *x*-axes represents relative humidity (RH) ranging from 15% to 95%. The total time for sorption and desorption was 330 hours. In the $T2_V$ plot, sorption (green circles) and desorption (yellow diamonds) are displayed on a smaller scale (maximum 0.5 m%, tertiary *y*-axis) to highlight an otherwise invisible hysteresis loop (crystallization delay) occurring between approximately 30% and 15% RH.

Comparison between modeled and experimental crystallization behavior

To further identify the RH points of interest the first derivative of the individual sorption and desorption measurements are calculated. The local maxima of the mean (*N*=4 for 0.5% h^{-1} and *N*=2 for 0.1% h^{-1}) rate of change (1st derivative) of sorption and desorption curves and the range of the hysteresis loops are summarized in Table 0-4. The table also presents the modeled (ECOS) RH points of interest for mutual deliquescence and crystallization. Additionally, it shows the mean (*N*=2) RH points where these processes were observed in the micrographs from the sorption and desorption experiments carried out under rapid (GenRH) and slow (SPS) RH changes. The combined methods allow a detailed analysis of the kinetic processes. For both mixture types sulfate-rich ($T1_V$, $T1_{VI}$) and calcium-rich ($T2_V$, $T2_{VI}$), deviations were observed between the modeled and the experimental RH points of interest.

These deviations are primarily attributed to the kinetic processes not considered in the modeled values. The experimental data allow us to better understand these processes under realistic changes

of humidity. Here we compare the first modeled mutual crystallization relative humidity (1^{st} $RH^{m}_{cry_x}$) with the initial crystallization RH observed in the micrographs under rapid and slow RH changes. Under rapid RH changes (0.6% s^{-1}), crystallization in $T1_V$ occurred 2% (incl. aphthitalite) and 12% (excl. aphthitalite) below the modeled values. For $T1_{VI}$ the deviation was 28%, while for the calcium-rich more hygroscopic mixtures the deviations below the modeled values are 26% for $T2_V$ and 24% for $T2_{VI}$. The differences under slow RH changes (0.5% h^{-1}) are 7% and 6% for $T1_V$, including and excluding aphthitalite. For $T1_{VI}$ they are 20%, while for $T2_V$ they are 13 to 21% and finally for $T2_{VI}$ a 10% deviation was observed.

As expected under slower RH changes (0.1% h^{-1}, desorption) initial crystallization was observed closer to the modeled values deviating only 3% and 4% for $T1_V$, including and excluding aphthitalite. While a 12% deviation was observed for $T1_{VI}$, the slower process also allowed an additional identification of niter crystallization 11% below the modeled value. Interestingly, for the more hygroscopic mixtures the deviations were similar under both 0.5% h^{-1} and 0.1% h^{-1}, with 13 and 11% for respectively $T2_V$ and $T2_{VI}$. Again, for $T2_{VI}$ an additional process was observed at 8% below the $RH^{m}_{cry_{car}}$. We can reasonably state that crystallization consistently occurs at lower RH then calculated due to a kinetic delay, likely caused by the supersaturation of the solution in relation to the rate of change, as further described in Rodriguez-Navarro and Doehne (1999), Flatt (2002), Desarnaud and Shahidzadeh-Bonn (2011), Desarnaud et al. (2014) (2015), and Stahlbuhk and Steiger (2022).

When investigating the dissolution behavior, initial dissolution RH values were closely in agreement with the modeled values for the sulfate-rich mixtures (T1), while significant deviations were observed for the hygroscopic T2 mixtures. The latter is related to the kinetically hindered crystallization of calcium nitrate and the continuous presence of solution throughout the experiment. For the completed dissolution processes (sorption) the deviations remained under 10% for slow (0.5% h^{-1}) and rapid (0.6% s^{-1}) humidity changes with a mean value of approximately 7% above the last modeled solid in solution, that is, the 1^{st} mutual crystallization RH. In comparison, under slower conditions (0.1% h^{-1}) the mean deviations were 3%, thus allowing for a higher accuracy, validating the modeled values.

Table 0-4 Summary of all RH (%) points of interest for mutual deliquescence and crystallization as modeled with ECOS/Runsalt, compared to the results of the experiments. The recorded RH points (mean *N*=2) for dissolution and crystallization are determined from the micrographs under rapid (0.6% s^{-1}) and slow (0.5% h^{-1} and 0.1% h^{-1}) RH changes. With RH steps of 5% and 2%, each RH step conditioned for either 1 h or a maximum of 6 h and 50 h, for the rapid and slow runs, respectively. Furthermore, the mean (*N*=4) RH ranges of the hysteresis loops between sorption and desorption curves are shown, as well as the maxima (max.) from the 1st derivative calculation of each individual curve and RH at which a change in wavenumber is identified in the Raman spectra (slow RH changes).

mixture	modeled	experimental									
	$RH^{m}_{del/cry}$	micrographs						mass change			Raman
		Rate of RH change at 20 °C									
		0.6% s^{-1}		0.5% h^{-1} *(0.1% h^{-1})*							0.5% h^{-1}
T1$_V$	92_{aph}	95	90	-	95 *(93)*	85 *(89)*	-	-	89	87 *(85)*	85
	67_{hal}, 66_{nit}, 64_{dar}	75	55	66 *(64)*	*(68)*	61 *(63)*	56 *(58)*	69-57 *(67-61)*	67 *(65)*	61 *(63)*	-
T1$_{VI}$	$73_{eps,blo}$	80	45	-	81 *(78)*	53 *(61)*	-	79-45 *(75-53)*	75 *(77)*	53 *(55)*	51
	65_{nit}	-	-	-	-	*(54)*	-		61 *(60)*		
	$59_{hal,nitra}$	-	-	61 *(61)*	-	-	45 *(48)*		49		
T2$_V$	66_{nit}	75	40	-	75 *(72)*	53 *(53)*	-	63-4	75 *(77)*	49 *(53)*	51
	57_{hal}	-	-	-	*(57)*	-	-		59 *(55)*		
	33_{nitro}	-	-	15	-	-	<15	33-15	-		
T2$_{VI}$	54_{nit}	60	30	-	63 *(63)*	44 *(43)*	-	53-37	49	39 *(43)*	39
	50_{hal}	-	-	-	*(50)*	-	-		36		
	31_{car}, $29_{nit(ro)}$	-	-	15	*(33)*	*(23)*	<15	37-15	15		
method	**A**	**B**	**C**	**D**	**E**	**F**	**G**	**H**	**I**	**J**	**K**

Legend for Table 5-2

-: empty cells, unidentified

A: modeled mutual (m) crystallization (cry) / deliquescence (del) relative humidity (RH)

B: completed dissolution observed at given RH

C: first crystallization observed at given RH

D: first dissolution observed at given RH during sorption

E: completed dissolution observed at given RH during sorption

F: first crystallization observed at given RH during desorption

G: completed crystallization observed at given RH during desorption

H: RH range of a hysteresis loop between sorption and desorption curves

I: first derivative maxima at given RH identified from the sorption curve

J: first derivative maxima at given RH identified from the desorption curve

K: RH when a change in wavenumber is identified in the Raman spectra

aph: aphthitalite, hal: halite, nit: niter, dar: darapskite, eps: epsomite, blo: bloedite, nitra: nitratine, nitro: nitrocalcite, car: carnallite.

Under rapid RH changes (0.6% s^{-1}) completed dissolution was observed 3% and 8% above the modeled values for $T1_V$, respectively excluding and including aphthitalite. Similar deviations were recorded

under a slow rate of the RH change (0.5% h^{-1}). For $T1_{VI}$ the deviations are 7% and 8%, respectively for rapid and slow changes, while for $T2_V$ and $T2_{VI}$, 9% and 6% are seen under both rates of change. The difference is less pronounced under slower conditions (0.1% h^{-1}), yet they remain significant for the calcium-rich mixtures (T2). A summary of the deviating RH values specific to each mixture type under rapid or slow RH changes is given in Table 0-5. Notably, initial dissolution was observed at the same RH (±2%) as modeled for the sulfate-rich mixtures (T1), while the deviation was at least 15% for the calcium-rich mixtures (T2) due to kinetically hindered crystallization of calcium nitrate.

As shown by the difference between RH values at which crystallization and dissolution occur when compared to the modeled values, the obtained sorption data (dissolution) allow for a more accurate indicator of $RH^{m}_{cry_x}$, also described by (Rörig-Dalgaard, 2021). When salt crystals dissolve, the water activity of the solution increases accounting for the steeper slopes during the sorption run. However, in complex mixtures, specifically ones with extreme hygroscopic properties (T2 mixtures) the mass change becomes negligible between solid and solution under increasing RH. This is because as the solid dissolves the solution picks up water molecules accounting for the mass loss. This phenomenon thus explains the discrepancies between the RH values determined via the sorption data and the micrographs.

Table 0-5 Summary of the experimental results considering kinetics of common mixtures under realistic humidity rate changes. The RH (%) deviations are shown between modeled and experimental RH points of interest (ΔRH), specifically the modeled mutual crystallization and mutual deliquescence RH compared to the observed RH values at which first crystallization and (first and completed) dissolution occurred in the different mixture types under rapid (0.6% s^{-1}) and slow (0.5% h^{-1} and 0.1% h^{-1}) RH changes.

mixture	modeled		experimental $-RH=$							
	$1^{st}\ RH^{m}_{cry_x}$	$RH^{m}_{del_x}$	$1^{st}cry-1^{st}RH^{m}_{cry_x}$			$1^{st}dis-RH^{m}_{del_x}$		$c.dis-1^{st}RH^{m}_{cry_x}$		
			Rate of RH change at 20 °C							
			0.6% s^{-1}	0.5% h^{-1}	0.1% h^{-1}	0.5% h^{-1}	0.1% h^{-1}	0.6% s^{-1}	0.5% h^{-1}	0.1% h^{-1}
$T1_V$	92_{aph}		-2	-7	-3	-	-	+3	+3	+1
	67_{hal}	64_{dar}	-12	-6	-4	+2	0	+8	-	+1
$T1_{VI}$	$73_{eps,blo}$	$59_{hal,nitra}$	-28	-20	-12	+2	+2	+7	+8	+5
$T2_V$	66_{nit}	33_{nitro}	-26	-13	-13	-18	-	+9	+9	+6
$T2_{VI}$	54_{nit}	29_{nitro}	-24	-10	-11	-12	-	+6	+9	+9
mean ΔRH			-18	-11	-9			+7	+7	+3

Legend for Table 5-3:
-: empty cells, observations and experimental data were inconclusive, processes could not be observed.
The RH steps under the rate of change are ±5% and ±2% for 0.6% s^{-1} and (0.5% and 0.1 h^{-1}), respectively. m: mutual, cry: crystallization, del: deliquescence, dis: dissolution, c.dis: completed dissolution (all solids are dissolved), *x*: associated solid, aph: aphthitalite, eps: epsomite, hal: halite, dar: darapskite, blo: bloedite, nitra: nitratine, nit: niter, nitro: nitrocalcite

The sorption and desorption curves obtained remain important to identify critical RH ranges in which the solids crystallize, determined from the 1^{st} derivative (maxima) of sorption and the hysteresis loops (Table 0-4).

The RH values identified are highly accurate for T1 mixtures, considering a 2% experimental resolution. These results are also in good agreement with the observations of 1st visible dissolution. Especially, for T2 mixtures deviations are recorded, with the modeled $RH^{m}_{cry_{nit}}$ at 66% compared to the 1st derivative of sorption at 75% for $T2_V$ and from modeled $RH^{m}_{cry_{nit}}$ 54% to 49% for $T2_{VI}$. However, the RH ranges of the hysteresis loops closely align with the majority of processes for all investigated mixtures, also showing crystallization delays between approximately 35% and 15% RH for more hygroscopic mixtures (T2). The latter is further illustrated with the sorption and desorption curves displayed on a smaller scale to highlight an otherwise invisible hysteresis loop (crystallization delay) occurring between approximately 30% and 15% RH, displayed for $T2_V$ in Fig. 0.16. Particularly, the behavior of KNO_3 in $T2_V$ showed a clear deviation, suggesting that model parameters may require refinement when K^+, NO_3^- and Ca^{2+} coexist in a mixture. It remains important to note that the model can be considered highly accurate and that the crystallization delays observed in both mixture types can primarily be attributed to kinetic delays.

Identification of salt phases and investigating crystal habit

The RH values at which crystallization and dissolution occur throughout the SPS measurements are further validated with the Raman spectra recorded at approximately each 5% RH step throughout the SPS desorption measurements (see 'Data records'). The first observed crystallization in the mixtures coincided with a change in wavenumber (cm^{-1}) identified in the Raman spectra. Initial crystallization was confirmed at 85%, 51%, 51% and 39% RH for $T1_V$, $T1_{VI}$, $T2_V$ and $T2_{VI}$, respectively. The results are closely in agreement with the observations of 1st crystallization as identified in micrographs throughout the SPS experiments. Specific bands are closely related to aphthitalite and niter in $T1_V$, nitratine, magnesium sulfate hydrates, arcanite and niter in $T1_{VI}$, while niter was identified in $T2_V$ and $T2_{VI}$. The Raman identification of solids during the faster GenRH experiments were carried out with higher resolution, thus allowing additional identification of darapskite, niter and aphthitalite for $T1_V$, magnesium sulfates, nitratine and niter for $T1_{VI}$, while niter and traces of nitrocalcite were identified in both $T2_V$ and $T2_{VI}$ including nitratine in the latter. The results confirm the modeled results while taking the limitations of thermodynamic calculations into account.

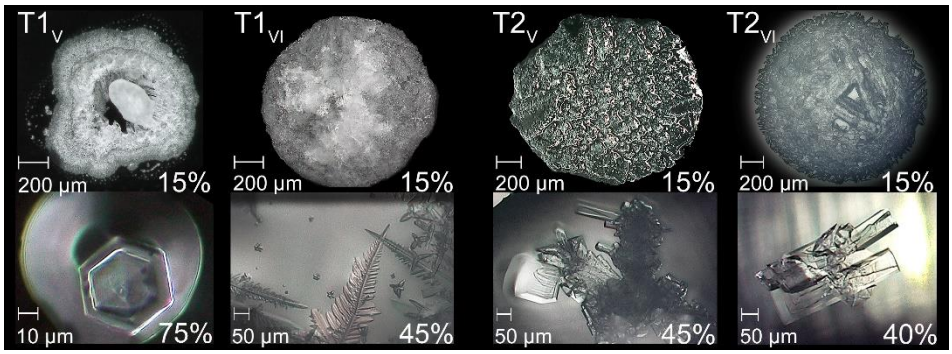

Fig. 0.17 Illustration of crystal habit identified in the micrographs under changing RH conditions and 20 °C for all investigated mixtures, from left to right $T1_V$ to $T2_{VI}$. The top images show the crystallized solutions (initial volume 0.5 µL) after rapid RH decrease (approximately 0.6% s^{-1}) from 95% to 15% RH. The bottom images example specific crystal habit, from left to right: first, hexagonal prism-shaped crystal associated with aphthitalite. Second, fern-like dendritic crystals identified as niter. Third, a clump of aggregated crystals with a mix of shapes, some of which have a tubular or rod-like morphology (niter), emerging from a central core and cubic shape associated with halite, and last, elongated tubular and cubic (hopper) crystals with multiple facets (niter and halite). Solution remained available in calcium-rich mixtures (T2) at 15% RH.

Additional XRD analysis was carried out on the dried solutions (see 'Data records'). Results were obtained for both sulfate-rich (T1) mixtures. As modeled by ECOS/Runsalt, darapskite, aphthitalite, niter and halite were identified in the dried mixture $T1_V$. As expected, thenardite was absent, as its formation in this mixture is the result of a solid-state decomposition reaction of darapskite and aphthitalite, which had not occurred within the experimental timeframe. This result validates the statement, that solid-state reactions might have limited effect on porous materials under daily changes in RH (Godts, Steiger, Orr, Stahlbuhk, et al., 2022). The mixture $T1_{VI}$ showed the presence of starkeyite, nitratine, halite and niter. Although the formation of starkeyite was not modeled, an issue with magnesium sulfate hydrates in ECOS was expected, as detailed in **Error! Reference source not found.**. In both cases the XRD results are in agreement with the ECOS modeled solids. On the other hand, despite the long-term conditioning of the calcium-rich (T2) mixtures, the XRD analysis was unable to identify any minerals. This was attributed to persistent calcium nitrate solution surrounding all solids, which had become extremely viscous and exhibited amorphous properties, thus obscuring the definitive crystalline characteristics required for identification (Fig. 0.17, top $T2_V$ and $T2_{VI}$).

To further aid the identification of salts and the possible relation with stone decay associated with crystal size (see (Benavente et al., 2004; Michael Steiger, 2005; Derluyn et al., 2014)), the habit of crystals was also investigated via ESEM-EDX (Fig. 0.18). The evaporation rate and surface tension have significant influence on crystal habit as described in (Sunagawa, 1981, 2005; Shahidzadeh et al., 2015), which implies different degrees of (super)saturation (Rodriguez-Navarro and Doehne, 1999; Flatt, 2002; Flatt et al., 2014). Additionally, it has been shown that a salt that crystallizes from a mixture has smaller dimensions when compared to its crystal size from a less complex ion solution (Stahlbuhk, 2021), more specifically crystal size is reduced in mixtures compared to single salt dimensions. Many different habits were identified in the micrographs, most notably, typical hexagonal structures and semispherical platy aggregates of aphthitalite, cubic and hopper crystal systems related to halite and sylvite, and orthorhombic crystals, that is, long prismatic shapes with needle-like or plate-like forms identified as niter. Other habits identified were different types of polyhedral crystals, with typical flat faces (facets) and sharp angles. Additionally, dendritic and needle morphologies were identified in all four mixtures that were mainly related to niter.

The more robust formed crystals were primarily obtained when the RH target was nearer to the critical crystallization RH of the related solid (for example Fig. 0.18 a. and c.). On the other hand, we observed more dendritic, microcrystalline, disordered, clusters and amorphous structures in the experiments where the rate of change is rapid and RH target is further away from the critical crystallization RH (for example Fig. 0.18 e.). Under these conditions, polycrystalline dendritic and microcrystalline patterns formed around the initial bulk, often out of the last remaining solution and sometimes growing up to three times the distance over the surface beyond the initial droplet circle. The identification of crystal habits and element distribution further validated the model calculated solids. This includes a clear identification of clusters related to sodium chloride (halite), potassium nitrate (niter), sodium potassium sulfate (aphthitalite) and calcium nitrate in solution (for example Fig. 0.18 b., d., f., and element distributions on the right).

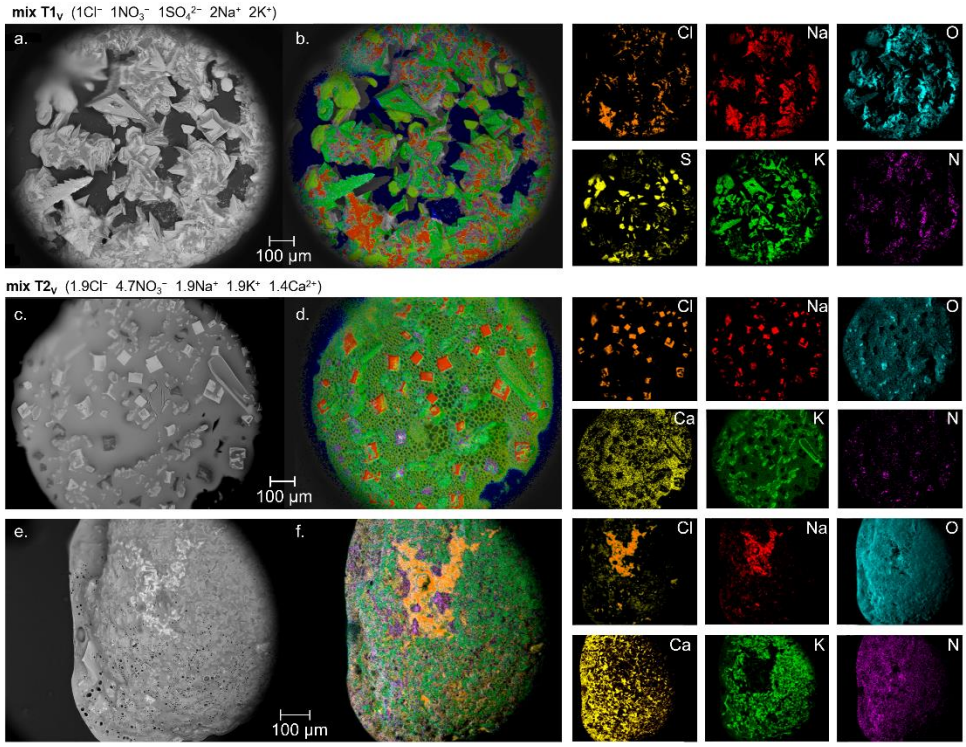

Fig. 0.18 Illustration of crystal habit ESEM image (left a, c and e) and layered EDX image (b, d and f) including element distribution (K-series) on the right for mixture $T1_V$ (a and b) $1Cl^- + 1NO_3^- + 1SO_4^{2-} + 2Na^+ + 2K^+$, and for mixture $T2_V$ (c and d) $1.9Cl^- + 4.7NO_3^- + 1.9Na^+ + 1.9K^+ + 1.4Ca^{2+}$, after a slow evaporation rate, while (e and f) show the same mix $T2_V$ after a fast evaporation rate. Images obtained between 0 and 1.2% RH and 5 °C (vacuum settings 9.79×10^{-4} or 10 Pa) after decreasing the chamber pressure in steps of 20% RH each hour from 95% to 15% (slow) or from solution directly under high vacuum (fast), at 5 °C. Note that solution remains available in mix T2 under both rates of evaporation at 0% RH, the bubbles in (d) are boiling solution caused by beam heating at the surface.

Understanding the kinetics of salt mixtures under varying relative humidity (RH) conditions is important for the conservation of built heritage to identify deviations from the calculated behavior and to incorporate crystallization and dissolution times in preventive management strategies. Several methods were combined in this research, including time-lapse micrographs and dynamic vapor sorption under changing humidity conditions, ranging from 15 to 95% RH (at 20 °C). The behavior of salt mixtures frequently identified in the built environment were established. These mixtures are either less or more hygroscopic, Type 1 sulfate-rich and Type 2 calcium-rich, respectively. The mixtures contain five or six ions: Cl^-, NO_3^-, Na^+, K^+, including either SO_4^{2-} or Ca^{2+}. When a sixth ion is present, it is the less common ion Mg^{2+}. Different rates of RH changes were chosen to mimic realistic climate scenarios, with rapid (0.6% s^{-1} = approximately 80% RH change within 133 s) and slow (0.5% h^{-1} = approximately 80% RH change over 160 h) humidity variations. Additionally, slower experiments (0.1% h^{-1}) were carried out to verify modeled RH points of interest and optimize the method.

Different analytical techniques were used to verify phase transitions and crystal habits associated with different RH conditions, such as, Environmental Scanning Electron Microscopy (ESEM), micro-Raman spectroscopy, X-ray Diffraction (XRD), and elemental mapping via Energy Dispersive X-ray Spectroscopy (EDX). The modeled (ECOS/Runsalt) behavior of the mixtures were verified with experimental observations, confirming that the model is accurate, while showing important deviations primarily attributed to kinetic factors, such as supersaturation. This reveals the necessity of kinetic

considerations in future models and risk assessment. Although kinetic variations were expected during desorption processes, the sorption or dissolution measurements should align with theoretical calculations. This discrepancy indicates that certain parameters within the model, particularly those related to calcium-rich (hygroscopic mixtures), require more attention.

The results show a relationship between kinetics of phase transitions and changes in RH. The onset of crystallization deviated by a mean value of −15% from the modeled crystallization RH, while dissolution showed a mean deviation of +7% from the dissolution RH. Interestingly, rates of RH change, between 0.6% s^{-1} and 0.5% h^{-1}, had a minor influence on these deviations, indicating that kinetics of crystallization and dissolution are slightly unresponsive to the different rates of environmental changes, spanning from hourly, to diurnal, up to a period of one week. Practical implications of these findings extend to both built heritage conservation and geological studies where daily changes in the environment influence crystallization cycles. In the context of built heritage, the results allow a more precise approach for in-situ preservation strategies, specifically in terms of climate adaptation and optimized environmental control. For geological applications, salt deposition and dissolution mechanisms can be predicted more precisely, such as, predicting salt weathering in natural rock formations, informing coastal erosion studies and improving models for soil salinity. The findings inform future modeling efforts of complex phenomena in built and natural environments, although additional parameters need to be considered, such as, different temperatures, water, wind, solar radiation, in-pore processes, and changes in the mixture composition. On the other hand, the results can be useful for laboratory experiments to understanding stone and built material decay processes over time, when crystallization cycles of a given mixture are related to pore filling, pressures, and material/salt properties.

More broadly, the insights are valuable for informing public policy and urban planning. For instance, the obtained data on how salt mixtures respond to varying RH conditions can inform the preservation techniques for historical monuments, thereby aiding in cultural preservation. Specifically, deviations are primarily seen when investigating crystallization, which is likely associated with a delayed process due to solution supersaturation before crystallization is possible. However, when the RH increases and remains close to the mutual deliquescence RH, completed dissolution can take more time when compared to complete crystallization processes. The differences between sulfate-rich and calcium-rich mixtures are especially clear, with higher accuracy of the model for sulfate-rich mixtures. While further deviations from the model for calcium-rich mixtures can be attributed to extremely concentrated solutions and kinetically hindered crystallization. Overall, the complex interplay between ion mixtures and RH fluctuations showed the significance of using combined analytical techniques and a need for multi-factor models in both environmental conservation and historical preservation planning.

General conclusions and outlook

The following text includes content adapted from the 'conclusions' section of the following published manuscript: Godts, S., Orr, S.A., Desarnaud, J., Steiger, M., Wilhelm, K., De Clercq H., Cnudde, V. and De Kock, T., 2021. NaCl-related weathering of stone: the importance of kinetics and salt mixtures in environmental risk assessment. Herit Sci. 9:44. 10.1186/s40494-021-00514-3.

This dissertation presents a comprehensive study aimed at enhancing our knowledge of salt mixtures, which are frequently recognized as agents of weathering in porous building materials. Theoretical, analytical, and experimental practices are explored for the analysis and interpretation of soluble ions that are found in building materials that undergo phase changes under changing environmental conditions. This links directly with ions related to geochemical processes where crystallization and

dissolution of salts are often misrepresented, as single salt rarely occur in realistic scenarios. In the section 'Analysis of salt mixtures' we explored the complexities of charge balance calculations, clarifying the ion compositions found in porous heritage materials. An improved calculation method was proposed and applied to an extensive dataset of 11412 samples. The results shed light on common ion mixtures and enhanced our understanding of salts in the built environment. In summary, the charge balance calculations follow two distinct pathways: i) an equal adjustment of all ions, or ii) adjustments to the cations in sequence related to the solubility of the theoretical solids. The latter, to identify the importance of undetected anions. The data analysis identified two principal mixture compositions that are equally present in the first centimeters of a substrate and a third less common one, all with respect to the removal of the theoretical gypsum content. Type 1, a sulfate-rich mixture includes an excess of sulfate ions. With the most important ions in order of magnitude SO_4^{2-}, Na^+, K^+, NO_3^-, Cl^-, and Mg^{2+}. Type 2, a calcium-rich mixture includes an excess of calcium ions. With the most important ions in order of magnitude NO_3^-, Ca^{2+}, Cl^-, Na^+, K^+, and Mg^{2+}. Type 3, a mixture containing an important content of carbonates related to an excess of sodium or potassium (relevant within Type 1).

The methodological advance presented in the section 'Analysis of salt mixtures' enabled a more refined approach towards the interpretation of ion data and allowed direct input for thermodynamic modeling. Furthermore, the data records and calculations have been made available for general use and future adaptations (Godts et al., 2022b). In the section 'Modeling salt behavior' salt mixture behavior is explored through thermodynamic modeling, which showed that the ECOS/Runsalt model is currently the most appropriate for the combined ions we encounter in the built environment. We addressed certain issues concerning the model's limitations and proposed solutions. The latter, not only of importance for its current use, also identifies specific areas of focus for model improvement, regarding calcium nitrate, potassium sulfate and magnesium sulfate hydrates. This includes possible influence of calcium sulfate or carbonates on the formation of different solids under specific conditions, and issues concerning more hygroscopic Type 2 (calcium-rich) mixtures and certain solids not included. However, the overall work in the section 'Modeling salt behavior' has substantially increased the utility of the ECOS/Runsalt model with the introduction of terminology and methodology, as it ensures uniformity in application and interpretation, crucial for advancing conservation science.

After the detailed investigation in the section 'Modeling salt behavior', we confidently used the model to further our understanding of salt mixture behavior in the section 'Identification of relevant salt mixtures', where we explore common salt mixtures and frequently occurring salts in stone weathering. The investigations give a detailed overview to classify and understand common salt mixtures, along with their critical RH thresholds. Specifically, with Type 1 mixtures showing less hygroscopic behavior because they contain more hydrating and sulfate salts, they are prone to crystallize and cause material decay, and often undergo cycles under relative humidity fluctuations around 61% to 72%. On the other hand, Type 2 mixtures are more hygroscopic due to more nitrate salts and can be linked to moisture stains and surface powdering, and they are mainly affected by lower RH levels around 28% to 46%. The analysis also confirmed that most samples contained at least five ions, with magnesium being less common. Four common mixtures were identified, consisting of sodium, potassium, nitrate, chloride, calcium or sulfate, with or without magnesium. Using the thermodynamic model ECOS/Runsalt, common solids and their behaviors for each mixture type were identified. For Type 1, these included niter, halite, aphthitalite, sodium and magnesium sulfates, bloedite, and darapskite. For Type 2, they were halite, calcium nitrate, niter, nitromagnesite, nitratine, and carnallite. Statistical analysis of the 11412 modeled samples confirmed these common solids, significantly reducing the potential phases to consider from over 85 to 14. It was observed that in

buildings with salt damage or moisture stains, the total salt content (excluding gypsum) is typically between 0.8-2% by weight in the first two centimeters of the material. Both Type 1 and Type 2 mixtures occur frequently in the first two centimeters of the surface, with Type 1 also identified at further depths and Type 2 tending to accumulate closer to the surface.

In the section 'Modeled versus experimental salt mixture behavior' the behavior of four mixtures were compared to their modeled ones to accurately predict phase changes under variable relative humidity (15-95%) at 20 °C. To replicate various realistic climatic conditions, rapid and slow RH changes were subjected to the mixtures (droplets), approximating an 80% RH change within minutes, over a week and a up to a month. Two of each mixture type were investigated, each containing five or six ions, Cl^-, NO_3^-, Na^+, K^+, including either SO_4^{2-} or Ca^{2+}, and excluding or including less common Mg^{2+}. The use of combined analytical techniques resulted in an innovative approach that presented important kinetic delays for crystallization and dissolution compared to the modeled behavior. These techniques included, time-lapse micrographs, dynamic vapor sorption, XRD, Raman and ESEM-EDX. The main results confirmed the accuracy of the ECOS/Runsalt model while noting deviations due to kinetic factors. Especially for Type 2 (calcium-rich) mixtures which showed remaining solution throughout the experiments under extreme dry environment. Other factors included kinetically hindered crystallization, delay effects due to the rate of supersaturation, and dissolution delays most likely caused by a combination of concentration gradients, surface tension, water activity, crystal microstructure, and surface characteristics. The processes are dynamic and complex, with various factors and inherent solution and crystal properties playing roles. These are areas of focus for fundamental research that need further attention, particularly in understanding the relationships between these factors and their impact on crystal behavior.

Implications for practice

This study offers significant impact for the practice by enhancing our knowledge about frequently identified salt mixture composition and behavior. This is an important step forward for developing more effective conservation strategies. The initial step in investigating salt decay involves sampling and ion analysis. The decision regarding the sampling method, specifically in terms of location (depth, height) and amount, primarily rests with a specialist. As described in section **Error! Reference source not found.**, the samples analyzed in this study are considered to represent best practice. The methodology for sampling remains unchanged as of this conclusion. For the ion analysis the introduction of an optimized method for charge balance calculations is an important step forward in accurately identifying the composition of salts in building materials. This improved methodology could be used as the basis for standard practice in future studies and could significantly enhance workflow procedures. However, some assumptions have been made regarding the salt content, which is considered a threshold for decay. This threshold was determined based on the expertise of specialists during the sampling process. Nonetheless, it is crucial to evaluate this salt content limit on a case-by-case basis in practical applications. Additionally, gypsum is often a major cause of decay when liquid water is present. This study focuses on salt mixture behavior under relative humidity changes below 95% RH, assuming that gypsum is less relevant. In practice, this assumption should not lead to the oversight of gypsum's potential impact. Its presence, especially in environments where liquid water is involved, can significantly contribute to decay processes. Consequently, while the results provide valuable insights into salt mixtures under varying humidity conditions, it is important for conservation scientists to carefully evaluate the role of gypsum in each specific case. This includes considering its interaction with other salts and the environmental conditions that might enhance its decay potential.

The availability of the data records, methodologies, and calculations made available in this dissertation allow general use and encourages further research and adaptations in this field. This open approach

facilitates collaborative efforts and the advancement of conservation science. Following appropriate analysis and data evaluation, the use of thermodynamic modeling is essential to understand mixture behavior. The modifications and improvements proposed for the ECOS/Runsalt model advance its utility in the conservation field. These advancements should be considered in future applications of the model, especially for studies involving salt mixtures in the built environment.

The improved data treatment and model use allowed a comprehensive analysis of large datasets, which led to the identification of frequently found salts and their behavior in a mixture. These are aspects that can be directly related to practical cases when looking at crystallization and dissolution events. The behavior can be linked to mixture compositions, which allows a better understanding of risk events and management decisions. Finally, little is known about the kinetics of salt mixtures, thus the identification of these processes showed their importance when interpreting model outputs. Specifically, for practical considerations this allows the understanding of the additional factor, such as, time and kinetic hindrance, affecting salt crystallization and dissolution. For example, when the critical crystallization relative humidity is defined by the thermodynamic behavior, the kinetic crystallization or dissolution delay can help indicate when phase changing can occur over time under realistic relative humidity changes. The findings also underline the need for incorporating these elements into future models. Bridging the theoretical and practical aspects of salt weathering is crucial for advancing risk assessment methodologies. This aspect is particularly important for conservation scientists aiming to predict and mitigate weathering effects on heritage materials.

Limitations and future work

The charge balance calculations presented include the most relevant ions found in the built environment, which are, chloride, nitrate, sulfate, sodium, potassium, magnesium, and calcium. However, in specific situations carbonate, fluoride, phosphate, oxalate, ammonia, acetate, or formate can occur. Extending the calculations with these ions can be helpful for future use cases. Additionally, the incorporation of the calculations in an online tool which can generate an overview of corrections applied would further benefit the overall understanding of the salt mixture identified. This is specifically important for equimolar contents of calcium sulfate and carbonate salts that are currently excluded from the mixture for modeling purposes. Although these corrections can be identified in the current calculation file, it remains critical to evaluate the results accordingly to avoid misinterpretation. The absence of these ions in standard models poses a challenge, as their presence can significantly alter the behavior and stability of salt mixtures. This oversight can lead to inaccuracies in modeling efforts, particularly in predicting salt crystallization and dissolution patterns under various environmental conditions. Therefore, integrating these ions into more comprehensive models is essential for a more accurate representation of real-world scenarios, enhancing the predictive power and reliability of our modeling efforts.

Moving forward, it remains important to investigate specific questions that were raised during the research presented in this dissertation. Future research activities should broaden their focus beyond droplet experiments, considering the additional influences when dealing with solutions in confined pore spaces. This is mainly important as further crystallization and dissolution delays have been documented in studies such as Desarnaud et al. (2014), (2015) and Godts et al. (2021). Hereby, the inertia of a porous media can influence the behavior of salt mixtures, as it moves through or interacts with the media. In this context future studies should explore, the influence of evaporation rates, capillary forces, pore-clogging, separation of solids from the original mixture, viscosity, and concentration gradients in the solution. This also includes other aspects, such as, pore-scale dynamics, imbibition, and wicking effects. The use of capillaries or micromodels simulating the pore-space in

combination with the analytical methods described in this dissertation can be particularly useful for future investigations to identify the above mentioned influencing factors.

The importance of considering salt kinetics when estimating the number of crystallization cycles in a given setting is influenced by many factors, such as the exposed surface area of crystals/solution (unconfined versus confined), the behavior of each individual mixture composition, the resolution and location of climate measurements. Crystallization and dissolution times in combination with accurate determination of critical RH events are important when using climate data for risk assessment. At low RH gradients, the crystallization and dissolution times drastically increase. The determination of relevant RH thresholds (RH equilibrium for a single salt or equilibria for a salt mixture) is also a critical factor. Additionally, the use of specific climatic location data is important for an accurate assessment and that climate data at low spatial resolution (i.e., one site used to represent an entire urban area) can significantly influence the frequency of cycles. Seasonal buffering is also of importance in the urban context and microclimates, rather than typically using measured meteorological data.

Furthermore, the use of an indicator based on a single salt does not represent the more common real-world scenario of salts present in a mixture. The application of a simple indicator (threshold, based on a variable 'averaging window' of time) demonstrates a significant difference in estimated number of cycles, further detailed in De Kock et al. (2021) and Godts et al. (2021). In summary, future research can build on the results presented in this dissertation and should channel efforts towards the refinement of existing thermodynamic models, perhaps embedding kinetic aspects in hygrothermal models, and embracing a broader spectrum of environmental variables such as temperature fluctuations, moisture dynamics, and material-specific responses. This evolution is essential to simulate salt behavior more realistically, thereby enhancing the predictive accuracy of conservation strategies under diverse climatic scenarios. While these aspects were not specifically addressed within this dissertation, they have been explored in related works, including Flatt et al. (2017), D'Altri et al. (2021), De Kock et al. (2021), Godts et al. (2021), Gulotta et al. (2021) and Chan (2023).

Final perspective

The findings presented support an overall approach for ion data analysis, and interpretation, predictive modeling and realistic (droplet) salt mixture behavior, which aid future research efforts and a more effective management of salt weathering challenges in conservation practices. The impact of this research extends beyond the confines of built heritage conservation to geological investigations. However, understanding the behavior of complex salt mixtures under real-world conditions remains an uncharted territory, especially considering the diversity of salts and environmental dynamics. Future research should aim to fill these gaps, thereby contributing to the development of more comprehensive and adaptable conservation methodologies. The road ahead requires a collaborative approach across various disciplines, the exchange of ideas, knowledge, and best practices can lead to important innovations and sustainable conservation solutions.

5. DISSEMINATION AND VALORIZATION

Key publications

1. Godts, S., 2024. Salts in the Built Environment. PhD dissertation, Ghent University and the University of Antwerp, Ghent, Belgium.
2. Godts, S., Steiger, M., Stahlbuhk, A., Orr, S.A., Desarnaud, J., De Clercq, H., Cnudde, V., De Kock, T., 2024. Modeled versus experimental salt mixture behavior under variable humidity. ACS Omega. 10.1021/acsomega.4c01486
3. Godts, S., Orr, S.A., Steiger, M., Stahlbuhk, A., De Kock, T., Desarnaud, J., De Clercq. H., Cnudde, V., 2023. Salt mixtures in stone weathering. Sci Rep 13, 13306. 10.1038/s41598-023-40590-y
4. Godts, S., Steiger, M., Orr, S.A., Stahlbuhk, A., Desarnaud, J., De Clercq, H., Cnudde, V., De Kock, T., 2022. Modeling Salt Behavior with ECOS/RUNSALT: Terminology, Methodology, Limitations, and Solutions. Heritage, 5, 3648-3663. 10.3390/heritage5040190
5. Godts, S., Steiger, M., Orr, S.A., De Kock, T., Desarnaud, J., De Clercq, H., Cnudde, V., 2022. Charge balance calculations for mixed salt systems applied to a large dataset from the built environment. Sci Data 9, 324. 10.1038/s41597-022-01445-9
6. Godts, S., Orr, S. A., Steiger, M., & De Kock, T., 2022. Mixed salt systems in the built environment - charge balance calculations [Data set]. Zenodo. 10.5281/zenodo.6280617
7. Godts, S., Orr, S.A., Desarnaud, J., Steiger, M., Wilhelm, K., De Clercq H., Cnudde, V. and De Kock, T., 2021. NaCl-related weathering of stone: the importance of kinetics and salt mixtures in environmental risk assessment. Herit Sci. 9:44. 10.1186/s40494-021-00514-3

International seminars and presentations

1. Godts, S., Stahlbuhk, A., Desarnaud, J., Orr, S.A., Crevals, V., De Clercq, H., De Kock, T., Cnudde, V., Steiger, M., 2023. Expect the unexpected: when increasing relative humidity causes non-hydrating salts to crystallize from a mixture, in: Abuku, M., Takatori, N. (Eds.), First International Conference in Asia on Salt Weathering of Buildings and Stone Sculptures. Presented at the SWBSS ASIA 2023, Japan Laboratory of Building Physics, Faculty of Architecture, Kindai University, Nara, Japan, pp. 135–146. https://repository.hawk-hhg.de/images/9/97/SWBSS_ASIA_2023_Proceedings.pdf
2. Desarnaud, J., Godts, S., Crevals, V., Dubois, S., de Bouw, M., and Vanhellemont, Y., 2023. A combination of salt analyses, thermodynamic modelling, and experimental observations to preserve Built Heritage: Case of Cordouan lighthouse, in: Abuku, M., Takatori, N. (Eds.), First International Conference in Asia on Salt Weathering of Buildings and Stone Sculptures. Presented at the SWBSS ASIA 2023, Japan Laboratory of Building Physics, Faculty of Architecture, Kindai University, Nara, Japan, pp. 91–102. https://repository.hawk-hhg.de/images/9/97/SWBSS_ASIA_2023_Proceedings.pdf
3. Crevals, V., Godts, S., Desarnaud, J., 2023. Desalination of brick masonry by means of a traditional lime plaster, in: Abuku, M., Takatori, N. (Eds.), First International Conference in Asia on Salt Weathering of Buildings and Stone Sculptures. Presented at the SWBSS ASIA 2023, Japan Laboratory of Building Physics, Faculty of Architecture, Kindai University, Nara, Japan, pp. 237–245. https://repository.hawk-hhg.de/images/9/97/SWBSS_ASIA_2023_Proceedings.pdf
4. Gulotta, D. and RILEM TC 271-ASC members, (incl. Godts, S.), 2023, The new RILEM TC 271-ASC recommendation for the durability assessment of porous building materials against salt crystallization, in: Abuku, M., Takatori, N. (Eds.), First International Conference in Asia on Salt Weathering of Buildings and Stone Sculptures. Presented at the SWBSS ASIA 2023, Japan Laboratory of Building Physics, Faculty of Architecture, Kindai University, Nara, Japan, pp. 221–224. https://repository.hawk-hhg.de/images/9/97/SWBSS_ASIA_2023_Proceedings.pdf

5. Crevals, V., Godts, S., Desarnaud, J., 2023. Salts in the 16th century mural painting of The Last Judgment in the leper hospice in Rumst, Belgium. Presented at the 2nd International Conference on Moisture in Buildings (ICMB23), online, 3-4 July 2023. https://doi.org/10.14293/icmb230054
6. Godts, S., et al., 2023. Identification of common salt mixtures and experimental verification of the calculated crystallization behavior. CrysPom VIII - The 8th International Workshop on Crystallization in Porous Media, 13-15 June 2023, Het Pand, Gent, Belgium.
7. Godts, S., et al., 2023. The Crystallization Behavior of Common Salt Mixtures Found in the Built Environment. Extended abstract and oral presentation. DACG 50, Dutch Association for Crystal Growth 50th Anniversary International Symposium, 20 -22 March 2023, Amsterdam Science Park, The Netherlands.
8. Godts, S. and Orr, S. A., 2022. Understanding salt mixture behavior: modeling and kinetics. ENBRI BBRI Expert Workshop, 21-22 Sep. 2022, Brussels
9. Orr, S. A. and Godts, S., 2022. Common salt mixtures in the built environment, Towards the integration of salts into hygrothermal studies. ENBRI BBRI Expert Workshop, 21-22 Sep. 2022, Brussels
10. Orr, S. A. and Godts, S. and De Kock. T., 2022. A data-driven approach to understanding the equilibria behaviour of salt mixtures in built cultural heritage. EGU General Assembly 23–27 May 2022, Vienna, Austria & Online. http://doi.org/10.5194/egusphere-egu22-5264
11. Godts, S., De Kock, T., Steiger, M., Orr, S. A., Desarnaud, J., De Clercq, H. and Cnudde. V., 2022. Common salt mixtures in the built environment, at DS2BE, Doctoral Seminars on Sustainability Research in the Built Environment. Ghent University. 24 & 25 May 2022, Ghent
12. Godts, S., Steiger, M., De Kock, T., Desarnaud, J., Orr, S.A., Cnudde, V. and De Clercq, H, 2021. Investigating the behavior of common salt mixtures in stone materials, in: Lubelli, B., Kamat, A. and Quis, W (eds.): Fifth International Conference on Salt Weathering of Buildings and Stone Sculptures: proceedings of SWBSS 2021 / 22-24 September 2021 Delft, the Netherlands, p. 49-51. https://books.bk.tudelft.nl/press/catalog/book/791
13. Crevals, V., Godts, S., and Desarnaud, J., 2021. Salt problems and climate control in the case of the church of Sint-Aldegondis in Mespelare, Belgium, an ECOS/Runsalt approach, in: Lubelli, B., Kamat, A. and Quis, W (eds.): Fifth International Conference on Salt Weathering of Buildings and Stone Sculptures: proceedings of SWBSS 2021 / 22-24 September 2021 Delft, the Netherlands, p. 13-20. https://books.bk.tudelft.nl/press/catalog/book/791
14. De Kock, T., Orr, S. A., Guilbert, D., Godts, S., Caluwaerts, S., Cnudde, V. and Desarnaud, J., 2021. Implications of using meteorological records to assess the environmental risk of salt crystallization cycles in stone, in: Lubelli, B., Kamat, A. and Quis, W (eds.): Fifth International Conference on Salt Weathering of Buildings and Stone Sculptures: proceedings of SWBSS 2021 / 22-24 September 2021 Delft, the Netherlands, p. 31-39. https://books.bk.tudelft.nl/press/catalog/book/791
15. Lubelli, B., and RILEM TC 271-ASC members (incl. Godts, S.), 2021. A new accelerated laboratory test for the assessment of the durability of materials with respect to salt crystallization, in: Lubelli, B., Kamat, A. and Quis, W (eds.): Fifth International Conference on Salt Weathering of Buildings and Stone Sculptures: proceedings of SWBSS 2021 / 22-24 September 2021 Delft, the Netherlands, p. 55-67. https://books.bk.tudelft.nl/press/catalog/book/791
16. Gulotta, D., Godts, S., De Kock, T. and Steiger, M., 2021. Comparative estimation of the pore filling of single salts in natural stone, in: Lubelli, B., Kamat, A. and Quis, W (eds.): Fifth International Conference on Salt Weathering of Buildings and Stone Sculptures: proceedings of SWBSS 2021 / 22-24 September 2021 Delft, the Netherlands, p. 79-88. https://books.bk.tudelft.nl/press/catalog/book/791

17. Nunes, C., Godts, S., Aguilar Sanchez, A.M., Slížková, Z., and Lubelli, B., 2021. Towards a new salt crystallisation test: comparison of salt contamination procedures, in: Lubelli, B., Kamat, A. and Quis, W (eds.): Fifth International Conference on Salt Weathering of Buildings and Stone Sculptures: proceedings of SWBSS 2021 / 22-24 September 2021 Delft, the Netherlands, p. 69-77. https://books.bk.tudelft.nl/press/catalog/book/791

18. Godts, S., Steiger, M., Desarnaud, J., Orr, S. A., Cnudde, V., De Clercq, H. and De Kock, T., 2021. Exploring the crystallization and dissolution behavior of NaCl, in: Derluyn, H. et al (eds): CRYSPOM VII: International workshop Crystallization in Porous Media, 7-9 June 2021 Pau, France

19. Crevals, V., Godts, S., Desarnaud, J., 2021. The influence of hygroscopic humidity from salts on moisture measurements in the case of the ‘ Boskapel ’ chapel in Imde-Meise , Belgium, in: 1st International Conference on Moisture in Buildings 2021 (ICMB21), online, 28-29 June 2021 http://doi.org/10.14293/ICMB210018

20. Qajar, J., Godts, S., Raoof, A., Cnudde, V. Phase transition of salt mixtures in porous media during drying using advanced optical microscopy, spectroscopy and X-ray tomography. EGU General Assembly 2024, Session: (MS10) Advances in imaging porous media: techniques, software and case studies.

21. De Groeve, M., Kale, E., Godts, S., Orr, S.A., De Kock, T., 2024. Impact of vertical greening on urban microclimate and historic building materials: A meta-analysis. Building and Environment, 253, 111365. https://doi.org/10.1016/j.buildenv.2024.111365.

22. Qajar, J., Godts, S., Baghery, M., Raoof, A., Cnudde, V., 2023. Microfluidic study of salt crystallization in porous media. Poster. Geosciences Research Day at Utrecht University, October 2023.
http://posters.geo.uu.nl/2023/Microfluidic_study_of_salt_crystallization_in_porous_media-Qajar_Godts_Baghery_Raoof_Cnudde-October2023.pdf

23. Lubelli, B., Rörig-Daalgard, I., Aguilar, A.M., and RILEM TC 271-ASC members (incl. Godts, S.), 2023. Recommendation of RILEM TC 271-ASC: New accelerated test procedure for the assessment of resistance of natural stone and fired-clay brick units against salt crystallization. Mater Struct 56, 101. https://doi.org/10.1617/s11527-023-02158-0

24. Nunes, C., Aguilar Sanchez, A.M., Godts, S., Gulotta, D., Ioannou, I., et al., 2021. Towards a more effective and reliable salt crystallisation test for porous building materials: Experimental research on salt contamination procedures and methods for assessment of the salt distribution. Construction and Building Materials, Elsevier, 298, https://doi.org/10.1016/j.conbuildmat.2021.123862

7. ACKNOWLEDGEMENTS

We wish to acknowledge the Belgium Science Policy (Belspo) for the financial support and recognizing the significance of Built Heritage Conservation. We also wish to acknowledge several (postgraduate) interns, Simone Semprini, Alexandre Gillon, Katrijn De Cock, and others for their initial experimental work with ESEM-EDX, XRD, micrograph analysis, and Raman spectroscopy, which helped to optimize the final methods and data gathering. We also acknowledge Mohamed Rich, Xavier Monfort, and countless interns over the years for the many site visits, sometimes deep underground or high up in church towers on wobbly scaffolding, and the thousands of tedious ion analysis preformed over the years. We also would like to thank Bhavesh Shah for his continuing efforts on a web tool integrating this work. As well as Zuzana Slizkova and Cristiana Lara Nunes at the Institute of Theoretical and Applied Mechanics (ITAM CAS, Prague) for providing ion data from four different sites in the Czech Republic to the dataset. The authors further acknowledge the funding for the GenRH humidity generator through “BOF, project UG_2832369580”, “JPI-JHEP project KISADAMA” and “FWO Research Grant 1521815N”.

8. REFERENCES

Archer, D. G., & Kirklin, D. R. (2002). Enthalpies of Solution of Sodium Chloride and Potassium Sulfate in Water. Thermodynamic Properties of the Potassium Sulfate + Water System. *Journal of Chemical & Engineering Data*, *47*(1), 33–46. https://doi.org/10.1021/je010118a

Arnold, A., & Küng, A. (1985). Crystallization and habit of salt efflorescences on walls I. In G. Félix (Ed.), *5th International Congress on Deterioration and Conservation of Stone, Lausanne, Switzerland, 25-27 September 1985* (pp. 255–267). Presses Romandes.

Arnold, A., & Zehnder, K. (1987). *Monitoring wall paintings affected by soluble salts* (S. Cather, Ed.; pp. 103–135). The Courtauld Institute of Fine Art and The Getty Conservation Institute.

Benavente, D., de Jongh, M., & Cañaveras, J. C. (2020). Weathering Processes and Mechanisms Caused by Capillary Waters and Pigeon Droppings on Porous Limestones. *Minerals*, *11*(1), 18. https://doi.org/10.3390/min11010018

Benavente, D., García del Cura, M. A., Fort, R., & Ordóñez, S. (2004). Durability estimation of porous building stones from pore structure and strength. *Engineering Geology*, *74*(1–2), 113–127. https://doi.org/10.1016/j.enggeo.2004.03.005

Benavente, D., Sanchez-Moral, S., Fernandez-Cortes, A., Cañaveras, J. C., Elez, J., & Saiz-Jimenez, C. (2011). Salt damage and microclimate in the Postumius Tomb, Roman Necropolis of Carmona, Spain. *Environmental Earth Sciences*, *63*(7–8), 1529–1543. https://doi.org/10.1007/s12665-010-0815-9

Bionda, D. (2005). *RUNSALT - A graphical user interface to the ECOS thermodynamic model for the prediction of the behaviour of salt mixtures under changing climate conditions. Http://science.sdf-eu.org/runsalt/* (Version 1.9) [Xlisp]. http://science.sdf-eu.org/runsalt/

Bionda, D. (2006). *Modelling indoor climate and salt behaviour in historical buildings*. Swiss Federal Institute of Technology.

Brimblecombe, P. (2003). *The Effects of Air Pollution on the Built Environment* (Vol. 2). PUBLISHED BY IMPERIAL COLLEGE PRESS AND DISTRIBUTED BY WORLD SCIENTIFIC PUBLISHING CO. https://doi.org/10.1142/p243

Chan, C. (2023). *Understanding common salt mixtures in the built environment: Temperature effect* [Master thesis]. UCL Institute for Sustainable Heritage.

Charola, A. E. (2000). Salts in the Deterioration of Porous Materials: An Overview. *Journal of the American Institute for Conservation*, *39*(3), 327–343. https://doi.org/10.1179/019713600806113176

Charola, A. E., Pühringer, J., & Steiger, M. (2007). Gypsum: A review of its role in the deterioration of building materials. *Environmental Geology*, *52*(2), 339–352. https://doi.org/10.1007/s00254-006-0566-9

Charola, A., & Lewin, S. (1979). Efflorescence on building stones—SEM in the characterization and elucidation of the mechanism of formation. *Scan Electron Microsc*, *79*(I), 379–387.

Clegg, S. L., & Brimblecombe, P. (2000). Pitzer Model of Electrolyte Solutions. In C. A. Price (Ed.), *An Expert Chemical Model for Determining the Environmental Conditions Needed to Prevent Salt Damage in Porous Materials: Project ENV4-CT95-0135 (1996-2000) Final Report; Protection and conservation of the European Cultural Heritage* (pp. 13–18). Archetype.

Clegg, S. L., & Pitzer, K. S. (1992). Thermodynamics of multicomponent, miscible, ionic solutions: Generalized equations for symmetrical electrolytes. *The Journal of Physical Chemistry*, *96*(8), 3513–3520. https://doi.org/10.1021/j100187a061

Clegg, S. L., Pitzer, K. S., & Brimblecombe, P. (1992). Thermodynamics of Multicomponent, Miscible, Ionic Solutions. 2. Mixtures Including Unsymmetrical Electrolytes. *J. Phys. Chem.*, *96*, 9470–9479. https://doi.org/10.1021/j100202a074

Costa, F. M. da C., Henriques Rosa, M. A. N., Canetto, M., & Sobral da Fonseca, M. J. (2022). The degradation of the “Study room” (Convent of Christ, Tomar, Portugal), from a preliminary analysis towards a sustainable maintenance. *Ge-Conservacion*, *21*(1), 95–107. https://doi.org/10.37558/gec.v21i1.1052

D’Altri, A. M., de Miranda, S., Beck, K., De Kock, T., & Derluyn, H. (2021). Towards a more effective and reliable salt crystallisation test for porous building materials: Predictive modelling of sodium chloride salt distribution. *Construction and Building Materials*, *304*, 124436. https://doi.org/10.1016/j.conbuildmat.2021.124436

De Clercq, H., Jovanović, M., Linnow, K., & Steiger, M. (2013). Performance of limestones laden with mixed salt solutions of Na2SO4–NaNO3 and Na2SO4–K2SO4. *Environmental Earth Sciences*, *69*(5), 1751–1761. https://doi.org/10.1007/s12665-012-2017-0

De Kock, T., Orr, S. A., Guilbert, D., Godts, S., Caluwaerts, S., Cnudde, V., & Desarnaud, J. (2021). Implications of using meteorological records to assess the environmental risk of salt crystallization cycles in stone. In B. Lubelli, A. Kamat, & W. J. Quist (Eds.), *Fifth International Conference on Salt Weathering of Buildings and Stone Sculptures: Proceedings of SWBSS 2021 / 22-24 September* (pp. 31–39). TU Delft Open.

Derluyn, H. (2012). *Salt transport and crystallization in porous limestone. Neutron-X-ray imaging and poromechanical modeling. DISS. ETH NO. 20673*.

Derluyn, H., Moonen, P., & Carmeliet, J. (2014). Deformation and damage due to drying-induced salt crystallization in porous limestone. *Journal of the Mechanics and Physics of Solids*, *63*, 242–255. https://doi.org/10.1016/j.jmps.2013.09.005

Desarnaud, J., Derluyn, H., Carmeliet, J., Bonn, D., & Shahidzadeh, N. (2014). Metastability Limit for the Nucleation of NaCl Crystals in Confinement. *The Journal of Physical Chemistry Letters*, *5*(5), 890–895. https://doi.org/10.1021/jz500090x

Desarnaud, J., Derluyn, H., Grementieri, L., Molari, L., de Miranda, S., Cnudde, V., & Shahidzadeh, N. (2016). *Salt weathering of sandstone during drying: Effect of primary and secondary crystallisation*. 299–307.

Desarnaud, J., Derluyn, H., Molari, L., de Miranda, S., Cnudde, V., & Shahidzadeh, N. (2015). Drying of salt contaminated porous media: Effect of primary and secondary nucleation. *Journal of Applied Physics*, *118*(11), 114901. https://doi.org/10.1063/1.4930292

Desarnaud, J., & Shahidzadeh-Bonn, N. (2011). Salt crystal purification by deliquescence/crystallization cycling. *EPL (Europhysics Letters)*, *95*(4), 48002. https://doi.org/10.1209/0295-5075/95/48002

Doehne, E. (2002). Salt Weathering: A Selective Review. *Geological Society Special Publications*, *205*, 51–64. https://doi.org/10.1144/GSL.SP.2002.205.01.05

Doehne, E., & Price, C. A. (2010). *Stone conservation: An overview of current research* (2nd ed). Getty Conservation Institute.

Ehret, W. F. (1932). Ternary Systems: CaCl2-Ca(NO3)2-H2O (25°), CaCl2-Ca(ClO3)2-H2O (25°) SrCl2-Sr(NO3)2-H2O (25°), KNO2-Pb(NO3)2-H2O (0°). *Journal of the American Chemical Society*, *54*, 3126–3134.

Evans, I. S. (1970). Salt crystallization and rock weathering: A review. *Rev Geomorphol Dyn.*, *19(4)*, 153–177.

Flatt, R., Aly Mohamed, N., Caruso, F., Derluyn, H., Desarnaud, J., Lubelli, B., Espinosa Marzal, R. M., Pel, L., Rodriguez-Navarro, C., Scherer, G. W., Shahidzadeh, N., & Steiger, M. (2017). Predicting salt damage in practice: A theoretical insight into laboratory tests. *RILEM Technical Letters*, *2*, 108–118. https://doi.org/10.21809/rilemtechlett.2017.41

Flatt, R., & Bocherens, P. (1962). Sur le système ternaire Ca^{++}_K^{+}_NO_3^{-}_H_2O. *Helv. Chim. Acta 45*, *45*(1), 187–195. https://doi.org/10.1002/hlca.19620450124

Flatt, R. J. (2002). Salt damage in porous materials: How high supersaturations are generated. *Journal of Crystal Growth*, *242*(3–4), 435–454. https://doi.org/10.1016/S0022-0248(02)01429-X

Flatt, R. J., Caruso, F., Sanchez, A. M. A., & Scherer, G. W. (2014). Chemo-mechanics of salt damage in stone. *Nature Communications*, *5*(1), 4823. https://doi.org/10.1038/ncomms5823

Flatt, R. J., Steiger, M., & Scherer, G. W. (2007). A commented translation of the paper by C.W. Correns and W. Steinborn on crystallization pressure. *Environmental Geology*, *52*(2), 187–203. https://doi.org/10.1007/s00254-006-0509-5

Godts, S. (2023). *Locations of 338 sites where in total 11412 drill samples were taken for the determination of quantitative ion concentrations (KMZ data file).* Figshare. 10.6084/m9.figshare.23616750

Godts, S., Hayen, R., & Clercq, H. D. (2014). Common Salt Mixtures Database: A Tool to Identify Research Needs. *3rd International Conference on Salt Weathering of Buildings and Stone Sculptures, Brussels, Belgium, 14–16 October 2014*, 14.

Godts, S., Hayen, R., & De Clercq, H. (2017). Investigating salt decay of stone materials related to the environment, a case study in the St. James church in Liège, Belgium. *Studies in Conservation*, *62*(6), 329–342. https://doi.org/10.1080/00393630.2016.1236997

Godts, S., Orr, S. A., Desarnaud, J., Steiger, M., Wilhelm, K., De Clercq, H., Cnudde, V., & De Kock, T. (2021). NaCl-related weathering of stone: The importance of kinetics and salt mixtures in environmental risk assessment. *Heritage Science*, *9*(44), 1:13. https://doi.org/10.1186/s40494-021-00514-3

Godts, S., Orr, S. A., Steiger, M., & De Kock, T. (2022). *Mixed salt systems in the built environment—Charge balance calculations [Data set]. Available at https://zenodo.org/record/6280617#.Y3yzyUnMJjF*. Zenodo. https://doi.org/10.5281/zenodo.6280617

Godts, S., Orr, S. A., Steiger, M., Stahlbuhk, A., De Kock, T., Desarnaud, J., De Clercq, H., & Cnudde, V. (2023). Salt mixtures in stone weathering. *Scientific Reports*, *13*(1), 13306. https://doi.org/10.1038/s41598-023-40590-y

Godts, S., Steiger, M., Orr, S. A., De Kock, T., Desarnaud, J., De Clercq, H., & Cnudde, V. (2022). Charge balance calculations for mixed salt systems applied to a large dataset from the built environment. *Scientific Data*, *9*(1), 324. https://doi.org/10.1038/s41597-022-01445-9

Godts, S., Steiger, M., Orr, S. A., Stahlbuhk, A., Desarnaud, J., De Clercq, H., Cnudde, V., & De Kock, T. (2022). Modeling Salt Behavior with ECOS/RUNSALT: Terminology, Methodology, Limitations, and Solutions. *Heritage*, *5*(4), 3648–3663. https://doi.org/10.3390/heritage5040190

Godts, S., Steiger, M., Stahlbuhk, A., Orr, S. A., Desarnaud, J., Clercq, H. D., Cnudde, V., & Kock, T. D. (2024). Modeled versus Experimental Salt Mixture Behavior under Variable Humidity. *ACS Omega*. https://doi.org/10.1021/acsomega.4c01486

Goudie, A., & Viles, H. (1997). *Salt Weathering Hazards*. John Wiley & Sons.

Grossi, C. M., Brimblecombe, P., Menendez, B., Benavente, D., Harris, I., & Déqué, M. (2011). Climatology of salt transitions and implications for stone weathering. *Sci Total Environ.*, *409(13)*, 2577–2585.

Gulotta, D., Godts, S., De Kock, T., & Steiger, M. (2021). Comparative estimation of the pore filling of single salts in natural stone. In B. Lubelli, A. A. Kamat, & W. J. Quist (Eds.), *Fifth International Conference on Salt Weathering of Buildings and Stone Sculptures, Delft, Netherlands, 22-24 September 2021*. TU Delft Open. https://hdl.handle.net/10067/1810480151162165141

Lindström, N., Heitmann, N., Linnow, K., & Steiger, M. (2015). Crystallization behavior of NaNO3–Na2SO4 salt mixtures in sandstone and comparison to single salt behavior. *Applied Geochemistry*, *63*, 116–132. https://doi.org/10.1016/j.apgeochem.2015.07.007

Lindström, N., Talreja, T., Linnow, K., Stahlbuhk, A., & Steiger, M. (2016). Crystallization behavior of Na_2SO_4–$MgSO_4$ salt mixtures in sandstone and comparison to single salt behavior. *Applied Geochemistry*, *69*, 50–70. https://doi.org/10.1016/j.apgeochem.2016.04.005

Lubelli, B., Cnudde, V., Diaz-Goncalves, T., Franzoni, E., van Hees, R. P. J., Ioannou, I., Menendez, B., Nunes, C., Siedel, H., Stefanidou, M., Verges-Belmin, V., & Viles, H. (2018). Towards a more effective and reliable salt crystallization test for porous building materials: State of the art. *Materials and Structures*, *51*(2), 55. https://doi.org/10.1617/s11527-018-1180-5

Lubelli, B., Rörig-Daalgard, I., Aguilar, A. M., Aškrabić, M., Beck, K., Bläuer, C., Cnudde, V., D'Altri, A. M., Derluyn, H., Desarnaud, J., Diaz Gonçalves, T., Flatt, R., Franzoni, E., Godts, S., Gulotta, D., van Hees, R., Ioannou, I., Kamat, A., De Kock, T., … Vergès-Belmin, V. (2023). Recommendation of RILEM TC 271-ASC: New accelerated test procedure for the assessment of resistance of natural stone and fired-clay brick units against salt crystallization. *Materials and Structures*, *56*(5), 101. https://doi.org/10.1617/s11527-023-02158-0

Meldrum, F. C., & O'Shaughnessy, C. (2020). Crystallization in Confinement. *Advanced Materials*, *32*(31), 2001068. https://doi.org/10.1002/adma.202001068

Menéndez, B. (2017). Estimation of salt mixture damage on built cultural heritage from environmental conditions using ECOS-RUNSALT model. *Journal of Cultural Heritage*, *24*, 22–30. https://doi.org/10.1016/j.culher.2016.11.006

Menéndez, B. (2018). Estimators of the Impact of Climate Change in Salt Weathering of Cultural Heritage. *Geosciences*, *8*(11), 401. https://doi.org/10.3390/geosciences8110401

Morillas, H., Maguregui, M., Paris, C., Bellot-Gurlet, L., Colomban, P., & Madariaga, J. M. (2015). The role of marine aerosol in the formation of (double) sulfate/nitrate salts in plasters. *Microchemical Journal*, *123*, 148–157. https://doi.org/10.1016/j.microc.2015.06.004

Piqué, F., Dei, L., & Ferroni, E. (1992). Physicochemical Aspects of the Deliquescence of Calcium Nitrate and Its Implications for Wall Painting Conservation. *Studies in Conservation*, *37*(4), 217–227. https://www.jstor.org/stable/1506351

Pitzer, K. S. (1981). The Treatment of Ionic Solutions over the Entire Miscibility Range. *Berichte Der Bunsengesellschaft Für Physikalische Chemie*, *85*(11), 952–959. https://doi.org/10.1002/bbpc.19810851107

Pitzer, K. S., & Simonson, J. M. (1986). Thermodynamics of multicomponent, miscible, ionic systems: Theory and equations. *The Journal of Physical Chemistry*, *90*(13), 3005–3009. https://doi.org/10.1021/j100404a042

Price, C. (2000). *An expert chemical model for determining the environmental conditions needed to prevent salt damage in porous materials: Protection and conservation of the European cultural heritage ; project ENV4-CT95-0135 (1996-2000) final report*. Archetype.

Rodriguez-Navarro, C., & Doehne, E. (1999). Salt weathering: Influence of evaporation rate, supersaturation and crystallization pattern. *Earth Surf. Process. Landforms*, 20. https://doi.org/10.1002/(SICI)1096-9837(199903)24:3<191::AID-ESP942>3.0.CO;2-G

Rörig-Dalgaard, I. (2021). Direct Measurements of the Deliquescence Relative Humidity in Salt Mixtures Including the Contribution from Metastable Phases. *ACS Omega*, *6*(25), 16297–16306. https://doi.org/10.1021/acsomega.1c00538

Sabbioni, C., Brimblecomb, P., & Cassar, M. (2012). *The atlas of climate change impact on European cultural heritage: Scientific analysis and management strategies*. Anthem.

Sawdy, A., & Heritage, A. (2007). Evaluating the influence of mixture composition on the kinetics of salt damage in wall paintings using time lapse video imaging with direct data annotation. *Environmental Geology*, *52*(2), 303–315. https://doi.org/10.1007/s00254-006-0496-6

Sawdy, A., Heritage, A., & Pel, L. (2008). A review of salt transport in porous media: Assessment methods and salt reduction treatments. *Salt Weathering on Buildings and Stone Sculptures (SWBSS)*.

Shahidzadeh, N., Schut, M. F. L., Desarnaud, J., Prat, M., & Bonn, D. (2015). Salt stains from evaporating droplets. *Scientific Reports*, *5*(1), 10335. https://doi.org/10.1038/srep10335

Shen, Y., Linnow, K., & Steiger, M. (2020). Crystallization Behavior and Damage Potential of Na_2SO_4–NaCl Mixtures in Porous Building Materials. *Crystal Growth & Design*, *20*(9), 5974–5985. https://doi.org/10.1021/acs.cgd.0c00671

Siedel, H. (2018). Salt efflorescence as indicator for sources of damaging salts on historic buildings and monuments: A statistical approach. *Environmental Earth Sciences*, *77*(16), 572. https://doi.org/10.1007/s12665-018-7752-4

Siegesmund, S., & Snethlage, R. (2014). *Stone in architecture: Properties, durability* (5th ed.). Springer.

Silcock, H. L. (1979). *Solubilities of Inorganic and Organic Compounds. Ternary and Multicomponent Systems of Inorganic Substances* (Vol. 3). Pergamon Press.

Stahlbuhk, A. (2021). *Untersuchung bauwerksrelevanter Nitratsalze im Hinblick auf ihr Schadenspotenzial, mit Studien zum Fallbeispiel des Wandmalereizyklus im Kreuzgang des Schleswiger Doms* [PhD Dissertation].

Stahlbuhk, A., & Steiger, M. (2022). Damage potential and supersaturation of KNO3 and relevance in the field of salt damage to porous building material. *Construction and Building Materials*, *325*, 126516. https://doi.org/10.1016/j.conbuildmat.2022.126516

Steiger, M. (2005a). Crystal growth in porous materials—II: Influence of crystal size on the crystallization pressure. *Journal of Crystal Growth*, *282*(3–4), 470–481. https://doi.org/10.1016/j.jcrysgro.2005.05.008

Steiger, M. (2005b). Salts in Porous Materials: Thermodynamics of Phase Transitions, Modeling and Preventive Conservation. *Restoration of Buildings and Monuments*, *11*(6), 419–432. https://doi.org/10.1515/rbm-2005-6002

Steiger, M. (Unpublished). *Dataset of Efflorescence reported in 112 journal articles and conference papers. University of Hamburg.* [Personal communication].

Steiger, M., Charola, A. E., & Sterflinger, K. (2014). Weathering and Deterioration. In S. Siegesmund & R. Snethlage (Eds.), *Stone in Architecture* (pp. 225–316). Springer Berlin Heidelberg. https://doi.org/10.1007/978-3-642-45155-3_4

Steiger, M., & Heritage, A. (2012, October 22). Modelling the crystallization behaviour of mixed salt systems: Input data requirements. *12th International Congress on the Deterioration and Conservation of Stone, New York, NY, USA*.

Steiger, M., Kiekbusch, J., & Nicolai, A. (2008). An improved model incorporating Pitzer's equations for calculation of thermodynamic properties of pore solutions implemented into an efficient program code. *Construction and Building Materials*, *22*(8), 1841–1850. https://doi.org/10.1016/j.conbuildmat.2007.04.020

Steiger, M., Linnow, K., Ehrhardt, D., & Rohde, M. (2011). Decomposition reactions of magnesium sulfate hydrates and phase equilibria in the $MgSO_4$–H_2O and Na^+–Mg^{2+}–Cl^-–SO_4^{2-}–H_2O systems with implications for Mars. *Geochimica et Cosmochimica Acta*, *75*(12), 3600–3626. https://doi.org/10.1016/j.gca.2011.03.038

Sunagawa, I. (1981). Characteristics of crystal growth in nature as seen from the morphology of mineral crystals. *Bulletin de Minéralogie*, *104*(2), 81–87. https://doi.org/10.3406/bulmi.1981.7438

Sunagawa, I. (2005). *Crystals Growth, Morphology and Perfection*. Cambridge University Press.

Vergès-Belmin, V. (2008). *ICOMOS-ISCS: Illustrated glossary on stone deterioration patterns* (English-French version). ICOMOS.

Von Konow, T. (2002). *Test results. The study of salt deterioration mechanisms. Decay of brick walls influenced by interior climate changes.* (T. von Konow, Ed.). Suomenlinnan Hoitokunta.

ANNEXES

Data records

The data records, as described in the section 'Analysis of salt mixtures', are available through Z*enodo* at https://doi.org/10.5281/zenodo.6090167 (Godts et al., 2022b). The contents include:

- Integrated database (11412 samples) and charge balance calculation sheet, including raw ion concentrations and balanced outputs (XLSX), in which each row represents an individual sample.
- Example database (25 mixtures) (XLSX). The database includes metadata, calculation abbreviations and a flowchart.

The Supporting Information referred to in the section 'Modeled versus experimental salt mixture behavior' is available at https://pubs.acs.org/doi/10.1021/acsomega.4c01486 (Godts et al., 2024). The contents include:

- Supplementary material 001 and 002: Raman reference spectra (in-house library), Raman spectra obtained throughout the desorption measurements at different RH values at 20 °C, and XRD spectra obtained for mixtures $T1_V$ and $T1_{VI}$ (PDF)
- Supplementary materials 003: Comparative data for mixtures $T1_V$, $T1_{VI}$, $T2_V$, and $T2_{VI}$; ECOS/RUNSALT raw data and outputs, selected sorption and desorption data and graphs; selected micrographs of crystallization and dissolution processes; and XRD analysis, Raman, and ESEM-EDX analysis data and figures (XLSX)

All raw data is stored on the internal servers of the Royal Institute for Cultural Heritage (KIK-IRPA, Jubelpark 1, 1000 Brussels, Belgium) under the Open Science Mandate of the Belgium Science Policy (Belspo) and is available at reasonable request to sebastiaan.godts@kikirpa.be or via info@kikirpa.be.

Code availability

Code is available, as described in the section 'Analysis of salt mixtures', through Zenodo (Godts et al., 2022b). The contents provide access to the calculations integrated into R, including in- and output of the dataset with descriptors. Specifically, R scripts for charge balance calculations (.R), Full set of raw ion concentrations for the R scripts (.txt), Example of 25 raw ion concentrations for the R scripts (.txt), Full set of balanced outputs from the R script (.txt), Example of 25 balanced outputs from the R script (.txt). The code is available under a CC BY 4.0 license permitting redistribution and reuse with appropriate credit.

List of abbreviations

Ions and salt minerals:

Cl^-: chloride ion

NO_3^-: nitrate ion

SO_4^{2-}: sulfate ion

Na^+: sodium ion

K^+: potassium ion

Mg^{2+}: magnesium ion

Ca^{2+}: calcium ion

F^-: fluoride

PO_4^{3-}: phosphate

$C_2O_4^{2-}$: oxalate

NH_4^+: ammonium

CH_3COO^-: acetate

$HCOO^-$: formate

H_2O: water

xH_2O: different possible states of hydration

Containing chloride (Cl^-):

NaCl: halite

KCl: sylvite

$CaCl_2$: calcium chloride

$CaCl_2 \cdot 6H_2O$: antarcticite

$KCl \cdot MgCl_2 \cdot 6H_2O$: carnallite

$KCl \cdot MgSO_4 \cdot 3H_2O$: kainite

Containing nitrate (NO_3^-):

KNO_3: niter

$Ca(NO_3)_2$: calcium nitrate

$Ca(NO_3)_2 \cdot 4H_2O$: nitrocalcite

$Mg(NO_3)_2$: nitromagnesite

$NaNO_3$: nitratine (nitronatrite)

$Mg(NO_3)_2 \cdot 6H_2O$: magnesium nitrate hexahydrate

$Ca(NO_3)_2 \cdot KNO_3 \cdot 3H_2O$: hydrated calcium nitrate and potassium nitrate

$Mg(NO_3)_2 \cdot Ca(NO_3)_2 \cdot 10H_2O$: hydrated magnesium calcium nitrate

$3Na_2SO_4 \cdot K_2SO_4 \cdot 2MgSO_4 \cdot 2NO_3 \cdot 6H_2O$: humberstonite

Containing sulfate (SO_4^{2-}):

$CaSO_4$: anhydrite

$CaSO_4 \cdot 2H_2O$: gypsum

K_2SO_4: arcanite

$MgSO_4 \cdot 7H_2O$: epsomite

$MgSO_4 \cdot 6H_2O$: hexahydrite

$MgSO_4 \cdot xH_2O$: magnesium sulfates

Na_2SO_4: thenardite

$Na_2SO_4 \cdot 10H_2O$: mirabilite

$Na_2SO_4 \cdot H_2O$: darapskite

$Na_2SO_4 \cdot MgSO_4 \cdot 4H_2O$: bloedite

$K_2SO_4 \cdot H_2O$: potassium sulfate hydrate

$K_2SO_4 \cdot MgSO_4 \cdot 6H_2O$: picromerite

$Na_2SO_4 \cdot CaSO_4$: glauberite

$Na_2SO_4 \cdot CaSO_4 \cdot 4H_2O$: wattevillite

$2Na_2SO_4 \cdot CaSO_4 \cdot 2H_2O$: eugsterite

$5Na_2SO_4 \cdot 3CaSO_4 \cdot 6H_2O$: hydroglauberite

$K_2SO_4 \cdot CaSO_4 \cdot H_2O$: syngenite

$K_2SO_4 \cdot 5CaSO_4 \cdot H_2O$: görgeyite

$K_2SO_4 \cdot MgSO_4 \cdot CaSO_4 \cdot 2H_2O$: polyhalite

Others:

$Na_2CO_3 \cdot 10H_2O$: natron

$Na_2CO_3 \cdot H_2O$: thermonatrite

$Na_3CO_3HCO_3 \cdot 2H_2O$: trona

$CaCO_3$: calcite

$Ca(OH)_2$: portlandite

Mixture types:

$T1_V$: Type 1 mixture (sulfate-rich) $_V$: five ions: Cl^-, NO_3^-, SO_4^{2-}, Na^+, K^+

$T1_{VI}$: Type 1 mixture (sulfate-rich) $_{VI}$: six ions: Cl^-, NO_3^-, SO_4^{2-}, Na^+, K^+, Mg^{2+}

$T2_V$: Type 2 mixture (calcium-rich) $_V$: five ions: Cl^-, NO_3^-, Na^+, K^+, Ca^{2+}

$T2_{VI}$: Type 2 mixture (calcium-rich) $_{VI}$: six ions: Cl^-, NO_3^-, Na^+, K^+, Mg^{2+}, Ca^{2+}

Type 3: mixtures containing carbonates (relative within Type 1)

Measurement units and scientific terms:

$RH^m_{cry_x}$: mutual crystallization relative humidity for salt

$RH^m_{dis_x}$: mutual dissolution relative humidity for salt

$RH^m_{del_x}$: mutual deliquescence relative humidity for salt

$RH^m_{tra_{[x-x]}}$: mutual transition relative humidity, either a phase change (hydration, dehydration), decomposition, or the formation (addition) of solids.

RH^m_{eq} : mutual equilibrium relative humidity

RH^m_{sat} : mutual saturation relative humidity

cr: crystalline form

SD: standard deviation

n / n_{tot} : fraction of crystalline salt

RH: relative humidity

T: temperature

°C: degrees Celsius

mol·kg^{-1}: moles per kilogram

wt.% (m%): weight (mass) percent

µL: microliter

µm: micrometer

t: time

% s^{-1}: percent per second (RH %)

% h^{-1}: percent per hour (RH %)

V: volume

mg/L: milligrams per liter

L: liter

V_m : molar volume

cm^{-1}: inverse centimeter, wavenumber (in Raman spectroscopy)

mW: milliwatt

nm: nanometer

sccm: standard cubic centimeter per minute

dm/dt: derivative of mass with respect to time

SD: standard deviation

Eq/kg: equivalents per kilogram

g/cm^3: grams per cubic centimeter

mEq/kg: milliequivalents per kilogram

M : molar mass of ion (kg/mol)

kg/mol: kilograms per mole, unit of molar mass

m(salt)/mol·kg^{-1}: solution concentration as molality, number of moles of dissolved salt per kilogram water

n: number of moles of crystalline salt

a_w : water activity

i : ion

z_i : charge of ion

w_i : weight Fraction

c_i : ion Concentration (mg/L)

V_w : volume of Water (L)

m_s : dry sample mass (mg)

e_i : initial charge equivalent content of an ion (Eq/kg)

Δ_e : charge imbalance (Eq/kg)

e_{cat} : total sum of cations (Eq/kg)

e_{ani} : total sum of anions (Eq/kg)

$e_{i,adj}$: adjusted and balanced concentration of an ion (Eq/kg)

$e_{adj,f}$: final adjusted ion content (Eq/kg)

e_{lim} : limited ion content (Eq/kg)

x_i : ion content as mole fraction

f_e : amount of substance as a fraction

Miscellaneous:

HIROX: manufacturer 3D-digital microscope

MXG-2500REZ, KH-8700: model of lens used in the microscope

GenRH/Mcell: model of humidity control equipment (surface measurement systems)

HC2-IC 102: model of humidity probe (rotronic)

VirsaTM and InVia: models of Raman spectrometer (Renishaw)

XRD: X-ray Diffraction (Bruker D8)

theta/2theta: configuration in XRD analysis

SPSx-1µ: model of sorption testing system (ProUmid)

WP 785: model (nm) Raman spectrometer laser (Wasatch Photonics)

ESEM-EDX: Environmental Scanning Electron Microscopy combined with Energy Dispersive X-ray Spectroscopy (Zeiss)

EHT: Extra High Tension, referring to the accelerating voltage in ESEM

LaB6: Lanthanum Hexaboride material used for cathode filaments in ESEM

NTS BSD: Nano Technology Systems BackScattered Detector in ESEM

ECOS/Runsalt: Environmental Control of Salts, thermodynamic model and its graphical user interface

B: solids that occur in both mixture types (identified in model outputs)

E: salts identified in model outputs that overlap with the ones identified in the ECOS outputs of the mean ion values per mixture type

m: unverified metastable phases